

Spatially varying magnetic anisotropies in ultrathin films

Dissertation

zur Erlangung des akademischen Grades

doctor rerum naturalium (Dr. rer. nat.)

vorgelegt der

Mathematisch-Naturwissenschaftlich-Technischen Fakultät
(mathematisch-naturwissenschaftlicher Bereich)
der Martin-Luther-Universität Halle-Wittenberg

von Herrn **Fabrizio Porrati**

geb. am: 31. Januar 1968 in Milano, Italien

Gutachterin/Gutachter:

1. J. Kirschner
2. A. De Simone
3. S. Trimper

Halle/Saale, 10 Juli 2002

Contents

Introduction	1
1 Energetics of a ferromagnet	5
1.1 Magnetic free energy	5
1.1.1 Exchange energy	5
1.1.2 Anisotropy energy	6
1.1.3 External field energy	7
1.1.4 Magnetostatic energy	7
1.2 Micromagnetic equations	8
1.3 Numerical micromagnetics	10
1.3.1 Energy minimization	11
1.4 Domain walls	12
2 Stripe domains in thin films	15
2.1 Films with perpendicular anisotropy	15
2.2 Domains separated by walls of negligible width	16
2.3 Domains separated by walls of finite width	19
2.3.1 Different contributions of the magnetostatic energy	19
2.3.2 Thickness dependence of the domain wall width	21
2.3.3 Transition single domain/multi-domain state	23
3 Films with spatially varying magnetic anisotropies	27
3.1 Uniform magnetization: second and fourth order magnetic anisotropy	27
3.2 Morphology and non uniform magnetization	30
3.2.1 Definition of the system on study: characteristic parameters	31
3.2.2 Scale dependence: uniformity, canting and coexistence	32
3.2.3 Uniform and non-uniform magnetization for $L \approx \lambda$	34
4 1-D model	43
4.1 Analytical solution	43
4.1.1 Magnetic profiles	44
4.1.2 Energies	49

4.2	Role of the dipolar interaction	53
5	Engineered magnetic domains	59
5.1	Alternating in/out-of-plane patterned domains	59
5.1.1	Tailoring the anisotropy and modifying the magnetic profiles	59
5.1.2	Types of multi-domain states	63
5.1.3	Diagram of the states for films with modulated anisotropies	67
5.2	Spin reorientation transition	69
5.2.1	Lateral modulation of the anisotropy and SRT	70
5.3	In-plane patterned domains	73
5.3.1	Experiment and micromagnetic simulation of Fe on W(001)	73
6	Discussion and conclusion	79
6.1	Introduction	79
6.2	Discussion	80
6.2.1	Characterization	80
6.2.2	Uniform magnetization	82
6.2.3	Modulation	83
6.2.4	Patterned magnetic domains	86
6.3	Conclusion	88
	Zusammenfassung	89
A	Derivation of equations	i
B	Curriculum vitae	vii
C	Erklärung	ix
D	Acknowledgments	xi

Introduction

The importance of thin film magnetism increases continuously. The semiconductor and the magnetic recording industries explore together spin-electronic devices based on magnetic thin films and multilayers. The giant magnetoresistive (GMR) effect used in the design of new read-heads have permitted a rapid growth of the storage capacity of hard disk drives that has reached more than 10 Gbits/in² [1]. The possibility to retain information after a power switch-off has generated great interest in the magnetic random access memory (MRAM). The heart of MRAM are magnetic storage cells constituted by two magnetic thin films separated by spacer either metallic ('spin-valve') or non-metallic (magnetic tunnel junction, MTJ).

One main challenge to obtain better performances in new magnetic devices is represented by the use of nanofabrication techniques that offer unprecedented capabilities in the manipulation of size, shape and composition of magnetic structures [2]. Nanosize and nanopatterning can be achieved by means of self-organization [3–5], growth on vicinal single crystal substrates [6] and lithography [7]. This last technique is particularly adapt to prepare model samples magnetically well ordered and morphologically well defined to study 2D and 1D systems.

In order to improve multi-layer devices a lot of efforts have been put in the study of perpendicular magnetic profiles in the last decade. Only recently the interest for lateral magnetic nanostructures [4, 6, 8] has grown driven by the possibilities of fabrication offered by the nanotechnology. Nanomagnetic systems have been investigated by spatially averaging techniques like the magneto-optical Kerr-effect (MOKE), often assisted by scanning tunneling microscopy (STM) for a structural and electronic analysis. With this approach the details of the domain structure remain unknown and the correlation between morphology and magnetism unclear [9]. The investigation of the magnetic properties below ~ 100 nm is possible by means of magnetic force microscopy (MFM) [10] and scanning electron microscopy with spin polarization analysis (SEMPA) [11]. Besides, recent advances in scanning tunneling microscopy and spectroscopy (STS) allow to image magnetic structures with a nanometric resolution by using ferromagnetic tips [12, 13]. In this way the connection between electronic, structural and magnetic properties at nanometer scale is set and lateral magnetic nanostructures can be properly investigated.

The modeling of systems by means of micromagnetics is of great help in order to interpret existing data and to plan new experiments. The theory of micromagnetism, whose

equations were introduced by Brown [14], constitutes a synthesis between the quantum theoretical description based on the Heisenberg model and the phenomenological description set on the classical equation of Maxwell [15]. Within this theory the microscopic behavior of magnetic materials can be studied and the macroscopic picture can be in principle obtained. With the advent of the nanotechnology the task of micromagnetics is to connect intrinsic properties of the materials with the morphological structure obtained by fabrication. In this direction the main question to be addressed is: How does the micromagnetic structure adapts at nanometer scale? The question is fundamental because at this scale the structural changes of the material compete with the micromagnetic characteristic length. At nanoscale new magnetic behaviours are expected, as recently theoretically examined [16] and experimentally detected [17]. The knowledge of micromagnetics can explain magnetoresistive effects at nanocontacts [16, 18] and is essential to develop new nano magnetic devices.

The fundamental theorem for magnetic particles, proven by Brown [19], establishes that below a certain critical size the lowest state in energy is the one of uniform magnetization. Thin films with uniform uniaxial anisotropy are uniformly magnetized in-plane or out-of-plane [20–22]. In spite of the different anisotropies acting on the surface and inside the film, the exchange anisotropy is thought to be strong enough to keep all the magnetic moments aligned along the same direction [23]. Magnetic domains are induced by the dipolar interaction in films sufficiently thick. Alternatively, domains can also be induced by local inhomogeneities, which is the topic of this thesis. In ultrathin films with spatially varying magnetic anisotropies a local rotation of the easy axis may be induced by capping [24], strain relief [25] or structural transformations.

The aim of this work is to give an overview of the micromagnetic properties of systems with spatially varying magnetic anisotropies. A main question arise: What kind of magnetization is obtained as a function of the anisotropy patterning and of the material parameters? The connection between macroscopic and microscopic picture is set by comparing experimental and theoretical hysteresis loops with the configuration obtained by solving the micromagnetic equations. The strength of the magnetic anisotropy and the direction of the easy axis are fundamental parameters to control the switch in magnetoelectronic components and to evaluate the blocking temperature that sets the superparamagnetic limit for nanoparticles. In this direction we have analyzed the hardness of the system as a function of the various parameters. The theoretical analysis, mainly applied to 1-D systems, is both analytical and numerical. Two levels of approximation have been used in the study. The first is based on an anisotropy-type description, i.e., the dependence of the dipolar interaction is considered anisotropy-like. The second level of approximation is obtained numerically and includes the exact value of the magnetostatic energy. Limits and applicability of these approaches are discussed as function of the system parameters.

Briefly, the thesis is divided as follow. In chapter 1, the free energy of a ferromagnet and the micromagnetic equations will be introduced. In chapter 2, the theoretical analysis concerning stripe domains in thin films is reviewed with emphasis to the transition between

single domain and multi-domain state. In chapter 3, the system studied is introduced and a description in the limit of small scale of the anisotropy patterning is given. In chapter 4, the analytical solution of the problem is given. In chapter 5, various possible magnetic configurations are analyzed and a diagram of the state is drawn. Moreover, the spin reorientation transition is studied as function of the system parameters and the theoretical solution compared with experimental results obtained for films of Fe on W(110) in-plane magnetized. Finally, in chapter 6 the results are discussed and the conclusion of the work is given.

Chapter 1

Energetics of a ferromagnet

1.1 Magnetic free energy

A ferromagnet can be described at different levels of complexity [29] as a function of the scale of the system. The macroscopic properties of the magnetic materials can be deduced by the analysis of the hysteresis loops [26]. The domain theory describes the magnetic structure at the scale of $1 - 10^3 \mu\text{m}$ [39]. The theory of micromagnetism is the base to describe magnetic microstructures at a scale of $1 - 10^3 \text{ nm}$ [14]. The goal of micromagnetics is to find the magnetization $\mathbf{M}(\mathbf{r})$ as a function of the position \mathbf{r} inside the sample, under the constrain of constant module, i.e., $|\mathbf{M}(\mathbf{r})| = \text{const.}$

The total free energy is given by:

$$G(\mathbf{M}; \mathbf{H}_a) = \int_V g_{tot}(\mathbf{M}(\mathbf{r}); \mathbf{H}_a) dV = \int_V (f_{ex} + f_{an} + f_{ms} + f_h) dV \quad (1.1)$$

where $g_{tot}(\mathbf{M}(\mathbf{r}); \mathbf{H}_a)$ is the total energy density given by the sum of exchange, anisotropy, magnetostatic and external field energies and \mathbf{H}_a is an applied external field. In the following we introduce the various energy terms involved in eq. (1.1).

1.1.1 Exchange energy

The exchange is the basic interaction in ferromagnetic materials. The origin of it is electrostatic, but the explanation involves quantum mechanics. In fact, two electrons with spin vector \mathbf{S}_i and \mathbf{S}_j can be parallel or anti-parallel; in the first case, as a consequence of the principle of exclusion of Pauli, the two electrons have separate orbits and thus a reduced Coulomb interaction. Therefore the configuration with parallel spins is the lowest in energy. This explains the tendency of the magnetic materials to be constituted of wide regions of uniform magnetization called magnetic domains. The exchange energy associated with spin \mathbf{S}_i and \mathbf{S}_j is given by:

$$f_{ij} = -2J\mathbf{S}_i \cdot \mathbf{S}_j \quad (1.2)$$

where J is the exchange integral; $J > 0$ for a ferromagnet, $J < 0$ for an antiferromagnet. If the sample consists of more than one magnetic domain, not all spins can be collinear. If the angle between neighbor spins is small it is possible to make a Taylor expansion of the exchange energy. In the continuum approximation we obtain [28]:

$$f_{ex}(\mathbf{m}(\mathbf{r})) = A((\nabla m_x)^2 + (\nabla m_y)^2 + (\nabla m_z)^2) \quad (1.3)$$

where $A = \frac{nJS^2}{a}$, called exchange stiffness constant, is a function of the number of atoms per unit cell n , the lattice constant a , and $\mathbf{m}(\mathbf{r}) = \mathbf{M}(\mathbf{r})/M_s$, with M_s the saturation magnetization. The exchange is a short range interaction, as deducible from the quantum mechanic formulation. In fact, the wave functions bounded to different electrons have to overlap significantly in order to contribute to the exchange integral J . Besides, the exchange energy is an isotropic quantity because it depends only on the angle between neighbor magnetic moments and not on their relative orientation, as clear from eq. (1.3). Higher order anisotropic contributions are usually neglected.

1.1.2 Anisotropy energy

In magnetic materials the magnetization is induced to lie along specific direction called easy axis. The spin-orbit interaction couples the electron spins, responsible for the magnetism, to the anisotropic orbitals in a crystalline structure. The ions of the crystal create an electric potential that couples the spins to the lattice. The anisotropy energy is proportional to the product $\mathbf{L} \cdot \mathbf{S}$ between the orbital momentum \mathbf{L} and the spin momentum \mathbf{S} . Therefore, in absence of magnetic field, the energetic minimum is obtained for \mathbf{S} parallel to \mathbf{L} . A higher order source of anisotropy can be the stress, either tensile or compressive, applied to a crystal lattice. The stress changes the distance between neighbor ions so that the electric potential, the electronic orbitals and finally the spin-orbit coupling are modified. Both the magnetocrystalline anisotropy and the stress induced anisotropy find their origin in the spin-orbit coupling.

Hexagonal crystals like cobalt exhibit a uniaxial magnetic anisotropy. In this case the anisotropy energy density is given by the expansion of $\sin^2\theta$ [28], where θ is the angle between the c -axis and the magnetization:

$$f_u(\mathbf{m}(\mathbf{r})) = k_0 + k_1 \sin^2\theta + k_2 \sin^4\theta + \dots \quad (1.4)$$

The anisotropy constants k_1 and k_2 depend on the temperature and can be obtained experimentally. The general formula in terms of expansion of direction cosine of \mathbf{m} was given by Akulov [31]. In a cubic crystal, called α_1 , α_2 and α_3 the cosine directors, the energy density result:

$$f_c(\mathbf{m}(\mathbf{r})) = k_0 + k_1(\alpha_1^2\alpha_2^2 + \alpha_2^2\alpha_3^2 + \alpha_3^2\alpha_1^2) + k_2(\alpha_1^2\alpha_2^2\alpha_3^2) + \dots \quad (1.5)$$

Equations (1.4) and (1.5) are volume energy densities. At surface the breaking of symmetry generates an additional term of anisotropy [29] given by:

$$f_s(\mathbf{m}(\mathbf{r})) = \frac{1}{2}k_s(\mathbf{n} \cdot \mathbf{m}(\mathbf{r}))^2 \quad (1.6)$$

where \mathbf{n} is a unitary vector perpendicular to the surface and the constant k_s can be taken from the experiments. Note that equation (1.6), called surface anisotropy energy, can favors both an in-plane or an out-of-plane magnetization [32] and therefore the sign of k_s can be positive or negative.

1.1.3 External field energy

The interaction between the magnetization $\mathbf{M}(\mathbf{r})$ and an applied external field \mathbf{H}_a results in the external field energy:

$$f_h(\mathbf{m}(\mathbf{r})) = -M_s\mathbf{H}_a \cdot \mathbf{m}(\mathbf{r}) \quad (1.7)$$

1.1.4 Magnetostatic energy

The magnetization $\mathbf{M}(\mathbf{r})$ can interact also with the magnetic field generated by the body itself. In this case the energy density is given by:

$$f_{ms}(\mathbf{m}(\mathbf{r})) = -\frac{1}{2}M_s\mathbf{H}_d \cdot \mathbf{m}(\mathbf{r}) \quad (1.8)$$

where the demagnetizing or stray field \mathbf{H}_d is generated by the sample itself. The factor $\frac{1}{2}$ is introduced in order to avoid counting twice the interaction between couples of magnetic moments.

In order to calculate the magnetostatic energy we first need to evaluate \mathbf{H}_d . In this view we have to introduce some fundamental relations for magnetized media based on the equations of Maxwell. In absence of conduction currents the following relation is valid:

$$\nabla \times \mathbf{H}_d = 0 \quad (1.9)$$

In analogy with electrostatics, we can define the magnetic scalar potential ϕ that is linked to \mathbf{H}_d :

$$\mathbf{H}_d = -\nabla\phi \quad (1.10)$$

The magnetic potential ϕ is solution of Poisson's equation. Considering the boundaries at the surface of the ferromagnet we obtain

$$\phi(\mathbf{r}) = -\int_V \frac{\nabla \cdot \mathbf{M}(\mathbf{r}')}{|\mathbf{r} - \mathbf{r}'|} d^3r' + \oint_S \frac{\mathbf{n} \cdot \mathbf{M}(\mathbf{r}')}{|\mathbf{r} - \mathbf{r}'|} dS' \quad (1.11)$$

where the first is a volume integral over the body of volume V and the second is a surface integral extended to the surface S of the body. The form of equation (1.11) is analog to

the electrostatic potential. In fact, the first integral can be interpreted as the potential due to a spatial distribution of a volume charge with density $\rho = -\nabla \cdot \mathbf{M}$; the second as the potential due to a surface charge with density $\sigma = \mathbf{n} \cdot \mathbf{M}$.

In general, the calculation of the stray field \mathbf{H}_d is complicated because it involves a three-fold integral, see eq. (1.11). In the case of a uniformly magnetized body $\nabla \cdot \mathbf{M} = 0$ and the first integral in eq. (1.11) vanishes. Moreover, \mathbf{M} can be taken out of the surface integral and the potential depends only on the shape of the body. In particular, if the body is of ellipsoidal shape, the demagnetizing field \mathbf{H}_d has the same direction as \mathbf{M} :

$$\mathbf{H}_d = -4\pi D \cdot \mathbf{M} \quad (1.12)$$

where D is a tensor. If \mathbf{M} is parallel to one of the principal axis of the ellipsoid D is a number and it is called demagnetizing factor. The trace of the tensor D is 1. In a sphere for symmetry reasons the three demagnetizing factors are equal, $D_x = D_y = D_z = \frac{1}{3}$. In an infinite cylinder along the z direction $D_z = 0$ while $D_x = D_y = \frac{1}{2}$. In fact no surface charges are present at infinity, when the cylinder is magnetized along z . Similarly, a film infinitely extended in the xy plane has demagnetizing factors $D_x = D_y = 0$ and $D_z = 1$. In all these cases it is easy to calculate the magnetostatic energy density from equations (1.12) and (1.8):

$$f_{ms} = 2\pi(D_x M_x^2 + D_y M_y^2 + D_z M_z^2) \quad (1.13)$$

where M_i are the projections of the magnetization along the reference axis. In particular in the case of the infinite film eq. (1.13) becomes:

$$f_{ms} = 2\pi M_z^2 = 2\pi M_s^2 \cos^2 \theta \quad (1.14)$$

where θ is the angle of the magnetization vector with respect to the axis z . Equation (1.14) is characteristic of systems with uniaxial anisotropy (see eq. (1.4)) and is called shape anisotropy, because it depends only on the shape of the body. In fact, equation (1.14) may be generalized to the case of spheroid with $D_x = D_y \neq 0$. In the next chapters we will make wide use of eq. (1.14) in order to study thin films with uniform and non-uniform uniaxial anisotropy. The minimum of equation (1.14) is obtained for $\theta = 90^\circ$, i.e., when the magnetization lies in-plane of the film. The direction of the easy axis is determined from the competition between shape and crystalline anisotropy.

Note that if the shape of the body is not ellipsoidal \mathbf{H}_d is generally not uniform even if \mathbf{M} is. In this case, equation (1.12) is no more valid.

1.2 Micromagnetic equations

The theory of micromagnetism developed in the 30ties with a study on the structure of magnetic walls between two antiparallel domains due to Landau and Lifshitz [27]. In the early 40ties W. F. Brown made fundamental steps to set the theory that he named

micromagnetics [14]. The theory considers in detail the magnetic microstructures that were neglected in domain theory [39]. The atomic nature of matter is ignored and the material is considered as continuous, i.e., the magnetization vector is taken as a continuous function of space.

In section 1 we introduced the energy terms useful to study the magnetization of a ferromagnet. In order to find the magnetization distribution we have to minimize the total energy of the system:

$$G(\mathbf{M}; \mathbf{H}_a) = \int_V (f_{ex}(\mathbf{m}(\mathbf{r})) + f_{an}(\mathbf{m}(\mathbf{r})) + f_h(\mathbf{m}(\mathbf{r})) + f_{ms}(\mathbf{m}(\mathbf{r})) d^3r + \int_S f_s(\mathbf{m}(\mathbf{r})) dS \quad (1.15)$$

where f are the energy densities. The set of local minima is found by means of variational calculus. The vector $\mathbf{m}(\mathbf{r})$ is varied in each point of the sample of a small quantity $\delta\mathbf{m}(\mathbf{r})$. The corresponding variation of the energy has to be zero, i. e. δG . In particular, the extreme is a minimum if the second-order variation of G is positive, i.e., $\delta^2 G \geq 0$. Following this scheme we will find the magnetization distribution for systems with spatially varying magnetic anisotropies, in chapter 4.

The solution of the variational problem takes the form of a stability condition to be fulfilled at equilibrium [26]. In each point of the magnetic body is defined an effective field \mathbf{H}_{eff} given by:

$$\mathbf{H}_{eff} = -\frac{\partial G(\mathbf{M}; \mathbf{H}_a)}{\partial \mathbf{M}} \quad (1.16)$$

The effective field creates a torque on the magnetization that must be zero at equilibrium. Therefore the stability condition to be fulfilled in each point of the magnetic body is:

$$\mathbf{m} \times \mathbf{H}_{eff} = 0 \quad (1.17)$$

Equation (1.17) is known as equation of Brown and it is completed by the boundary conditions:

$$\mathbf{m} \times \left(2A \frac{\partial \mathbf{m}}{\partial n} + \frac{\partial f_s}{\partial \mathbf{m}} \right) \quad (1.18)$$

where \mathbf{n} is the unity vector normal to the surface and A is the exchange stiffness constant. In absence of surface anisotropy equation (1.18) becomes:

$$\frac{\partial \mathbf{m}}{\partial n} = 0 \quad (1.19)$$

where the condition $\mathbf{m} \cdot \partial \mathbf{m} / \partial n = 0$, valid for any vector of constant magnitude, has been used.

If the system is not in equilibrium equation (1.17) is not fulfilled and the vector \mathbf{m} precess around the field \mathbf{H}_{eff} . From the experiments is known that the precession decays in a finite time [27]. As a consequence the temporal variation of \mathbf{m} can be written as

$$\frac{\partial \mathbf{m}}{\partial t} = \gamma_G \mathbf{m} \times \left(\mathbf{H}_{eff} - \alpha_G \frac{\partial \mathbf{m}}{\partial t} \right) \quad (1.20)$$

where α_G is a phenomenological damping parameter and γ_G is proportional to the Lande' factor γ , i.e., $\gamma_G = \mu_0 \gamma$. Equation (1.20), called Gilbert's equation, is the generalization of eq. (1.17) to the dynamical case. If $\alpha_G \rightarrow 0$ the damping vanishes and the precession continues for ever. If $\alpha_G \rightarrow \infty$ the precession is negligible compared with the damping term. Finally, if $\partial \mathbf{m} / \partial t = 0$ the equation (1.17) is recovered.

1.3 Numerical micromagnetics

The spatial distribution of the magnetization is obtained from eq. (1.17) in the case of statics and from eq. (1.20) in the case of dynamics. The effective field \mathbf{H}_{eff} necessary to solve these equations is determined from the total system energy $G(\mathbf{M}; \mathbf{H}_a)$, see equation (1.16). In general the calculation of $G(\mathbf{M}; \mathbf{H}_a)$ is not easy because it involves a six-fold integral in the evaluation of the magnetostatic energy. In fact, while the exchange and the anisotropy energy can be obtained directly by solving the volume integral of eq. (1.15), the magnetostatic energy is obtained through the double volume integration of eq. (1.11) and eq. (1.15). Because of this complexity numerics started to be employed since the mid 60s [33] and is nowadays widely used in micromagnetic modeling of advanced magnetic materials [131].

Many of the numerical computations are based on the method developed by LaBonte [27] who computed a one-dimensional wall in thin films [33] in the mid 60ies. Some years later Labonte [34] and Hubert [35] solved independently the problem of a two-dimensional wall. In numerical micromagnetics the magnetic body is divided in elements of volume ΔV whose shape depends on the numerical method used. Inside each element the magnetization is constant in module and free to vary arbitrarily in direction. The continuous media is approximated by a discrete numbers of points each located at the center of one element. Therefore the integrals and the derivatives in the energy expressions are replaced by finite sums and differences in terms of the unknown magnetization components [34]. Finally, the total energy is minimized in order to obtain the magnetization distribution.

In this thesis the numerical computations are performed by using a commercial code written by Scheinfein [37] based on the method developed by LaBonte. Let us briefly consider the original problem of a two-dimensional domain wall solved by LaBonte [34]. In order to study a two dimensional wall in a magnetic film we can divide the body in $N_x \times N_y$ infinite long rectangular prisms of side $\Delta = a/N_x = b/N_y$ centered in $1 \leq I \leq N_x$, $1 \leq J \leq N_y$, see Fig. 1.1. Each prism exhibits uniform magnetization $\mathbf{M}(I, J) = M_s \mathbf{m}(I, J)$ with $\mathbf{m}(I, J) = \alpha(I, J) \mathbf{i} + \beta(I, J) \mathbf{j} + \gamma(I, J) \mathbf{k}$. The boundaries are considered by introducing additional points along the constraint edges $x = \pm a/2$ and along the film surfaces $y = \pm b/2$. The left and right column of points are denoted by $I = 0$ and $I = N_x + 1$; the bottom and top rows by $J = 0$ and $J = N_y + 1$. The constraint

boundary conditions at the edges of the film may be expressed as $\mathbf{m}(0, J) = -\mathbf{k}$ and $\mathbf{m}(N_x + 1, J) = +\mathbf{k}$ for the range $1 \leq J \leq N_y$. These constraints simulate the presence of two in-plane magnetic domains with opposite magnetization located at the sides of the wall. Since in this example the surface anisotropy is supposed to be zero equation (1.19) can be used. As a consequence $\mathbf{m}(I, 1) = \mathbf{m}(I, 0)$ and $\mathbf{m}(I, N_y + 1) = \mathbf{m}(I, N_y)$ over the range $1 \leq I \leq N_x$. The energy expressions are developed directly in terms of the discrete distribution $\{\mathbf{m}(I, J)\}$ [34].

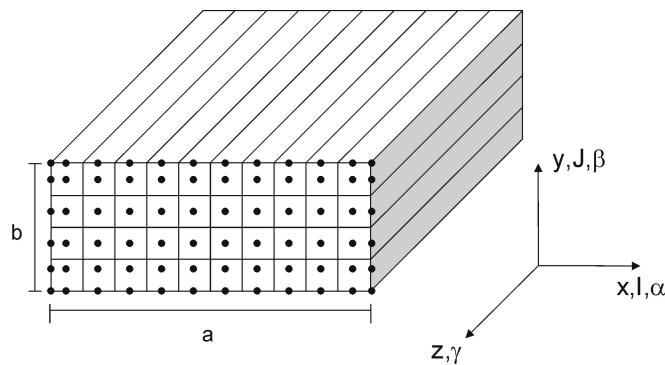


Figure 1.1: *Discrete partition for the study of a two-dimensional domain wall [34]. The film is infinite in the z direction, it has width a and thickness b. Inside each prism the magnetization is constant, i. e. $|\mathbf{m}(I, J)| = \text{const}$.*

1.3.1 Energy minimization

The magnetization distribution can be obtained either integrating the discretized Gilbert's equation (1.20) in time [133] or minimizing the total energy to reach the equilibrium condition of Brown's equation (1.17).

In the relaxation method the effective field $\mathbf{H}(I, J)$ is computed for a particular point in the grid with the magnetization distribution held fixed. This field is normalized to $\mathbf{h}(I, J) = \mathbf{H}(I, J) / |\mathbf{H}(I, J)|$ and the difference $\delta(I, J) = |\mathbf{h}(I, J) - \mathbf{m}(I, J)|$ is stored as the most recent misalignment at location (I, J) . The current value of $\mathbf{m}(I, J)$ is then replaced by $\mathbf{h}(I, J)$ and a new location is selected. In this manner the entire distribution is swept through and $\{\mathbf{m}(I, J)\}$ is reset point by point. After each complete sweep, the maximum value within the set $\{\delta(I, J)\}$ is found and compared with a preset tolerance; this procedure is continued until the maximum deviation falls below the tolerance [34]. At this point the system has reached the equilibrium and Brown's equation (1.17) is fulfilled.

The time integration method solves numerically the dynamic Gilbert's equation (1.20) or the equivalent Landau-Lifshitz's equation [27]. This method is suitable to study dynamic problems like wall motion or the variation of the magnetization after a magnetic

field is applied. For calculations of equilibrium wall configurations both methods can be used. It has been shown [133] that they yield equivalent equilibrium magnetization structures for thin Permalloy and Fe films in agreement with the experimental surface domain magnetization profiles. In order to choose the numerical method the calculation time has to be considered. In the code used in this thesis [37], on the one hand the relaxation method leads to a more rapid convergence than the time integration method. On the other hand, in the relaxation method the CPU time depends on the square of the number of cells, i.e., N^2 , in the magnetostatic self-field computation. As a consequence, the time integration method with Fast Fourier Transformation (FFT) can be 100-1000 times faster for large problems, even with a 10-100 times slower convergence. In this work, the relatively low number of cells used ($N \approx 10^3$) led to choose the relaxation method scheme for the minimization of static magnetization structures.

Two parameters have to be chosen carefully in order to obtain a reliable results from the simulations: the grid density, i.e., the size of the unit cells, and the convergence criterion, i.e., when to end the simulation. No clear-cut criterion is known to chose the grid density. Nevertheless two obvious limits has to be considered. On the one hand, the mesh should not be too fine, so that the computation is numerically feasible. On the other hand, the mesh should be sufficiently fine to allow the microstructure to be fully developed [27]. In order to find the right mesh for the problem successive computations with increasing cell density has to be performed and compared until no modification of the magnetization configuration are found.

1.4 Domain walls

At the boundaries between neighboring domains the magnetic moments gradually change direction in order to minimize the total energy of the system. The details of the transition region, called domain wall, can be calculated using the methods of variational calculus (see section 1.2) or numerical micromagnetics (section 1.3). The first calculation of domain walls was carried out by Landau and Lifshitz for an infinite crystal with uniaxial anisotropy [29, 134]. In this case the direction of the magnetization changes of 180° in a region separating two domains of opposite magnetization. As a consequence a wall, generally called Bloch wall, forms between the two neighbor domains, see Fig. 1.2.

The rotation of the magnetization takes place along the direction of the x -axis. Since the crystal is considered infinite, the contribution of the surface charges is zero. Besides, in order to minimize the contribution of the magnetostatic energy the vector \mathbf{m} lies in the yz plane so that $\nabla \cdot \mathbf{m}=0$. Therefore the total energy per unit area is

$$G(\mathbf{M}) = \int_{-\infty}^{\infty} \left[k_1 \sin^2 \theta_x + A \left(\frac{d\theta}{dx} \right)^2 \right] dx \quad (1.21)$$

i.e., the sum between anisotropy and exchange energy. The angular dependence of the magnetization is obtained after minimization by means of variational calculus (see for

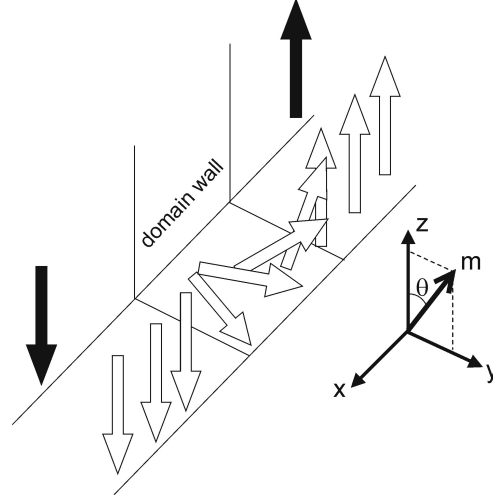


Figure 1.2: Bloch wall separating domains with opposite magnetization.

instance [26, 27]):

$$\theta_x = \text{acos} \left(-\text{th} \frac{x}{\lambda} \right) \quad (1.22)$$

where $\lambda = \sqrt{A/k_1}$ is the magnetic characteristic length. The classical definition of domain width is based on the slope of the magnetization angle θ_x [29]. Its value is:

$$\delta_w = \pi \sqrt{\frac{A}{k_1}} \quad (1.23)$$

By integrating the energy density over x we obtain the total energy density per unit surface:

$$\gamma = 4\sqrt{Ak_1} \quad (1.24)$$

If the anisotropy is cubic, as for instance in iron or nickel, there are three axis along the three cubic axis. In this case the orientation of the magnetization in neighboring domains may be at 90° or 180° . The structure and the energy of 90° domain walls can be calculated in the same way as shown in this section for the 180° Bloch wall. The walls considered in this thesis are anisotropy-like, but also other kind of walls are possible in thin films. In order to reduce the stray field energy the magnetization vector may rotate in-plane in sufficiently thin films forming a Néel wall. In this case no surface charges but only some volume charges contribute to the magnetostatic energy.

In order to study different domain configurations the walls between neighbor domains are assumed to have zero width [39]. In fact, for domains of the order of micrometers

the domain wall width is negligible. Nevertheless the energy of the wall has to be considered and included into the total energy. Then the total energy is minimized and the energy value obtained is compared with the one of other possible domain configurations. If the scale of the system reduces the domain structure is no more negligible and the micromagnetic equation have to be used to describe the magnetization distribution. In the next chapter we will study the effect of the reduction of the scale for a system with perpendicular uniform uniaxial anisotropy.

Chapter 2

Stripe domains in thin films

2.1 Films with perpendicular anisotropy

In the first part of this chapter, we discuss the magnetization of films with perpendicular uniaxial anisotropy. The easy axis of the anisotropy is chosen parallel to the film normal and favors an out-of-plane magnetization. The tendency of the magnetization to rotate out-of-plane, however, is hindered by the presence of the magnetic charges on the surface of the film which contribute to the magnetostatic energy. As a consequence, the magnetostatic energy (or the shape anisotropy) is smallest when the magnetization lies in the plane of the film. The competition between uniaxial and shape anisotropy determines whether the magnetization tends to be perpendicular or parallel to the film normal, provided that the magnetization is uniform. The two quantities are compared by means of the quality factor [29]

$$Q = \frac{2k_u}{\mu_0 M_s^2} \quad (2.1)$$

the ratio between the uniaxial and the shape anisotropy. The uniaxial anisotropy is a function of the thickness t of the film and it is given by the sum of the volume anisotropy constant k_b and of the surface anisotropy constant k_s divided by t :

$$k_u(t) = k_b + \frac{k_s}{t} \quad (2.2)$$

If $Q < 1$, the shape anisotropy is dominant and the magnetization tends to lie in-plane. If $Q > 1$, the uniaxial anisotropy forces the anisotropy to lie out-of-plane.

So far we have seen that the tendency of the magnetization to lie in or out-of-plane is connected to the ratio of uniaxial and shape anisotropies. To understand whether the system shows magnetic domains or a single domain, we have to analyse the energy of these configurations. In general, magnetic domains occur when the gain in magnetostatic energy due to the domain structure is bigger than the energy required to form the domain walls.

2.2 Domains separated by walls of negligible width

In order to calculate the total energy of a stripe configuration, some studies [38, 40, 42] follow the pioneering work of Kittel [39] who considered a series of stripes of width D , with the magnetization pointing alternatively up and down (Fig. 2.1). The stripes are assumed uniformly magnetised and separated by a wall of width δ_w much smaller than the domains D .

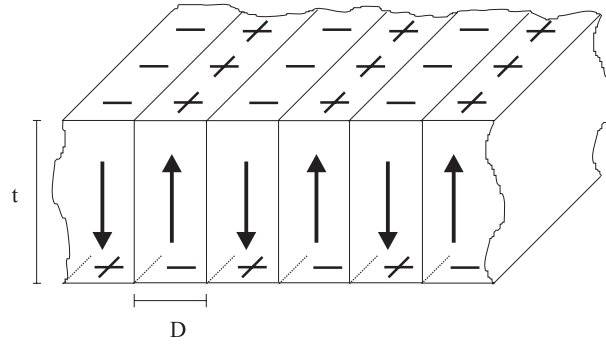


Figure 2.1: *Series of stripe domains for a thick film, i.e., for thickness t much bigger than the domain width D . The magnetization is uniform within each stripe and the wall width δ_w is negligible with respect to the domain width D .*

The relevant energy is given by the sum of the magnetostatic energy and of the wall energy. The total wall energy per unit area of the stripe domain configuration in Fig. 2.1 is given by

$$e_w = \gamma_w \frac{t}{D} \quad (2.3)$$

where $\gamma_w = 4\sqrt{Ak}$ is the energy of a Bloch wall and t/D is the total domain wall area [28]. In the limit of thick films, i.e., $t \gg D$, the magnetostatic field created by the charges on one surface of the slab does not interact with the field of the other surface. Therefore the value of magnetostatic energy is two times the value obtained for a single surface of the slab. The field created by the surface charges with alternating sign $\pm M_s$, is given by the Fourier expansion of a square-wave of amplitude $2\pi M_s^2$. The magnetostatic energy density per unit area for one single surface results [39]:

$$e_{ms} = 0.85 M_s^2 D \quad (2.4)$$

The dependence of the domain width D from the thickness of the slab t is obtained by minimizing the energy, given by the sum of eq. (2.3) and (2.4), with respect to D . The result is that in the limit of thick films, the domain width grows with the root of the

thickness: $D \sim \sqrt{t}$. If the thickness of the film is smaller or comparable to the domain width, i.e., $t \leq D$, the two surfaces interact magnetostatically. The magnetic field \mathbf{H} is approximately the same of a film uniformly magnetized, except for regions of size t around the wall Fig. 2.2 [26].

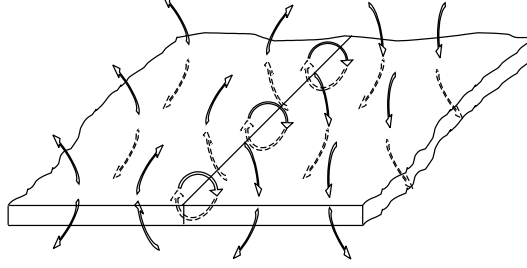


Figure 2.2: *Stripe domains in the limit of small thickness, i.e., $t \ll D$. The stray field crosses the film, side to side, and it is similar to the stray field of a single domain state, uniformly magnetized out-of-plane. The difference is localized around the border of successive stripes; in this region the flux closure slightly reduces the magnetostatic energy with respect to the value of a single domain state. The arrows indicate the stray field direction.*

In this case the magnetostatic energy is a function of the thickness t and it is found by expanding the magnetic potential in a double Fourier series given by [40, 42]:

$$e_{ms} = \frac{16M_s^2 D}{\pi^2} \sum_{n=1}^{\infty} \frac{1}{2n} \left(1 - \exp\left(-\frac{2n\pi t}{D}\right)\right) \quad (2.5)$$

In the limit of thick films, the exponential of eq. (2.5) is negligible and the magnetostatic energy tends to the value given by Kittel, eq. (2.4). In the limit of thin films, i.e., $t \ll D$, the exponential can be expanded to the first order, so that $\exp\left(-\frac{2n\pi t}{D}\right) \cong 1 - 2n\pi t/D$ and eq. (2.5) becomes:

$$e_{ms} = 2\pi M_s^2 t \quad (2.6)$$

This expression shows that in the limit of thin films, the magnetostatic energy reaches the value of a film of thickness t , uniformly magnetized parallel to the normal. An analytical study of the system in the limit of thin films, has been performed by Kaplan and Gehring [38]. Using the Taylor expansion of t/D up to the second order, they give the expression for the magnetostatic energy:

$$e_{ms} = 2\pi M_s^2 t \left(1 - 0.67 \frac{t}{D} + \frac{2t}{\pi D} \ln \frac{t}{D}\right) \quad (2.7)$$

The comparison of this equation with eq. (2.6) shows that the difference in magnetostatic energy between the stripe-domains state and the single domain state is vanishing with the thickness t . The minimization of the total energy, obtained after summation

of equations (2.3) and (2.5), gives the value of the domain width $D(t)$ as a function of the thickness of the film. The numerical solution is plotted in logarithmic scale in Fig. (2.3) [43].

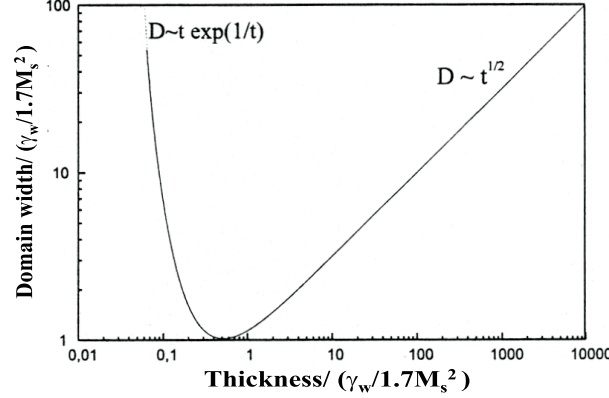


Figure 2.3: Domain width $D(t)$ as a function of t , thickness of the film. The curve is obtained numerically by minimizing the total energy which is given by the sum of equations (2.3) and (2.5) [43]. The axes are normalized to the minimum of the domain width, $D_m = \gamma_m / 1.7 M_s^2$. In the limit of thick films, i.e., $t \gg D$, the domain width follows the law of Kittel, $D \sim \sqrt{t}$. In the limit of thin films, i.e., $t \ll D$, the domain width increases with $D \sim t \exp\left(\frac{1}{t}\right)$

In the limit of thick films, the curve follows the prediction of Kittel. The minimum is obtained by decreasing the thickness of the slab when the charges of the two surfaces start to interact. The critical width, i.e., $D_m = \gamma_m / 1.7 M_s^2$, is a function of the material and its value is usually between 20 nm and 50 nm. For thinner films the domain width increases rapidly with exponential law: $D \sim t \exp\left(\frac{1}{t}\right)$. The same behaviour is found analytically [38], after the minimization of the total energy, sum of equations (2.3) and (2.7). In this case the domain width is given by:

$$D(t) = 0.95t \exp\left(\frac{\pi D_0}{2t}\right) \quad (2.8)$$

where $D_0 = \gamma_m / 2 \pi M_s^2$ is the characteristic dipolar length. Equation (2.8) can be inserted in the expression of the total energy that results [45] :

$$e_t = 2\pi M_s^2 t \left(1 - 0.67 \exp\left(-\frac{\pi D_0}{2t}\right)\right) \quad (2.9)$$

The total energy of the single domain state is equal to its magnetostatic energy and it is given by eq. (2.6). In the limit of thick films, i.e., $t \gg D$, the gain in magnetostatic

energy due to the flux closure is sufficiently high to guarantee that the energy for a stripe domain configuration is lower than for a single domain state. By decreasing the thickness of the film, the gain in magnetostatic energy becomes comparable to the wall energy and the domain formation is less efficient. In the limit of thin films, i.e., $t \ll D$, the energy for the stripe domain configuration is given by eq. (2.9). From this equation we notice that for every thickness of the slab, the value of the total energy is smaller than for a single domain state. However, the rapid increasing of the domain width, rules out the possibility to have a multi-domain state in a real sample of finite dimensions below a certain critical thickness t_c , when the domain width becomes of the same order of the extension of the thin film.

2.3 Domains separated by walls of finite width

So far we have considered a system with uniform magnetization within the magnetic domain and with a wall negligible with respect to the domain width. In reality, the Bloch wall between two domains has a finite width and this contributes to the total energy of the system. For certain sets of the parameters of the system, the dimension of the wall becomes comparable with respect to the domain size and the picture of domains separated by narrow walls loses its meaning. In such a case, the magnetization profile can be described by a sine-like function between two maximal values which are a function of the domain width [46]. The goal of this paragraph is to describe films with uniform perpendicular anisotropy taking into account the effect of Bloch walls of finite width between domains of opposite out of the plane magnetization.

2.3.1 Different contributions of the magnetostatic energy

The magnetostatic energy of a sample of volume V is given by:

$$F_{\text{ms}} = -2\pi \int_v \mathbf{M}(\mathbf{r}) \cdot \mathbf{H}(\mathbf{r}) d\mathbf{r} \quad (2.10)$$

The dipolar field $\mathbf{H}(\mathbf{r})$ is the result of the interactions of all the magnetic moments distributed in the sample. Therefore the magnetostatic energy density is a non-local quantity, depending on the distribution of all the magnetic charges upon the sample. On the other hand, the anisotropy is a local quantity which depends on the symmetry of the magnetic material considered. In thin films it is possible to write the magnetostatic energy as a sum of an anisotropy-type energy density term, proportional to the area of the film, plus a term describing the influence of the wall fine structure [47]. In this way it is possible to evaluate the rotation of the magnetization which takes place in the region of the wall.

With the exception of some particular cases, the integral (2.10) has no analytical solution and the magnetostatic energy can be calculated only numerically. In the case of

a uniformly magnetised film, however, the magnetostatic energy density results:

$$f_{\text{ms}} = 2\pi M_s^2 \cos^2\theta \quad (2.11)$$

where θ is the angle between the magnetization and the normal of the film. If the film is magnetized parallel to the normal, θ is zero and eq. (2.11) equals eq. (2.6). Since in a system with perpendicular uniaxial anisotropy the angular dependence of the anisotropy energy is of the same form as eq. (2.11), it is convenient to define the following effective anisotropy:

$$k_{\text{eff}} = k_{\text{u}} - 2\pi M_s^2 \quad (2.12)$$

so that the total energy density of the system results:

$$f_{\text{t}} = c + k_{\text{eff}} \sin^2\theta \quad (2.13)$$

In this way the uniformly magnetized system is fully described by anisotropy-type local quantities. It is useful to underline that the magnetostatic energy, although absorbed in the effective anisotropy constant as shown in eq. (2.13), is still a non-local quantity, a function of the mutual interaction of all the spins distributed in the sample. In general the magnetization along the sample is not uniform and the magnetization can rotate forming a Bloch wall, as sketched in Fig. 2.4 for a thin film.

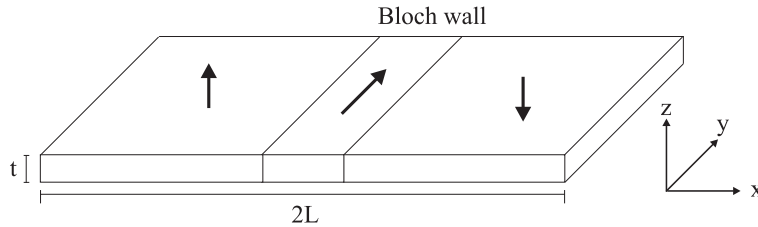


Figure 2.4: *Infinitely long slab of thickness t and width $2L$. The Bloch wall between the two domains has the width $\delta_w = \pi\sqrt{\frac{A}{k}}$.*

In case of a thin film not uniformly magnetized along the x direction the magnetostatic energy per unit length can be written in the following way [44]:

$$f_{\text{ms}}(L, t) = 2\pi Lt \int M_z^2(x) dx + \frac{Lt^2}{4} \int \frac{dM_z(x)}{dx} \frac{dM_z(x')}{dx'} \ln \frac{|x - x'|}{t} dx dx' \quad (2.14)$$

where L is the length of the unit cell. The first part of the equation corresponds to the anisotropy-like term. It is proportional to the area of the film and it contains the local magnetization $M_z(x)$, which is integrated across the wall. The second term represents the correction to the magnetostatic energy due to the rotation of the magnetization, as

shown by the derivative under integration, and it is negative. In the case of uniform magnetization the derivative is zero and eq. (2.14) reduces to eq. (2.11). In the limit of vanishing thickness, i.e., $t \rightarrow 0$, only the first term remains and the value of the magnetostatic energy can be compared to the one of eq. (2.6). In both cases the demagnetizing factor is equal to one, but the value of the magnetostatic energy is different. In fact, while eq. (2.6) refers to a film uniformly magnetized out of plane, the first term of eq. (2.14) refers to a system with non uniform magnetization. In this latter case both the average value of the magnetic charges and the magnetostatic energy reduce. In general, as will be clear in section 2.3.3, the second term of eq. (2.14) must be considered to guarantee the existence of magnetic domains in systems with uniform uniaxial anisotropy. The goal of section 5.1 will be to show that systems with alternated anisotropy can have magnetic domains even neglecting the correction to the magnetostatic energy.

2.3.2 Thickness dependence of the domain wall width

Before we analyze the formation of a multi-domain state, we study the thickness dependence of a Bloch wall clarifying the role of the different contributions to the magnetostatic energy introduced in the last section.

The surface charges of opposite signs on the two sides of a Bloch wall generate a stray field whose intensity is a function of the thickness of the slab. In order to measure the effect of the stray field at first we calculate the energy and the wall profile in the case of vanishing thickness. In this case no stray field is created around the Bloch wall. Therefore the correction to the magnetostatic energy is zero and the system can be described by means of anisotropy-type quantities, as seen in section 2.3.1. This state can be obtained by assuming zero magnetostatic energy and the value given by eq. (2.12) for the anisotropy.

With reference to Fig. 2.4, we consider a Bloch wall of width δ_w dividing an infinite film [48] of thickness t in two regions, oppositely magnetized. In the example, the exchange constant is $A=1.05 \cdot 10^6 \text{erg/cm}^3$, the uniaxial anisotropy constant $k_u=1.35 \cdot 10^7 \text{erg/cm}^3$, and the spontaneous magnetization is $M_s=1440 \text{emu/cm}^3$. The profile of the wall for different thickness is plotted in Fig. 2.5. The shape of the wall is determined by the minimization of the anisotropy energy, the exchange energy and the magnetostatic energy. In particular both the contributions of the magnetostatic energy introduced in section 2.3.1 play a role in the determination of the wall structure. In fact, on the one hand the anisotropy-type term tends to enlarge the wall in order to minimize the surface charge density (principle of charges avoiding), on the other hand the correction to the magnetostatic energy tends to narrow it because of the flux closure generated around the wall (see Fig. 2.2). The weight of the two contributions is a function of the thickness of the film as can be seen by defining the following general expression of the effective anisotropy:

$$k_{\text{eff}}(t) = k_u(t) - \alpha(t)2\pi M_s^2 \quad (2.15)$$

The function $\alpha(t)$ measures the contribution of the correction to the magnetostatic energy

and has the following limits:

$$\lim_{t \rightarrow 0} \alpha(t) = 1 \quad \lim_{t \gg \delta_w} \alpha(t) = 0 \quad (2.16)$$

The two values are obtained respectively for a film with vanishing thickness and for a thick film. When the thickness of the film tends to zero, the effect of the circular field created around the wall is small and the anisotropy-type term is sufficient to describe the magnetostatic energy. The wall profile obtained in such a case is drawn as a solid line in Fig. 2.5.

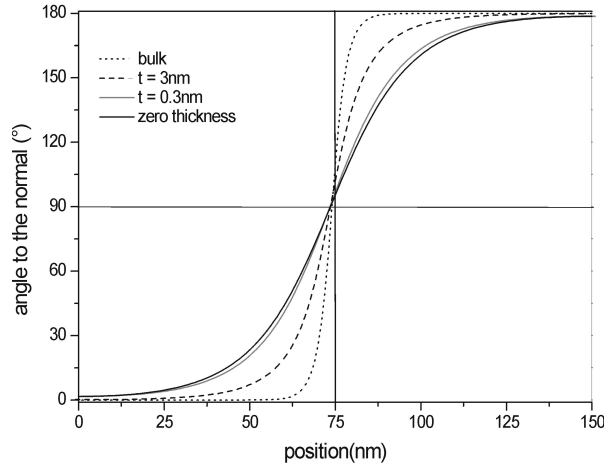


Figure 2.5: Influence of the thickness t of the film on the width of the Bloch wall. To study the dependency of the magnetostatic energy, the uniaxial anisotropy constant $k(t)$ is considered thickness independent. The dotted and the solid line are the lower and the upper limit for the wall width. The limits correspond to the bulk value (dotted line) and to the zero thickness film (solid line). By increasing the thickness of the film the influence of the circular field created by the surface charges around the Bloch wall increases blocking the expansion of the wall.

In this case the magnetostatic energy tends to $2\pi M_s^2$ and the width of the wall tends to

$$\delta_w = \pi \sqrt{\frac{A}{k_{\text{eff}}}} \quad (2.17)$$

This equation represents the upper limit of the wall width for a system with uniaxial anisotropy k_u . The plot in grey in Fig. 2.5 represents the case of an ultrathin film with vanishing thickness, $t = 0.3$ nm, when the circular magnetic field plays still a negligible role. By increasing the thickness of the film the effect of the field becomes stronger and the wall reduces its extension, as we can see in the dashed profile of Fig. 2.5. In the

limit of thick films, i.e., for $t \gg d$, the width of the wall is given by equation 1.23, which represents the lower limit for a system with uniaxial anisotropy k_u . Hence, by means of the function $\alpha(t)$, the thickness dependence of the circular magnetic field created by the surface charges is described. The validity of this function goes beyond the limit of thin films for which eq. (2.14) has been calculated, but does not describe completely the thickness dependence of the effective anisotropy which are present as well in the uniaxial anisotropy term of eq. (2.15).

2.3.3 Transition single domain/multi-domain state

In this section, first we want to compare the energy of a single domain state with the one of a multi-domain state, in order to find the critical domain size of the transition for systems with finite walls width. The domain size at the transition is a function of the thickness as well as of the hardness of the material represented by Q . Secondly we show that a multi domain state cannot exist if the dipolar interaction is neglected and only local quantities are considered to describe the system. Finally we compare the transition to the case of systems with negligible wall width.

In general, a multi-domain state is energetically favorable in comparison to a single domain state if the energy required to form a wall is lower than the gain in magnetostatic energy due to the stray field. The formation of a multi-domain state can be analyzed in simple terms by considering two domains, opposite magnetized and separated by a Bloch wall, as shown in Fig. 2.4, and comparing the energy obtained with the one of a single domain state. The energy of the wall is independent on the length L of the slab. As a consequence the energy to pay to form the multi-domain state is constant with the length L . On the contrary, the gain in magnetostatic energy density per unit area increases with L . Therefore, for a certain critical value of the length L_0 , the energy of the multi-domain state becomes favorable.

The situation is well represented by the following equation, obtained by integration of eq. (2.14), using the profile of the Bloch wall $M_s = M_t \tanh(x/\delta)$ [41, 44]:

$$\frac{\Delta F}{Lt} = \gamma_w + \frac{\mu_0 M_s^2 t}{\pi} \ln \frac{2c_w \delta}{L} \quad (2.18)$$

where $c_w \approx 1.356$ is a numerical factor.

Equation (2.18) gives the energy difference between single and multi-domain state; it is positive for $L < L_0$ and negative for $L > L_0$. The term responsible for the domain formation is the logarithm and comes from the non-local part of the magnetostatic energy written in eq. (2.14). This term, which has to be negative in order to reduce the value of the total energy, drives the transition by increasing L , length of the slab. The critical length L_0 , normalized to the exchange length l_{ex} , is obtained from eq. (2.18) for $\Delta F=0$:

$$\frac{L_0}{l_{ex}} = \frac{1.9}{\sqrt{2Q-1}} \exp \frac{8.9\sqrt{2Q-1}}{\frac{t}{l_{ex}}} \quad (2.19)$$

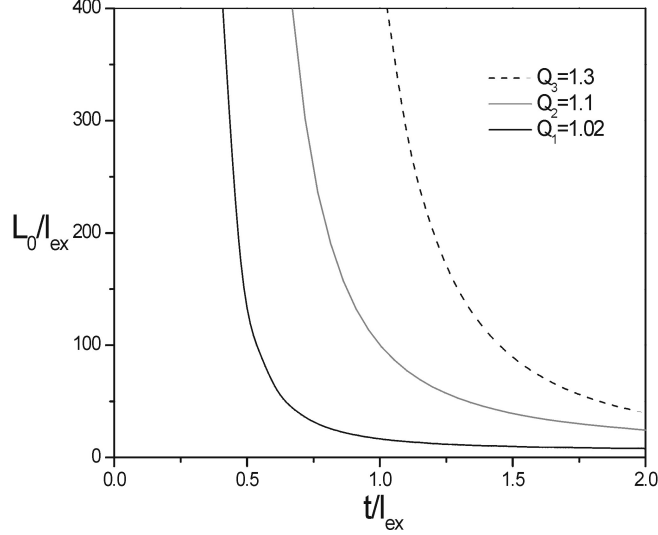


Figure 2.6: Thickness of the film versus L_0 , the critical length for the transition to the multi-domain state. The plots are normalized to the exchange length l_{ex} and refer to eq. (2.18) for different values of Q . With increasing Q or decreasing t , l_0 shifts to higher values. In this way the drop in magnetostatic energy balances the increase of the wall energy.

The thickness of the film versus the critical length L_0 , for different values of Q , is plotted in Fig. (2.6). As already shown in section 2.2 for the case of negligible wall width, the domain size increases rapidly with thickness decreasing, till the size of the sample is reached and the multi domain state cannot exist anymore. This happens because the gain in magnetostatic energy decreases with the thickness and therefore the length L of the slab has to increase to allow domain formation.

The dependence of the domain size on the hardness of the material is clear if we consider the effective anisotropy, whose value increases with Q , as can be deduced from eq. (2.15). As a consequence the wall energy increases and, in order to obtain a multi domain configuration, the length L of the slab has to become bigger so that the gain in magnetostatic energy can be comparable to the energy paid to form the wall.

Before comparing the different models introduced in the last sections, we show that the existence of the stray field created around the Bloch wall is essential to understand the formation of a multi-domain state. Let us consider once more a system with uniaxial perpendicular effective anisotropy, described only by means of the exchange energy and the anisotropy-type energy terms. If the system is uniformly magnetized out-of-plane, the exchange and the effective anisotropy energy are zero. As soon as a wall is formed and some of the magnetic moments are tilted away from the normal of the film, the effective anisotropy energy and the exchange energy are no more zero. Therefore, if the dipolar

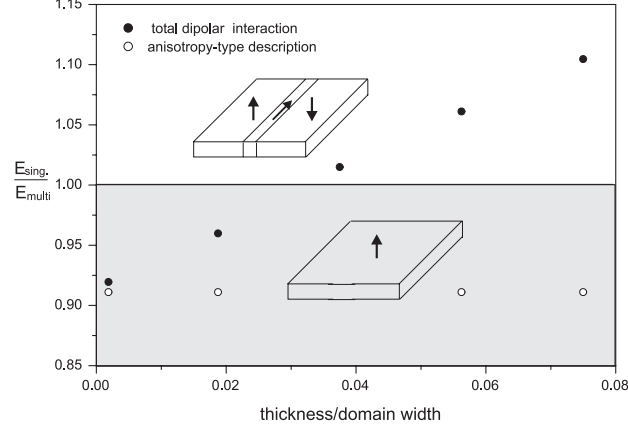


Figure 2.7: Ratio of the total energy between single-domain and multi-domain state vs. the thickness of the slab, normalized to the domain width. If the system is described by means of anisotropy-type terms, the only possible state is the single domain. If the stray field created around the Bloch wall is considered, at a certain critical thickness the system splits into magnetic domains.

interaction is not considered in its complete form, the energy of the system increases and the single domain state is the lowest in energy. This shows that the complete non-local dipolar interaction is the fundamental quantity to be considered to explain the formation of a multi-domain state for a system with perpendicular uniaxial anisotropy. In Fig. 2.7 we compare the energies of a multi-domain state with a single-domain state as a function of the thickness, normalized to a fixed value of the domain width. The numerical calculation is performed in the case of an anisotropy-type description (white dots in Fig. 2.7), when the circular magnetic field is not considered, and in the case of total dipolar interaction (black dots in Fig. 2.7). If the correction to the dipolar energy is not considered, the ratio of the total energy is constant with the thickness and the single domain state has lower energy than the multi-domain state. This happens because the magnetostatic energy density is thickness independent for both states. If the correction is considered, the magnetostatic energy density is no more thickness independent. As a consequence the total energy of the multi-domain state decreases linearly with the thickness allowing the transition to the multi-domain state.

The analysis carried out in this section has the purpose to determine the conditions for which it is favorable to have a multi-domain configuration. To complete the picture, we want to study the influence of the presence of the domain wall in the determination of the domain size by comparing eq. (2.18) with eq. (2.8), calculated with the assumption of uniform magnetization and negligible wall width. The two curves are plotted in Fig. 2.8,

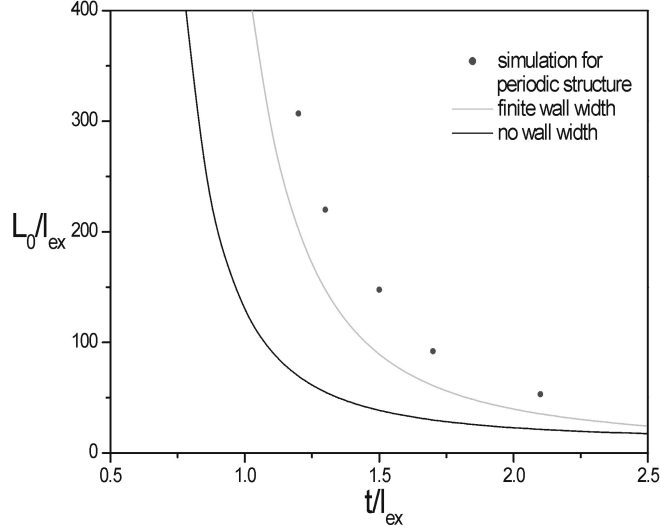


Figure 2.8: L_0 , critical length for the transition to the multi-domain state versus t , thickness of the film. The plots shown, normalized to the exchange length l_{ex} , are for a value of $Q=1.3$. The black plot refers to eq. (2.8), where the wall-width is neglected. The dashed plot refers to eq. (2.18), where the wall width is considered finite. The black points result from numeric simulation performed with periodic boundary conditions.

for $Q=1.3$. Fixing an arbitrary value of the thickness of the slab we notice that the domain size is significantly larger if the wall is included in the description. In this case the average perpendicular magnetization around the region of the wall is smaller than for a system with negligible wall width. As a consequence the gain in magnetostatic energy due to the flux closure is limited by the presence of the wall and the transition to the multi-domain state shifts to larger values of the domain size. Therefore, the assumptions of uniform magnetization and negligible wall width made in section 2.2, cause an overestimation of the gain in magnetostatic energy and a significant underestimation of the value of the domain size. To calculate correctly the size of the unit cell in the case of finite wall width, we have to bound the system periodically. In this way a new Bloch wall forms at the edge of the slab and the unit cell of the multi-domain state is given by the sum of the domain width and of the wall width. This choice, not considered in the derivation of eq. (2.18) [41], yields a further shift of the value of the domain size, as shown in Fig. 2.8. The difference is due to the presence of the Bloch wall at the edge of the slab and to the consequent reduction of the average magnetization around it.

Chapter 3

Films with spatially varying magnetic anisotropies

The magnetic anisotropy can be spatially varied by means of various nano-patterning techniques. The aim of the next two chapters is to describe the magnetic behaviour of these systems by means of micromagnetics. In particular we will answer the following questions: What is the magnetization as a function of the scale of the anisotropy pattern? What is the weight of the different interactions determining the free energy of the system? How does the system behave when an external field is applied?

The investigation of these questions will show that the hypothesis of non-uniform magnetization is essential to describe these films and that the analysis of the magnetic microstructure is necessary to explain the macroscopic properties of the system.

3.1 Uniform magnetization: second and fourth order magnetic anisotropy

Before to study films with spatially varying magnetic anisotropies, we resume the main features of the phenomenological model used in literature to describe systems with uniform magnetization. The purpose of this presentation is to point out the limits of such a description and to show the necessity of a non-uniform approach to study systems with patterned anisotropies.

First principle calculations performed in the monolayer regime show that the breaking of translational symmetry perpendicular to the surface leads to an easy axis that can be either in-plane or out-of-plane [49]. Often in the limit of ultrathin films the observed magnetization is uniform, either out-of-plane or in-plane [22, 121], as theoretically predicted [20, 21, 40].

The angular dependence of the free energy density for a uniformly magnetized film

can be written in the following way:

$$f(t, T, \theta) = k_1^{\text{eff}}(t, T)\sin^2\theta + k_2(t, T)\sin^4\theta \quad (3.1)$$

being θ the angle between the magnetization vector \mathbf{M} and the normal to the surface. The thickness and the temperature dependence of the free energy is contained in the first and second order anisotropy constants:

$$k_1^{\text{eff}}(t, T) = k_{1b}(T) + \frac{2k_{1s}(T)}{t} - 2\pi M_s^2 \quad (3.2)$$

$$k_2(t, T) = k_{2b}(T) + \frac{2k_{2s}(T)}{t} \quad (3.3)$$

where $k_{1b}(T)$, $k_{1s}(T)$ and $k_{2b}(T)$, $k_{2s}(T)$ are the first and second order anisotropy constants in bulk and at the surface of the film. The last term of the equation (3.2) is the shape anisotropy of the system and its value is the result of the assumption of uniform magnetization. The explicit thickness dependence of the phenomenological equations (3.2) and (3.3) is experimentally widely verified [50–52] and theoretically justified [53]. The temperature dependence of the magnetic anisotropy is implicit [54] and complex to treat. Theoretically the problem was originally examined by considering the spin-orbit interaction as a small perturbation of the exchange coupling [55]. Later it has been shown that the entropy contributes to the determination of the easy axis favoring an in-plane magnetization [56]. Experimentally it has been found that the volume anisotropy is a function of the temperature through the dependence of the bulk magnetostriction constants [57, 58].

The minimization of equation (3.1) with respect to θ gives four states with uniform magnetization as a function of different combinations of the first and second order anisotropy constants. The magnetization is, see Fig. 3.1:

- 1) out-of-plane for $k_1 > 0$; $-\frac{1}{2}k_1 < k_2 < \infty$
- 2) canted for $k_1 < 0$; $-\frac{1}{2}k_1 < k_2 < \infty$
- 3) in-plane for $-\infty < k_1 < -2k_2$; $-\infty < k_2 < -\frac{1}{2}k_1$
- 4) coexistence for $k_2 < 0$; $0 < k_1 < -\frac{1}{2}k_2$.

To each point of the diagram of Fig. 3.1 corresponds a minimum that is absolute in the case of regions 1 – 3 and metastable, with two minima, in the case of region 4. In particular region 4 the state of lowest energy results:

- out-of-plane for $-k_2 \leq k_1 \leq -2k_2$,
- in-plane for $0 \leq k_1 \leq -k_2$.

From Fig. 3.1 we notice that in order to describe the states of canting and coexistence it is necessary to introduce a fourth order anisotropy term, while the second order anisotropy is sufficient to describe uniform in-plane or out-of-plane magnetization. The system can move from a state of equilibrium into a new metastable state if the temperature and the thickness of the film are varied. The final state can be in the same region of the phase diagram or in a new one. In this last case the transition takes place either directly between the initial and the final magnetic phase or indirectly with the involvement of

a third magnetic phase. In particular the film can transit from an out-of-plane to an in-plane state of uniform magnetization in three different ways [54, 61]:

- a) continuously through the canted state
- b) discontinuously without involvement of a third state
- c) discontinuously through the coexistence state.

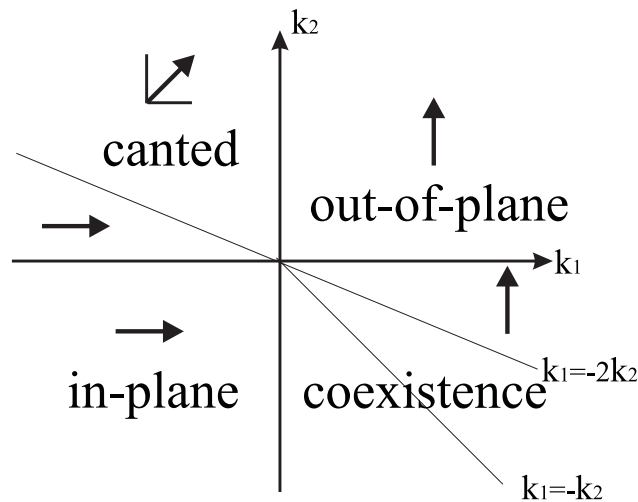


Figure 3.1: Anisotropy space diagram obtained after minimization of equation (3.1). The magnetization is uniform along the lateral extension of the film.

Indications of the transition *a*) have been observed in various systems [58, 61–63]. This transition is often attributed due to the temperature dependence of the bulk magnetostriction constants [57–59, 62, 78]. The transitions *b*) and *c*) have been mentioned respectively by Grolier *et al.* [63] for Au/Co/Au sandwiches and Fritzsche *et al.* [61] for Pd/Co/Pd(111).

The previous analysis refers to films uniformly magnetized. Other systems reorient as a function of the thickness and the temperature by involving domain formation, see for instance [64–67]. Clearly, as soon as domains form the phenomenological approach based on the uniform magnetization fails [68] and the picture of non-uniform magnetization has to be considered. In particular we will see that non-uniform magnetization is necessary to describe systems with a lateral variation of the magnetic anisotropy.

3.2 Morphology and non uniform magnetization

In chapter 2 we have shown that the size of domains of dipolar origin increases beyond the sample dimension in the limit of ultrathin films. Therefore the possibility to have magnetic domains for system with uniform uniaxial anisotropy is limited to a certain range of thickness. In this section we first define and then we study systems with lateral varying magnetic anisotropies which can present magnetic domains induced by the anisotropies and not by the dipolar interaction.

By definition the effect of the surface anisotropy is confined to the top and to the bottom layer while the shape anisotropy energy is proportional to the film thickness. If the surface anisotropy favors an out-of-plane magnetization, with increasing thickness the magnetization reorients in-plane. Some questions arise: Is the exchange stiffness A_{ex} strong enough to keep the magnetization uniform? For which values of the parameters the magnetization is non-uniform so that a twisted configuration can be observed? O’Handley and Woods [69] studying a semi-infinite magnetic system find a critical value of the surface anisotropy above which the magnetization tilts in the out-of-plane direction in the layers close to the surface. This phenomenon, called surface magnetic reconstruction [71], has been observed in the case of Gd(0001) crystals [72]. Thiaville and Fert [23] study a thin film between two interfaces and find that the magnetization is uniform or twisted as a function of the film thickness. In the case of zero applied external field the phase diagram presents in-plane, out-of-plane and twisted configurations. Mainly, in the case of transition metals, the magnetization is either in-plane or out-of-plane. In the case of Fe, the twisted configuration is obtained if the thickness of the film is $11.1 \text{ nm} \leq t \leq 11.3 \text{ nm}$. Since this thickness interval is almost negligible, we can consider the uniform magnetization a good approximation to study transition metal thin films. It has to be noticed that in the case of rare earth metals and especially in alloys, where the value of the exchange stiffness A_{ex} is reduced, the thickness interval of the twisted configuration enlarges so that the assumption of uniform magnetization is no more valid.

Although the vertical modulation of the magnetization is never obtained in thin films of pure transition metals with uniform uniaxial anisotropy, twisted configurations can be obtained if the magnetic anisotropy is locally tuned on a scale of the order of the magnetic characteristic length. This is the case of a magnetic layer capped by a material, either magnetic or non-magnetic, with opposite direction of the effective uniaxial anisotropy [73, 74]. The same phenomenon takes place if the capping is partial and the variation of the anisotropy is lateral [4, 24, 75–78]. In principle, systems with vertical and lateral variation of the magnetization constitute the most general case to be treated. In our investigation we will consider films uniformly magnetized in the vertical direction with laterally varying magnetic anisotropies.

3.2.1 Definition of the system on study: characteristic parameters

In this section we study films with spatially varying uniaxial anisotropies. In the following all the analytical calculations and the main part of the simulations are performed in the case of periodic magnetic configuration. This choice simplifies the theoretical investigation and it is useful to describe systems of stripes obtained by means of patterning techniques.

The unit cell of the system is sketched in Fig. 3.2. It is formed by two infinitely long stripes of width L_1 and L_2 . The easy axis of the effective anisotropies of the two stripes is respectively out-of-plane and in-plane, i.e., $k_1 > 0$ and $k_2 < 0$ or $Q_1 > 1$ and $Q_2 < 1$, see equation (2.1). Periodic boundary conditions are imposed in the x and y directions to model a series of infinitely long stripes with alternating uniaxial anisotropy. As indicated in the last section the thickness of the film is chosen much smaller than the magnetic characteristic length. Thus, with reference to Fig. 3.2, the magnetization is uniform in the z direction.

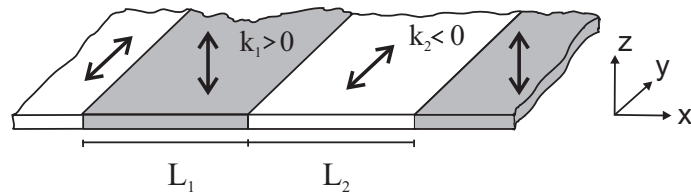


Figure 3.2: *Unit cell of a series of infinitely long stripes with alternating uniaxial anisotropies.*

The nature of the parameters involved can be intrinsic or extrinsic. To the first category belong the material parameters that define the magnetic properties of the film. The extrinsic parameters define the geometry of the anisotropy pattern. The thickness of the film belongs to the second category of parameters. Nevertheless, since we use a uniform approximation to determine the anisotropy in the z direction of the film, the thickness is just a scaling variable of the effective anisotropy and it can be included in the group of intrinsic parameters. The geometry of the pattern can be defined by the relative importance of the two stripes (R) and the density of unit cells (ρ):

$$R = \frac{L_1}{L_1 + L_2} \quad (3.4)$$

and

$$\rho = \frac{2}{L_1 + L_2} \quad (3.5)$$

where the factor 2 refers to the number of stripes in the unit cell. Once the intrinsic parameters are fixed by the choice of the magnetic sub-layer and of the capping material,

only the ratio R and the density of stripes ρ determine the magnetic moment distribution in our study. It has to be noticed that the capping material can be both magnetic or non-magnetic. In the first case the local change in the direction of the easy axis is due to the thickness dependence of the shape anisotropy. In the second case it is due to the variation of the surface energy.

3.2.2 Scale dependence: uniformity, canting and coexistence

In this section we study the general features of systems with laterally varying magnetic anisotropies. The investigation takes place at macroscopic level. In particular we study the system as a function of its scale. Therefore, fixing the ratio R , we obtain different magnetic states as a function of the stripes density ρ . The complete solution of the problem will be given in chapter 4 in the framework of the micromagnetic theory.

We consider a system of stripes with alternating uniaxial anisotropies as shown in Fig. 3.2. This situation is realized for example in the case of Fe films grown on stepped W(110) surfaces [81]. Here stripes of 2ML and 1ML of Fe are alternating. The effective anisotropies are respectively $k_1^{eff} = 1 \cdot 10^7$ erg/cm³ and $k_2^{eff} = -4 \cdot 10^7$ erg/cm³. The negative value shows that in the first layer the anisotropy favors an in-plane magnetization, while in the second it favors an out-of-plane orientation. Experiments on this system have been performed for a value of the unit cell of 8 nm [17, 82]. In the following we investigate the magnetization as a function of the width of the unit cell.

The analysis starts by considering a unit cell of width $L = 8$ nm and $L_1 = L_2 = 4$ nm, i.e., $\rho = 0.25$ nm⁻¹ and $R = 0.5$. In this case the unit cell is comparable with the magnetic characteristic length, i.e., $L \approx \lambda$. To study the system we calculate the magnetization as a function of an external field applied perpendicularly to the film. The result of the simulation is plotted in Fig. 3.3. The axis of the abscisse is normalized to the anisotropy field necessary to reverse the magnetization of 1ML and it is given by $H_{an} = 2k_1^{eff}/\mu_0 M_s = 50$ kOe. As a starting condition we choose a uniform magnetization perpendicular to the film surface. As soon as the external field reduces, the magnetization decreases. The reduction of the average magnetization is continuous until the coercive field is reached. Notice that both the remanence M_r and the coercive field H_c are different from zero. This result can be interpreted in the framework of the theory of Stoner and Wohlfarth for single particles [84]. These authors studied the field dependence of the direction of the magnetization of a uniformly magnetized ellipsoid. The shape of the hysteresis loops is a function of the angle α between the applied field and the easy axis. The remanence and the coercivity decrease with increasing α . The shape of the hysteresis loop in Fig. 3.3 indicates a behavior similar to the one of a single particle with $\alpha \simeq 75^\circ$. Therefore in systems with a unit cell comparable with the magnetic characteristic length the indicative behavior of the magnetization is uniform. This means that successive stripes with alternating uniaxial anisotropy are strongly coupled by exchange and they behave like a single particle.

In this analysis we have considered the averaged magnetization \mathbf{M} , as it could be obtained experimentally by means of MOKE [83], as we will see in chapter 5. In order

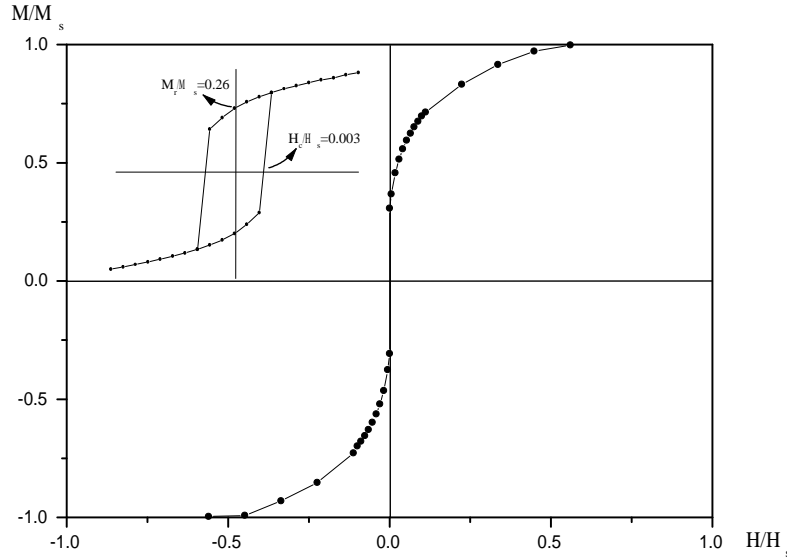


Figure 3.3: *Hysteresis polar loop for a film with patterned anisotropy with scale comparable with the magnetic characteristic length, i.e., $L \approx \lambda$. Since $k_2^{eff} > k_1^{eff}$, the average magnetization \mathbf{M} decreases together with applied external field until the remanence M_r is reached. The stripes are exchange coupled by the reduced dimension. The inset is a magnified view of the same loop and shows that a small coercive field drives the film out from the canted state obtained at remanence.*

to have more information about the system it is necessary to calculate the magnetization as a function of the position by means of micromagnetics. In the next section we will see that micromagnetics is the key to explain the canting shown in Fig. 3.3.

Now we increase the width of the unit cell to 50 nm keeping the value of the coverage of the system constant. In this way the density of stripes reduce to $\rho = 0.04 \text{ nm}^{-1}$ and the scale of the anisotropy patterning is bigger than the magnetic characteristic length, i.e., $L \gg \lambda$. Like in the former case, we study the main features of the system calculating the magnetization as a function of an applied external field. The resulting hysteresis loop is plotted in Fig. 3.4. The saturation is obtained by applying a field of around 50 kOe perpendicular to the film surface. This is the same value necessary to reverse a film with in-plane easy axis of 1ML. As soon as the field reduces, the magnetization decreases until the value $M_r = 0.67$ is reached at zero applied external field. This value can be explained if we assume that the magnetization in the regions with thickness of 1ML rotates in-plane. Therefore only two third of the unit cell remains out-of-plane magnetized and we expect to have a state that consists of in-plane and out-of-plane magnetic domains.

Summarizing, we have seen that the hysteresis loops of films with spatially varying magnetic anisotropies depends on the scale of the system. The analysis provides a macro-

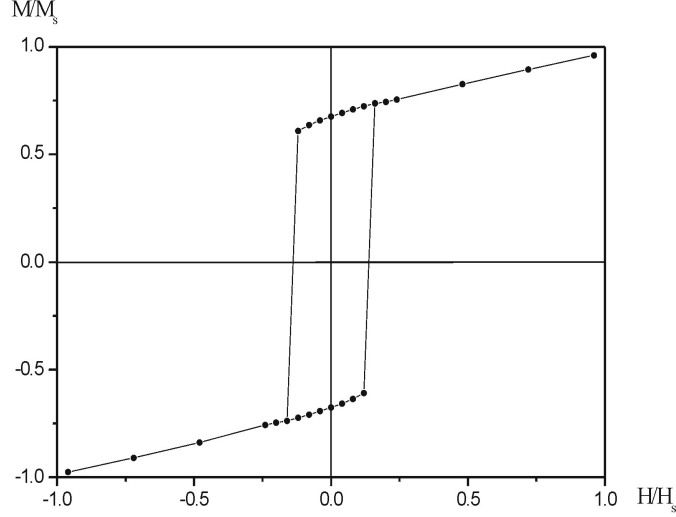


Figure 3.4: *Hysteresis loop referring to a unit cell of 50 nm. The value at remanence, $M_r = 0.67$, indicates that the system consists of magnetic domains.*

scopic tool to investigate the system but it does not clarify completely the nature of the canting found for $L \approx \lambda$ and the existence of magnetic domains for $L \gg \lambda$.

From the point of view of the applications it is interesting to notice that the change of scale causes a decreasing of the coercive field of two orders of magnitude.

3.2.3 Uniform and non-uniform magnetization for $L \approx \lambda$

In the last section we have seen that a system with spatially varying magnetic anisotropies can present a state of canting. The nature of this state could not be clarified at macroscopic level. In this section we show that the analysis of the magnetic microstructure explains the canting for a scale of the anisotropy patterning of the order of the magnetic characteristic length, i.e., $L \approx \lambda$. In the following we introduce a simple model based on the assumption of uniform magnetization valid for partially covered thin films. We show that this assumption is correct until one of the two effective anisotropies of the film dominates, while it fails when they are balanced. In this case a state of non-uniform magnetization appears that can be described by means of a fourth order anisotropy term whose strength is a function of the scale of the pattern.

With reference to Fig. 3.2, let us consider a unit cell of width L composed of two stripes L_1 and L_2 , in general of different width, having effective anisotropy k_1^{eff} and k_2^{eff} , respectively. The scale of the unit cell is supposed to be small so that the magnetization can be considered uniform. In this case the exchange energy is zero and the free energy

is given by the sum of magnetostatic and anisotropy energy. Since in general $k_1 \neq k_2$ we have to weight the two quantities with the respective stripe width in order to obtain the anisotropy energy. Thus the free energy results:

$$f(\theta) = (k_1 R + k_2(1 - R)) \cdot \sin^2\theta + k_{sh} \cdot \cos^2\theta \quad (3.6)$$

with $k_{sh} = 2\pi M_s^2$ and $R = L_1/L$. Equation (3.6) shows that both k_1 and k_2 favors an out-of-plane magnetization contrary to the shape anisotropy. Besides, the absence of modulation permits to describe the system in the framework of an anisotropy type description. Equation (3.6) can be written in the following compact form:

$$f(\theta) = k_{sh} + k_{tot}\sin^2\theta \quad (3.7)$$

being

$$k_{tot} = k_1^{eff} R + k_2^{eff}(1 - R) = A + B \quad (3.8)$$

Fixing the intrinsic parameters, the free energy is a function of the ratio R , while it does not depend on the scale of the system since the magnetization is assumed to be uniform. Equation (3.7) shows that the strength and the direction of the easy axis is a function of the effective anisotropy weighted by the stripe width. In particular the magnetization points in-plane and out-of-plane for $k_{tot} < 0$ and $k_{tot} > 0$ respectively.

A first check of the model can be done by comparing the analytical expression (3.7) with the energy calculated numerically [37]. Let us consider a film of about 3 ML of Co grown on Pd(111) partially covered by islands of Pd. The crystalline anisotropy constants of the covered and uncovered regions are $k_{Pd} = 1.96 * 10^7 \text{erg/cm}^3$ and $k_{Co} = 0.86 * 10^7 \text{erg/cm}^3$ [85, 86]. The value of the magnetization at saturation for bulk systems is $M_s = 1440 \text{emu/cm}^3$ and thus the shape anisotropy is equal to $k_{sh} = 1.3 * 10^7 \text{erg/cm}^3$. As a consequence $k_{Pd}^{eff} = 0.66 * 10^7 \text{erg/cm}^3$ and $k_{Co}^{eff} = -0.44 * 10^7 \text{erg/cm}^3$ favor respectively an out-of-plane and an in-plane magnetization. The total energy of the system as a function of the coverage and angle to the normal is plotted in Fig. 3.5 in the case of unit cell $L = 5 \text{ nm}$. For $0 \text{ nm} \leq L_{Pd} < 2 \text{ nm}$ the Co component is dominant and the system has an in-plane uniaxial anisotropy. For $2 \text{ nm} \leq L_{Pd} < 5 \text{ nm}$ the coverage of Pd is sufficient to change the easy axis of the film in the out-of-plane direction. Thus we see that with coverage increasing the easy axis reorients from in-plane to out-of-plane. The transition takes place for $L_{Pd} = 2 \text{ nm}$ when no angular variation is detected and the magnet behaves like a soft magnet. In Fig. 3.5 the values calculated analytically and numerically are plotted respectively with symbols and lines. The good agreement shows that the idea to describe the system by means of weighted effective anisotropies in the limit of a film with uniform magnetization is correct.

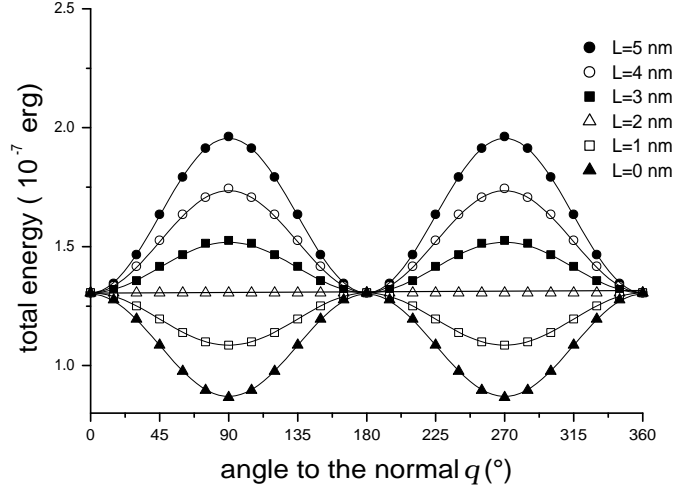


Figure 3.5: Total energy as a function of the angle to the normal. The hypothesis of uniform magnetization is used to calculate both the numerical and the analytical values, respectively plotted as points and lines. With coverage increasing the easy axis change from in-plane to out-of-plane. The transition takes place when the effective anisotropies balance, *i. e.* $k_{Pd}L_{Pd} = k_{Co}L_{Co}$.

Still two questions need an answer: Is the assumption of uniform magnetization correct? Is it possible to obtain an ideally soft magnet? In order to answer these questions we study the magnetization process as a function of the ratio R .

Let us consider a field applied in the direction perpendicular to the sample surface. The starting magnetization is uniform out-of-plane. The analysis of the loops plotted in Fig. 3.6 confirm that the direction of the easy axis reorients from in-plane to out-of-plane with increasing coverage, as modeled by means of equation (3.7). Besides, the shape of the loops proves that the magnetization is uniform for the coverage and for the scale of the unit cell considered. Therefore we may conclude that in a film with spatially varying magnetic anisotropies with a scale of the unit cell of the order of the magnetic characteristic length, *i. e.*, $L \approx \lambda$, the magnetization is uniform if one of the two weighted effective anisotropies dominates.

It is interesting to note that the field necessary to reverse the magnetization is a function of the coverage. This field, called anisotropy field in system uniformly magnetized with uniaxial anisotropy that rotates coherently, defines the hardness of the magnet and it can be extracted directly from the plots in Fig. 3.6. In fact, in the case of easy axis loop the anisotropy field corresponds to the coercive field, while in the case of hard axis loop it is given by the field necessary to saturate the film. The anisotropy field and the uniaxial anisotropy are proportional and related by:

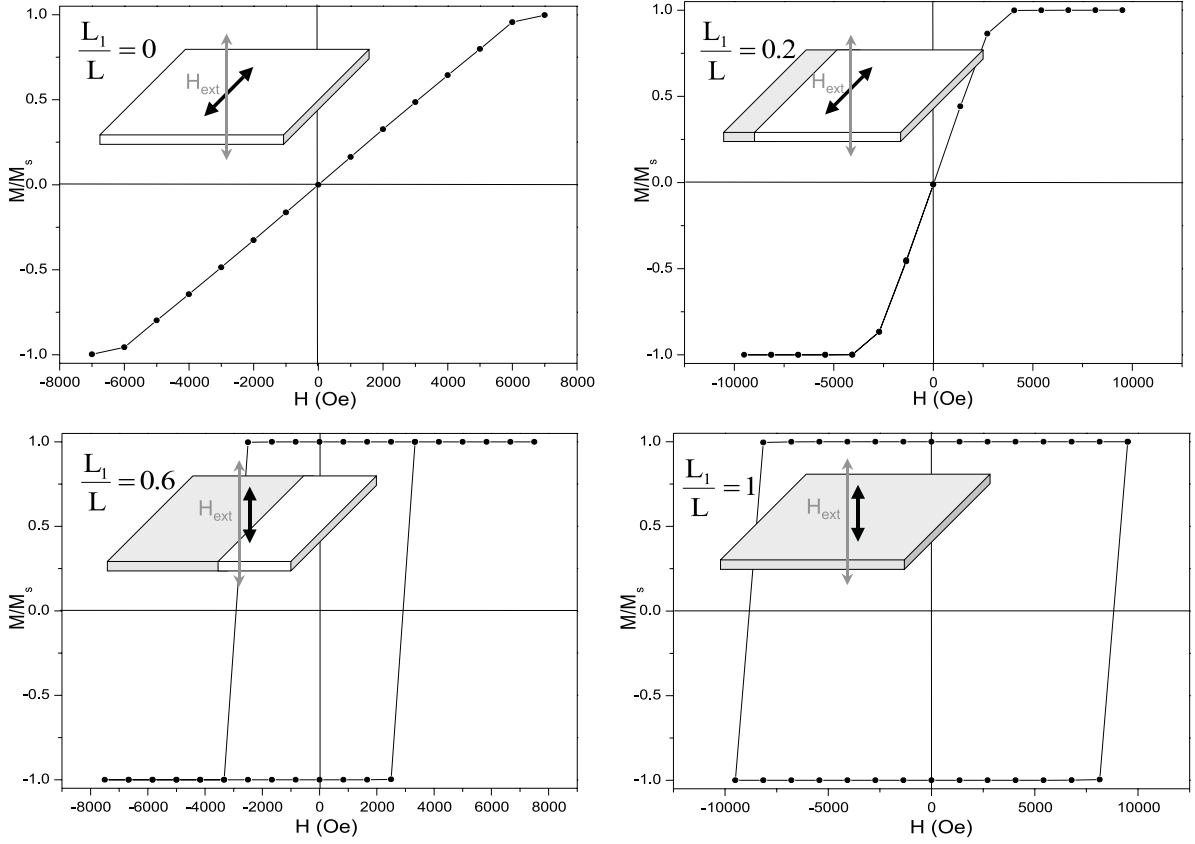


Figure 3.6: Magnetization vs. external field applied perpendicularly to the sample. The easy axis reorients from parallel to normal with coverage increasing, as indicated by the black arrow. The shape of the loops shows that in the cases considered the film is uniformly magnetized.

$$H_{an} = \frac{2k_{tot}}{\mu_0 M_s} \quad (3.9)$$

Knowing the anisotropy field, from equation (3.9) we can calculate k_{tot} as a function of the ratio R . The values obtained in this way are compared to equation (3.8) in Fig. 3.7. The perfect agreement is a further proof that the model used is valid for $k_{tot} \neq 0$, in the limit of $L \approx \lambda$ assuming coherent rotation.

The analysis of the magnetization as a function of the external applied field can be extended to the regime in which the weighted anisotropies balance. What happens at compensation? Can we expect an ideally soft magnet?

In Fig. 3.8 the hysteresis loop obtained for $k_{tot} = 0$ is plotted. In particular we report the projection of the magnetization in the direction of the external field, applied at 45° with respect to the normal. Since at remanence the magnetization is saturated, we deduce

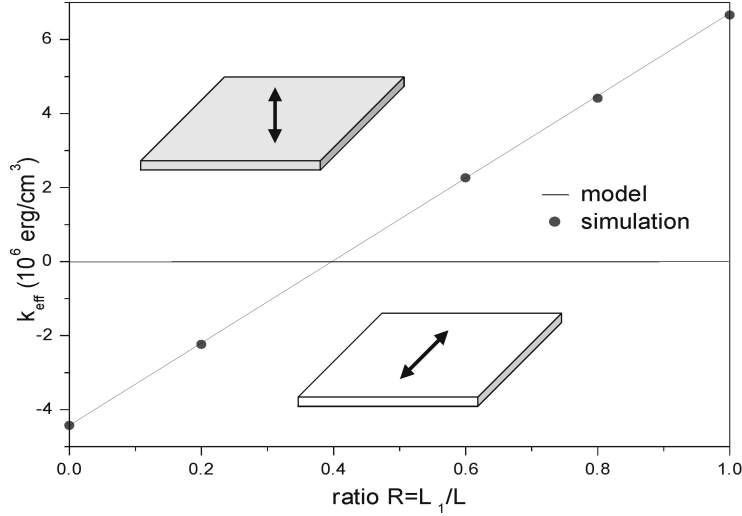


Figure 3.7: Hardness of the magnet, represented by k_{tot} , vs. the ratio R . The line is calculated using equation (3.8). The points from Fig. 3.6 and equation (3.9). The accordance shows that the idea to describe the system by means of weighted effective anisotropies in the limit of small scale of the system, i.e., $L \approx \lambda$, is correct.

that the system has an easy axis at 45° with respect to the normal. Moreover the system is not completely soft, as clear from the non-zero coercive field. It has to be noticed that the rotation of the magnetization is not abrupt but it involves a third state, as indicated by the point at almost zero magnetization. This behaviour reflects the existence of a four-fold anisotropy that appears as soon as the uniaxial anisotropies average out.

As explained in section 3.2.2, the analysis of the hysteresis loops give a macroscopic picture of the magnetic properties of the system. In order to describe the canted state of Fig. 3.8 we could insert an higher order anisotropy term in equation (3.8). In this way we would describe the system in the framework of the phenomenological model that assume the uniform magnetization of the film, as seen in section 3.1. Such a description would be arbitrary since it is not based on a physical interpretation of the four-fold anisotropy.

In order to find an explanation for the canting reported in Fig. 3.8 we have to analyze the magnetic microstructure at compensation, i.e., for $k_{\text{tot}} = 0$. In Fig. 3.9 we plot the projection to the normal of the magnetization as function of the position. The simulation is performed for a sample with a unit cell of 5 nm in absence of external field. From the figure it is evident that the magnetization is not uniform, but oscillates around 45° . The reason is that none of the two weighted anisotropies dominates and thus the magnetization tends to follow the constriction of the alternating anisotropies. The angular gap $\Delta\vartheta$ increases with the size of the unit cell, since the exchange is a short range interaction. The profile plotted in Fig. 3.9 is asymmetric. This reflects the different values of the effective anisotropies in two successive stripes. In particular we notice that the deviation from the average is larger in the region with in-plane anisotropy than in the region with out-of-plane anisotropy, since the stripe is wider.

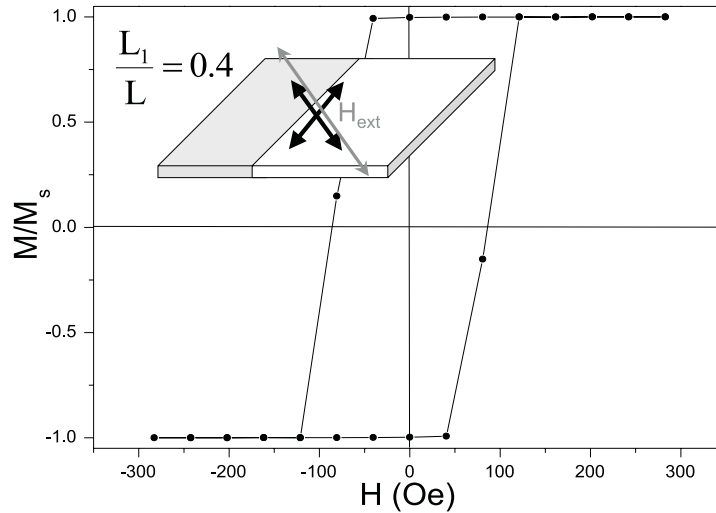


Figure 3.8: *Hysteresis loop at compensation, i.e., for $k_{tot} = 0$. The external field is applied at 45° to the normal. The shape of the loop indicate a four-fold anisotropy whose nature is not of crystalline origin.*

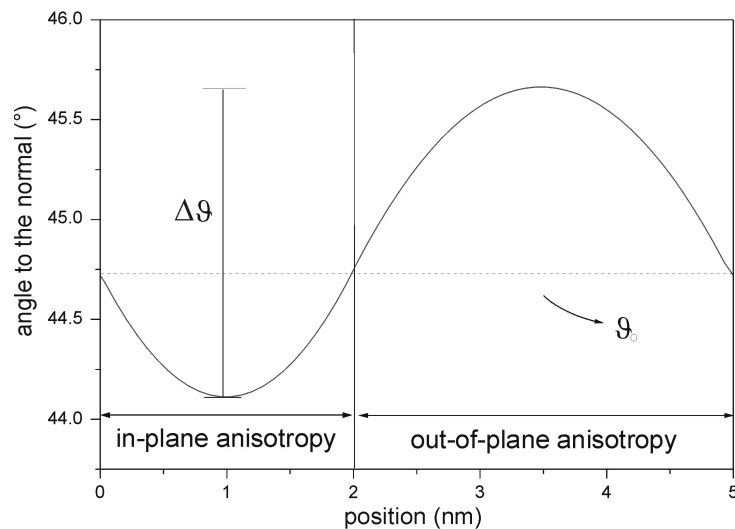


Figure 3.9: *Magnetization profile versus the position inside a unit cell of 5 nm. The oscillation shows up in the limit of $k_{tot} \approx 0$, when the assumption of uniform magnetization breaks down. The angle ϑ_0 at the border of two successive stripes slightly differs from the minimum at 45° because the weighted anisotropies do not compensate perfectly.*

According to Fig. 3.5, for $k_{tot} = 0$ no angular dependence of the total energy is expected in the limit of uniform magnetization. Does it hold for the case of non-uniform magnetization? The answer is given in Fig. 3.10 where the total energy is plotted versus

the average angle to the normal.

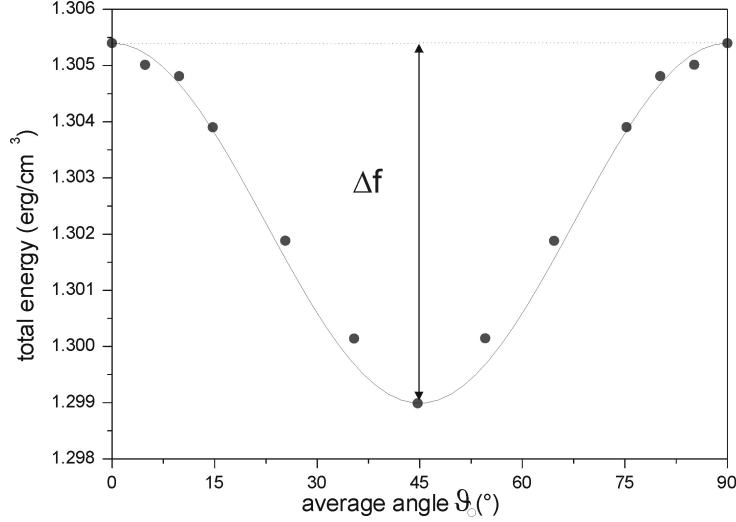


Figure 3.10: *Angular dependence of the total energy for films non-uniformly magnetized. The curve has a minimum at 45° that is the image of the four-fold anisotropy shown in Fig. 3.8. The depth of the minimum is function of the width of the unit cell.*

The total energy is a function of the angle θ_0 , i.e., the angle to the normal of the magnetization obtained at the border of two successive stripes. The minimum is at 45° with respect to the normal. Therefore, a fourth order magnetic anisotropy due to the microstructure shows up at compensation of the two weighted effective anisotropies. The angular gap $\Delta\vartheta$ versus θ_0 is plotted in Fig. 3.11. The plot shows that the split between neighbor magnetic moments is maximum at 45° with respect to the normal. Note that the minimum of the total energy and the maximum of the angular gap $\Delta\vartheta$ are at 45° .

In order to explain this finding we extend the model represented by equation (3.7) to systems with non-uniform magnetization in the limit of $\lambda \approx L$. In this case $\Delta\vartheta \ll \vartheta_0$ and the magnetization can be assumed constant inside each stripe. Therefore we can describe the system by means of two split magnetic moments, see Fig. 3.12. In general the deviation in the two stripes is not the same because the effective anisotropies are not equal. In the stripe with out-of-plane anisotropy the magnetization rotates in the direction to the normal of the quantity $\frac{\Delta\vartheta_1}{2}$. In the stripe with in-plane anisotropy it rotates in the opposite direction of the angle $\frac{\Delta\vartheta_2}{2}$. The splitting decreases the anisotropy energy and increases the exchange energy.

As a consequence equation (3.7) becomes:

$$f(\theta) = k_{sh} + A\sin^2\left(\theta_0 - \frac{\Delta\vartheta_1}{2}\right) + B\sin^2\left(\theta_0 + \frac{\Delta\vartheta_2}{2}\right) \quad (3.10)$$

In the limit of small deviations, i.e., $\Delta\vartheta_1, \Delta\vartheta_2 \approx 0$, equation (3.10) is:

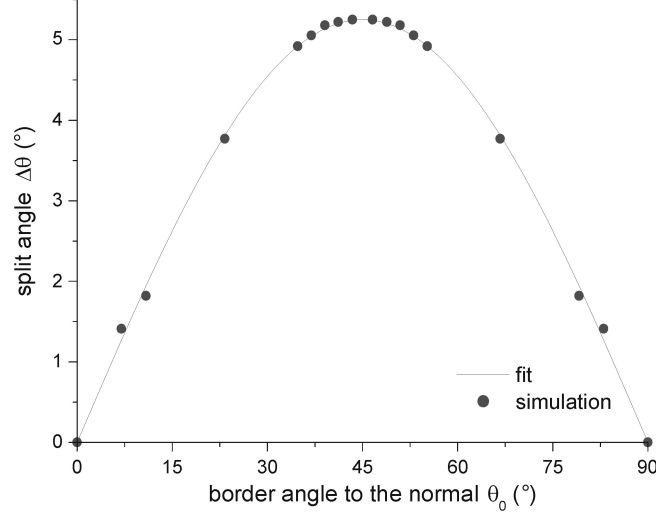


Figure 3.11: *Split angle $\Delta\vartheta$ as a function of the angle ϑ_0 at the border of two successive stripes. The plot refers to a unit cell of 10 nm. The gain in anisotropy energy, that is maximum at 45° , allows the splitting with consequent increasing of the exchange energy.*

$$f(\theta) \approx k_{sh} + (A + B)\sin^2\theta_0 + \frac{B - A}{2}\Delta\vartheta\sin(2\vartheta_0) \quad (3.11)$$

with $\Delta\vartheta = \frac{\Delta\vartheta_1}{2} + \frac{\Delta\vartheta_2}{2}$. The second order anisotropy vanishes for $A=-B$, i.e., when the weighted effective anisotropies balance. In this case equation (3.11) reduces to:

$$f(\theta) \approx k_{sh} - A\Delta\vartheta\sin(2\vartheta_0) \quad (3.12)$$

This higher order anisotropy term has a minimum at 45° with respect to the normal and it describes the four-fold anisotropy obtained in the simulation plotted in Fig. 3.10. The angle $\Delta\vartheta$, that determines the depth of the minimum in Fig. 3.10, increases with the width of the unit cell and it is a function of the exchange stiffness constant¹.

The model based on two magnetic moments is useful to explain the minimum of the total energy obtained for $\vartheta_0 = 45^\circ$ with respect to the normal. In fact, considering two magnetic moments, the exchange energy is a function of the split angle $\Delta\vartheta$ and not of their orientation in the space. On the contrary the anisotropy energy is a function of ϑ_0 and therefore it determines the angular dependence of the total energy. In particular the gain in anisotropy energy due to the splitting is maximum for $\vartheta_0 = 45^\circ$, as follows from the slope of the sine in equation (3.10). As a consequence the minimum of the total energy is obtained for $\vartheta_0 = 45^\circ$. In the description presented above the dipolar interaction

¹A similar result can be obtained by following the fluctuation mechanism for biquadratic exchange coupling in magnetic sandwiches studied by Slonczewski [24, 79, 80].

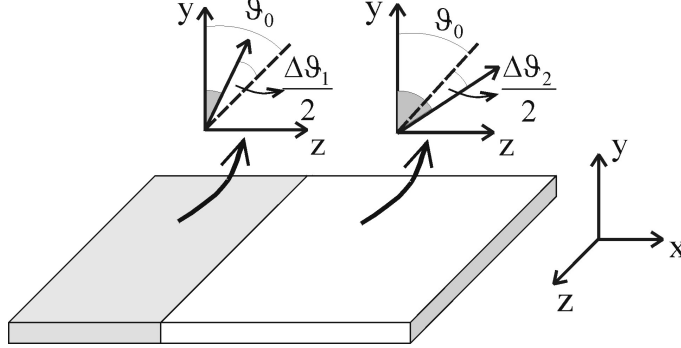


Figure 3.12: *Thin film with anisotropy alternatively in-plane (white stripe) and out-of-plane (dark stripe). The magnetization is assumed to be constant inside each stripe. The system is described by means of two magnetic moments that split by the angle $\Delta\vartheta$.*

is included in the anisotropy energy. The correction due to the non-uniformity of the magnetization, as introduced in section 2.3.1, are neglected. This assumption is the more justified the smaller the modulation of the magnetization around ϑ_0 .

Summarizing, in this section we have studied the system with alternating anisotropies in the limit of unit cell of the order of the magnetic characteristic length, i. e. $L \approx \lambda$. We have shown that the system can be modeled in the framework of the anisotropy-type description. In particular if one of the two weighted effective anisotropies dominates the system is described by means of a second order anisotropy in the limit of a film uniformly magnetized. In the limit of balanced weighted anisotropies the microscopic analysis shows a non-uniform magnetization that is the origin of the canted state. As a consequence the system is described by means of a fourth order anisotropy due to the magnetic microstructure.

Chapter 4

1-D model for systems with modulated anisotropies

In this chapter we solve the micromagnetic problem associated with systems with spatially varying magnetic anisotropies. The problem has already been addressed in chapter 3 in the case of small width of the unit cell L in comparison with the magnetic characteristic length λ , i.e., $L \ll \lambda$. Here the treatment is generalized to all scales of the system. In particular, in the first part of the chapter we solve analytically the equation of Brown [14] for the geometry considered. Therefore, in the framework of the anisotropy-type description, we calculate the magnetic profile and the energies of the configuration. The comparison of this solution with a magnetic profile obtained experimentally by means of SEMPA [11, 97], MFM [10] or spin-polarized STM [12, 13, 98], gives a tool to find out the anisotropy constants of the system. Moreover, once the total energy is known as a function of L we have the necessary information to study the stability of the system when an external field is applied.

In the second part of the chapter we compare the analytical solution obtained in the framework of the anisotropy-type description with the numerical one that fully includes the dipolar interaction. We study when this higher order description becomes important as a function of the scale of the system, the effective anisotropy and the thickness of the film.

4.1 Analytical solution

Often the solution of the micromagnetic equation of the free energy can be obtained only numerically. This is mainly due to the difficulty to calculate the magnetostatic energy. An exact analytical solution is possible just in a few cases. One of these is an infinitely thin film with arbitrary magnetic moments distribution, if the divergence of the magnetization vector \mathbf{M} is equal to zero. In this case the magnetostatic energy becomes part of the anisotropy energy, as described in chapter 2, and the minimization of the

total free energy by means of the variational method, i.e., the solution of the equation of Brown [14], leads to the magnetization distribution.

The anisotropy-type description is used in many geometries to calculate the total energy of the system. The form of the micromagnetic equation is identical, but specific boundary conditions lead to different solutions. Some authors calculated the magnetization direction as function of the vertical depth for thin films of a single material [23, 69, 99]. The problem for a triple-layer sandwich composed by a soft magnet of finite thickness between two hard magnets of infinite thickness was solved by Leineweber and Kronmüller [100]. A system of two films with different thickness, composition and anisotropy easy axis was studied by Xiao Hu and Kawazoe [73]. The problem for thin films with spatially varying magnetic anisotropies was addressed by Elmers [75]. The author calculated the critical values of uniform and non-uniform magnetization using the Jacobi criterion, but do not give the analytical solution to calculate profiles and energies of the system. In our work we give the complete solution of the problem focusing in particular on the scale dependence of the magnetic profiles and the energies.

4.1.1 Magnetic profiles

The geometry of our problem is recalled in Fig. 4.1. The unit cell is constituted by two stripes of length L_1 and L_2 , in general not equal. The effective anisotropy is respectively out-of-plane and in-plane. Periodical boundary conditions are imposed to model the infinite alternation of anisotropies. Since the geometry repeats along the x direction, the magnetization must be symmetric with respect to the center of each stripe.

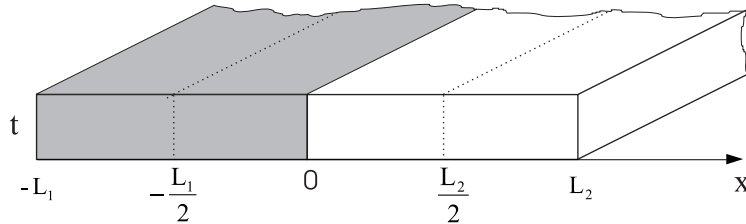


Figure 4.1: *Unit cell for system with alternated uniaxial anisotropies. The effective anisotropy is out-of-plane in the stripe of width L_1 and in-plane in the stripe of width L_2 .*

Moreover, the magnetization rotates parallel to the stripe extension to avoid any divergence of the magnetization vector \mathbf{M} . In this way only the surface magnetic charges contribute to the magnetostatic energy. The slab is sufficiently thin so that \mathbf{M} is uniform in the vertical direction. Therefore the geometry is one dimensional and the magnetization varies only along x , i.e., $\mathbf{M}=\mathbf{M}(x)$.

The free energy per unit area of the unit cell is given by [75, 100]:

$$G(L_1, L_2) = \int_{-L_1}^0 f_1(x) dx + \int_0^{L_2} f_2(x) dx \quad (4.1)$$

where the energy densities f_1 and f_2 are given by:

$$f_1(x) = A_{1,ex} \left(\frac{d\theta}{dx} \right)^2 + k_{sh} + k_1^{eff} \sin^2 \theta \quad -L_1 \leq x \leq 0 \quad (4.2)$$

$$f_2(x) = A_{2,ex} \left(\frac{d\theta}{dx} \right)^2 + k_{sh} + k_2^{eff} \sin^2 \theta \quad 0 \leq x \leq L_2 \quad (4.3)$$

The first term of equations (4.2) and (4.3) is the exchange energy density, being $A_{1,ex}$ and $A_{2,ex}$ the exchange stiffness constants. The remaining part is the sum of the magnetostatic energy and of the anisotropy energy with $k_{sh} = 2\pi M_s^2$, $k_1^{eff} = k_1 - k_{sh} > 0$, that favors an out-of-plane magnetization and $k_2^{eff} = k_2 - k_{sh} < 0$ that favors an in-plane magnetization. Minimizing equation (4.1) we obtain the position dependence of θ_x . By applying the variational method [101], see Appendix A, we obtain:

$$\left(\frac{d\theta}{dx} \right)^2 = \frac{\sin^2 \theta}{\lambda_1^2} + c_1 \quad -L_1 \leq x \leq 0 \quad (4.4)$$

$$\left(\frac{d\theta}{dx} \right)^2 = -\frac{\sin^2 \theta}{\lambda_2^2} + c_2 \quad 0 \leq x \leq L_2 \quad (4.5)$$

with $\lambda_1 = \sqrt{\frac{A_{1,ex}}{k_1^{eff}}}$ and $\lambda_2 = \sqrt{-\frac{A_{2,ex}}{k_2^{eff}}}$ positive quantities, c_1 and c_2 constants to be determined. Since the structure is periodical along the x direction, the derivative of θ at the center of the stripes must be zero, i.e., $\lim_{x \rightarrow -\frac{L_1}{2}} \frac{d\theta}{dx} = 0$ and $\lim_{x \rightarrow \frac{L_2}{2}} \frac{d\theta}{dx} = 0$. By using these conditions we find the constants c_1 and c_2 . In this way equations (4.4) and (4.5) become:

$$\left(\frac{d\theta}{dx} \right)^2 = \frac{\sin^2 \theta - \sin^2 \theta_{-\frac{L_1}{2}}}{\lambda_1^2} \quad -L_1 \leq x \leq 0 \quad (4.6)$$

$$\left(\frac{d\theta}{dx} \right)^2 = \frac{\sin^2 \theta_{\frac{L_2}{2}} - \sin^2 \theta}{\lambda_2^2} \quad 0 \leq x \leq L_2 \quad (4.7)$$

Taking the square root and integrating along the x direction, equation (4.7) results:

$$\int_{\theta_0}^{\theta_x} \frac{d\theta}{\sqrt{1 - m \sin^2 \theta}} = \frac{x}{\lambda_2 \sqrt{m}} \quad (4.8)$$

where θ_0 , the angle to the normal of the magnetization at the border between two stripes, is an unknown parameter and $m = (\sin^2 \theta_{\frac{L_2}{2}})^{-1}$. Since equation (4.8) is the difference

between elliptical integrals of the first kind, see Appendix and citations [102, 103], we obtain:

$$F(\theta_x|m) - F(\theta_0|m) = \frac{x}{\lambda_2\sqrt{m}} \quad (4.9)$$

By means of the properties of the elliptical integrals, see Appendix, equation (4.9) transforms in:

$$F(\operatorname{asin}\left(\frac{\sin\theta_x}{\sin\theta_{\frac{L_2}{2}}}\right)|\sin^2\theta_{\frac{L_2}{2}}) - F(\operatorname{asin}\left(\frac{\sin\theta_0}{\sin\theta_{\frac{L_2}{2}}}\right)|\sin^2\theta_{\frac{L_2}{2}}) = \frac{x}{\lambda_2} \quad (4.10)$$

Equation (4.10) is valid for $0 \leq x \leq L_2$ and is symmetric with respect to the center of the stripe, i. e. $x = \frac{L_2}{2}$. In the same way from equation (4.6) we obtain, see Appendix:

$$F(\operatorname{asin}\left(\frac{\cos\theta_x}{\cos\theta_{-\frac{L_1}{2}}}\right)|\cos^2\theta_{-\frac{L_1}{2}}) - F(\operatorname{asin}\left(\frac{\cos\theta_0}{\cos\theta_{-\frac{L_1}{2}}}\right)|\cos^2\theta_{-\frac{L_1}{2}}) = -\frac{x}{\lambda_1} \quad (4.11)$$

valid for $-L_1 \leq x \leq 0$. To extract θ_x from equations (4.10) and (4.11) we use the following condition of continuity of the derivatives, known as Weierstrass-Erdmann law [73]:

$$A_{1,ex}\left(\frac{d\theta}{dx}\right)_{x=-0} = A_{2,ex}\left(\frac{d\theta}{dx}\right)_{x=+0} \quad (4.12)$$

By inserting equations (4.6) and (4.7) in equation (4.12), after some calculations we obtain:

$$\cos^2\theta_{-\frac{L_1}{2}} = \cos^2\theta_0(1 + \xi) - \xi\cos^2\theta_{\frac{L_2}{2}} \quad (4.13)$$

with $\xi = \left(\frac{k_2^{eff}}{k_1^{eff}}\right)^2$. Equations (4.11), (4.10) and (4.13) constitute the system of equations from which θ_x can be extracted.

To obtain θ_0 we can proceed as follow. By inserting $x = \frac{L_2}{2}$ and $x = -\frac{L_1}{2}$ in equations (4.10) and (4.11) we obtain:

$$\theta_{\frac{L_2}{2}} = \theta_{\frac{L_2}{2}}(\theta_0) \quad (4.14)$$

$$\theta_{-\frac{L_1}{2}} = \theta_{-\frac{L_1}{2}}(\theta_0) \quad (4.15)$$

The successive substitution of the relations (4.14) and (4.15) in equation (4.13) gives θ_0 . Knowing θ_0 it is easy to calculate $\theta_{\frac{L_2}{2}}$ and $\theta_{-\frac{L_1}{2}}$ from (4.14) and (4.15) and finally θ_x from equations (4.10) and (4.11) respectively for $0 \leq x \leq L_2$ and $-L_1 \leq x \leq 0$.

Now we analyze the main features of the magnetic profiles with an example. We consider a system whose unit cell has width L . The easy axis of the effective anisotropy is out-of-plane and in-plane in the stripes of length L_1 and L_2 respectively. The ratio between L_1 and L is $R = 0.4$. The values of the effective anisotropy and of the exchange

stiffness constant are the same in both the stripes, i.e., $k_1^{eff} = k_2^{eff} = 1 \cdot 10^7 \frac{\text{erg}}{\text{cm}^3}$ and $A_1 = A_2 = 1 \cdot 10^{-6} \frac{\text{erg}}{\text{cm}}$. In Fig. 4.2 θ_x is plotted for a value of the width of the unit cell $L = 15$ nm. Note that since $L_1 \neq L_2$ the angular dependence of the magnetization is asymmetric with respect to the center of the unit cell. Therefore the weighted effective anisotropies are not balanced and we expect an angle $\theta_0 \neq 45^\circ$ at the border between two successive stripes. In particular in the example $\theta_0 > 45^\circ$ because $L_2 > L_1$.

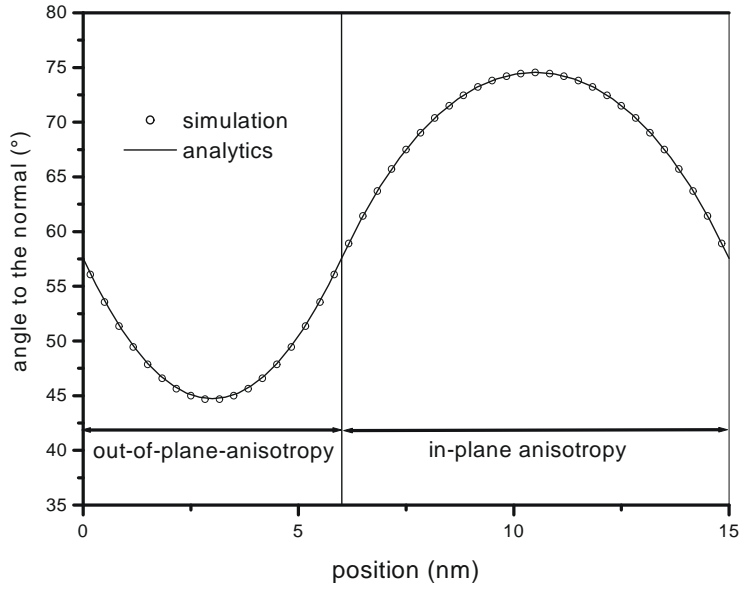


Figure 4.2: Angle to the normal θ_x for a system with $\lambda_1 = \lambda_2$. Since $L_2 > L_1$, $\theta_0 > 45^\circ$ and the magnetic profile is asymmetric with respect to center of the unit cell. The accordance between simulation and analytics shows that equations (4.10) and (4.11) are correct in the limit of anisotropy-type description.

Note that in the experiments we should find mostly asymmetric profiles, because in general the weighted anisotropies do not balance. In order to test the analytically calculated profile we performed a numerical simulation [37] assuming the anisotropy-type description, i.e., the magnetostatic energy has the same form of the anisotropy. Technically this condition is obtained by considering the saturation magnetization $M_s = 0$ and assuming the anisotropy to be a constant equal to the effective anisotropy. Fig. 4.2 shows a perfect agreement between the two calculated magnetic profiles.

Figure 4.2 refers to a specific value of the unit cell: $L = 15$ nm. To prove the general validity of the analytical solution we have calculated the magnetic profile by varying the width of the unit cell and keeping the value of $R = 0.4$. In particular we have determined

the angles to the normal at the center of the two stripes, i. e. $\theta_{\frac{L_1}{2}}$ and $\theta_{\frac{L_2}{2}}$, and at the border between them, i.e., θ_0 as a function of the width of the unit cell. The result of this calculation is shown in Fig. 4.3 where the values obtained numerically and analytically are compared showing an excellent agreement.

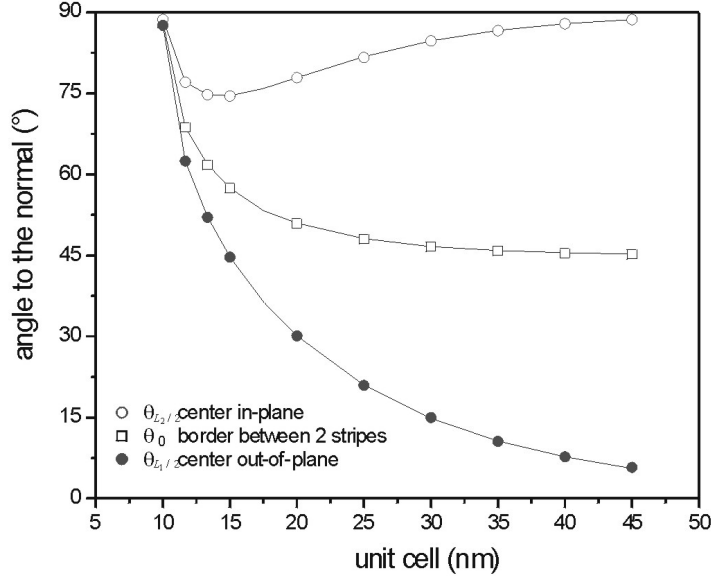


Figure 4.3: Angle to the normal vs. width of the unit cell. The dots and the lines are respectively the numerical and the analytical values. $\theta_{\frac{-L_1}{2}}$ and $\theta_{\frac{L_2}{2}}$ are the angles to the normal at the center of the stripes of width L_1 and L_2 ; θ_0 is located at the center of the unit cell. The ratio $R = 0.4$ is the same for all the values of the unit cell. Since $L_2 > L_1$, the in-plane component dominates for $L < 10$ nm and the film results uniformly magnetized.

For $L = 45$ nm the unit cell is sufficiently wide to permit the magnetization to follow the constriction of the anisotropy. As a consequence at the center of the stripes the magnetization is parallel to the axis of the uniaxial anisotropy. In this way it results $\theta_{\frac{L_1}{2}} \approx 0^\circ$ and $\theta_{\frac{L_2}{2}} \approx 90^\circ$. For the symmetry reasons the angle at the center of the unit cell is $\theta_0 = 45^\circ$. Shrinking the width of the system the relative importance of the exchange energy increases and therefore the amplitude of the modulation of the magnetization reduces, as can be seen from the difference $\Delta\theta = \theta_{\frac{L_2}{2}} - \theta_{\frac{-L_1}{2}}$. Since $L_2 > L_1$, the weighted effective anisotropies are not balanced and the angle θ_0 tends to rotate in-plane with the reduction of L . $\theta_{\frac{-L_1}{2}}(L)$ behaves similarly. The behavior of the two curves with respect to the width of the unit cell is monotonic, while $\theta_{\frac{L_2}{2}}(L)$ has a minimum around $L = 15$ nm. The existence of the minimum shows that there are two factors determining the direction of the magnetization. One is the exchange energy that tries to reduce $\Delta\theta$ and the other is

the unbalance of the weighted effective anisotropies that tends to rotate the magnetization into the plane.

It is important to notice that for $L \approx \lambda$ ($\lambda \approx 3\text{nm}$) the magnetization is uniform and for $L \gg \lambda$ it is non-uniform (see Fig. 4.3). Therefore we may deduce that not only the relative weight of the two effective anisotropies can induce a transition between uniform and non-uniform magnetization as seen in chapter 3, but also the scale of the system. In chapter 5 we will study the spin reorientation transition in systems with modulated anisotropy as a function of the coverage φ and of the density of stripes ρ . We will see that the reorientation transition is driven by the coverage variation and that its sharpness, i.e., the coverage interval necessary to the magnetization to reorient, is a function of the scale of the system.

4.1.2 Energies

In this subsection, using the analytical expressions obtained in the last section, we calculate the energies of the system as a function of the width of the unit cell. The main goal is to give a formula useful to predict the stability of thin films with spatially varying magnetic anisotropies.

Exchange energy

The exchange energy per unit volume is given by:

$$f_{ex} = \frac{2}{L} A_{1,ex} \int_{-\frac{L_1}{2}}^0 \left(\frac{d\theta}{dx} \right)^2 dx + \frac{2}{L} A_{2,ex} \int_0^{\frac{L_2}{2}} \left(\frac{d\theta}{dx} \right)^2 dx \quad (4.16)$$

where in general the constants $A_{1,ex}$ and $A_{2,ex}$ are not equal. After integration, see Appendix, equation (4.16) transforms in:

$$f_{ex} = \frac{2A_{1,ex}}{\lambda_1 L} (\Delta E(\phi_1|m_1) - (1 - m_1) \frac{L_1}{2\lambda_1}) + \frac{2A_{2,ex}}{\lambda_2 L} (\Delta E(\phi_2|m_2) - (1 - m_2) \frac{L_2}{2\lambda_2}) \quad (4.17)$$

with $\Delta E(\phi_1|m_1) = E(\phi_{-\frac{L_1}{2}}|m_1) - E(\phi_0|m_1)$, $\Delta E(\phi_2|m_2) = E(\phi_{\frac{L_2}{2}}|m_2) - E(\phi_0|m_2)$, $m_1 = \cos^2 \theta_{-\frac{L_1}{2}}$ and $m_2 = \sin^2 \theta_{\frac{L_2}{2}}$. A compact form of equation (4.17) is obtained when $A_{1,ex} = A_{2,ex} = A_{ex}$, $L_1 = L_2 = \frac{L}{2}$ and $\lambda_1 = \lambda_2 = \lambda$:

$$f_{ex} = \frac{4A_{ex}}{\lambda L} (E(\phi_{\frac{L}{4}}|m) - E(\phi_0|m) - (1 - m) \frac{L}{4\lambda}) \quad (4.18)$$

In the derivation of equation (4.18) also the condition of symmetry $\theta_{-\frac{L_1}{2}} + \theta_{\frac{L_2}{2}} = \frac{\pi}{2}$, that leads to $m_1 = m_2 = m$ and $\phi_{-\frac{L_1}{2}} = \phi_{\frac{L_2}{2}} = \phi_{\frac{L}{4}}$ has been used. This condition is valid if the weighted effective anisotropies balance. Note that the ratios $\frac{L_1}{\lambda_1}$, $\frac{L_2}{\lambda_2}$ and $\frac{L}{\lambda}$ can be written as difference of elliptical integrals of the first kind, see eq. (A.15) in Appendix, and therefore equations (4.17) and (4.18) become a difference between elliptical integrals

of the second and first kind. In Fig. 4.4 the exchange energy density is plotted as a function of L , width of the unit cell. The system considered is Ni on Cu(110) partially covered by H_2 . The film of Ni on Cu(110) with a thickness below 10ML is in-plane magnetized [62]. Adsorption of H_2 changes the surface anisotropy [120] so that an out-of-plane magnetization becomes favorable. Here we choose to study this system because of its potential suitability to experimental studies. In fact, by ion beam irradiation [130] it is possible to remove H_2 and it is easy to prepare films with spatially varying magnetic anisotropies.

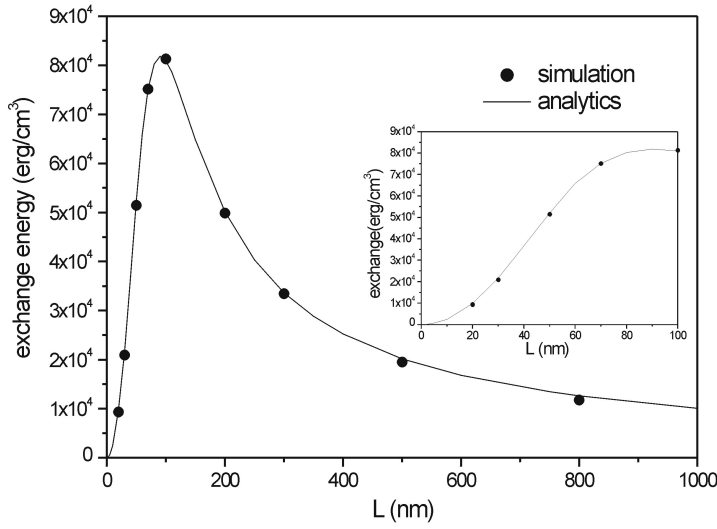


Figure 4.4: Exchange energy density vs. L , width of the unit cell. The curve refers to the system Ni on Cu(110) partially covered by H_2 after adsorption. The dots are the simulation, the curve is the analytical equation (4.18). The initial increasing, detailed in the inset, is due to the split of neighbor magnetic moments. The process ends if the geometry does not constrain any more the magnetic structure. A further increase of L does not change the angular difference between successive magnetic moments and the exchange energy density decreases with power law L^{-1} .

The sum of the interface and the surface anisotropy is $k_{s+i,Ni} = -0.611 \frac{\text{erg}}{\text{cm}^2}$ for Ni on Cu(110) and $k_{s+i,H_2} = -0.396 \frac{\text{erg}}{\text{cm}^2}$ when H_2 is adsorbed. Considering that the value of the volume anisotropy is $k_v = 0.439 \cdot 10^7 \frac{\text{erg}}{\text{cm}^3}$ and the shape anisotropy is $k_{sh} = 1.098 \cdot 10^6 \frac{\text{erg}}{\text{cm}^3}$, for a thickness of 9ML we have: $k_{H_2}^{eff} = -k_{Ni}^{eff} = 0.702 \cdot 10^6 \frac{\text{erg}}{\text{cm}^3}$. By means of equation (4.18) we can study the exchange energy as a function of the width of the unit cell. As shown in chapter 3 the angle $d\theta$ between neighbor stripes increases with L . As a consequence also the exchange energy increases since it is proportional to the square of the derivative of the angle to the normal, i.e., $f_{ex} \propto (\frac{d\theta}{dx})^2$. If L is wide enough so that the magnetic structure is free from geometrical constrictions, any further increase of the width of the unit cell does not increase the exchange energy. Therefore, having reached a

maximum, the exchange energy density decreases with power law L^{-1} .

Anisotropy energy

In the anisotropy-type description the influence of the stray field is not fully considered. Therefore the sum of the magnetostatic energy and of the anisotropy energy is given by:

$$f_{ms} + f_{an} = k_{sh} + \frac{2}{L}k_1^{eff} \int_{-\frac{L_1}{2}}^0 \sin^2\theta_x dx + \frac{2}{L}k_2^{eff} \int_0^{\frac{L_2}{2}} \sin^2\theta_x dx \quad (4.19)$$

where $k_{sh} = 2\pi M_s^2$, $k_1^{eff} = k_1 - k_{sh}$ and $k_2^{eff} = k_2 - k_{sh}$. The magnetostatic energy and the anisotropy energy favor respectively an in-plane and an out-of-plane magnetization. After integration, see Appendix, equation (4.19) becomes:

$$f_{ms} + f_{an} = k_{sh} + \frac{2k_1^{eff}\lambda_1}{L}\Delta E(\phi_1|m_1) - \frac{2k_2^{eff}\lambda_2}{L}\Delta E(\phi_2|m_2) + \frac{L_2k_2^{eff}}{L} \quad (4.20)$$

When the effective anisotropies balance, the equation (4.20) transforms in:

$$f_{ms} + f_{an} = \frac{k_{sh} + k_2}{2} + \frac{4k_1^{eff}\lambda_1}{L}(E(\phi_{\frac{L}{4}}|m) - E(\phi_0|m)) \quad (4.21)$$

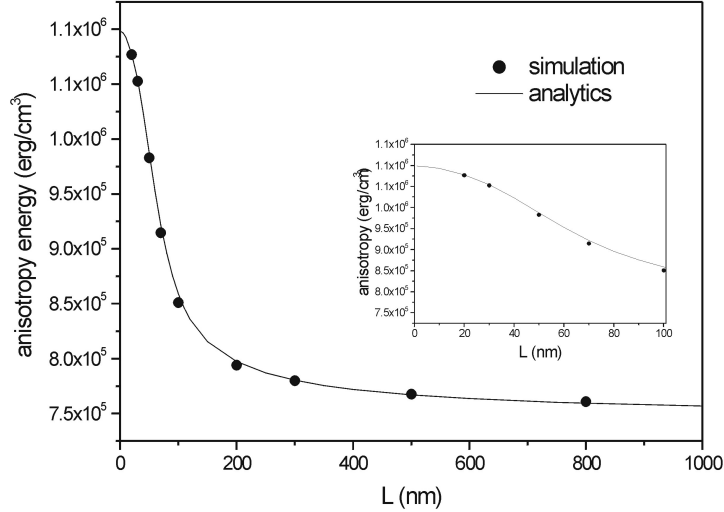


Figure 4.5: *Effective anisotropy energy vs. L , width of the unit cell. The curve refers to the system Ni on Cu(110) partially covered by H_2 . The maximum value is obtained for $L \rightarrow 0$ when the magnetization is uniform at 45° with respect to the normal. The minimum is reached for large width of the unit cell when the magnetization alternates from in-plane to out-of-plane in successive stripes.*

Equation (4.21) as a function of L is plotted in Fig. 4.5 in the case of Ni on Cu(110) partially covered by H_2 . The second term equation (4.21) is a positive number that reduces

with L increasing. In the limit of large unit cell the magnetization in successive stripes alternates between in-plane and out-of-plane directions. Therefore, since $L_1 = L_2 = \frac{L}{2}$, the magnetostatic energy density is half of the value obtained for a film magnetized uniformly out-of-plane, i.e., $f_{ms} = \frac{k_{sh}}{2}$ because the magnetic surface charges are only present in the stripes with out-of-plane anisotropy. Similarly the anisotropy energy density due to the contribution inside the stripes of Ni, which are in-plane magnetized, is $f_{an} = \frac{k_{Ni}}{2} = \frac{k_2}{2}$. In the limit of vanishing width of the unit cell, the magnetization is uniform at 45° with respect to the normal. As a consequence the integrand function contained in equation (4.19) is constant and the integration is straightforward. Considered that $k_1^{eff} = -k_2^{eff}$, it follows $f_{ms} + f_{an} = k_{sh}$. In this way we find that in the limit of small unit cell, i.e., for $L \rightarrow 0$, the effective anisotropy energy is equal to the magnetostatic energy of a film uniformly magnetized out-of-plane. It is interesting to notice that the derivative of the anisotropy energy changes sign for $L \approx 50$ nm. The same behavior is found in the plot of the exchange energy, see inset of Fig. 4.4. The existence of the point of inflection is an image of two competing factors that contribute to the variation of the energy as a function of L . For $L < 50$ nm the dependence of the fine structure, represented by the elliptical integrals, dominates the energy variation; for $L > 50$ nm the geometrical scale factor $\frac{1}{L}$ becomes dominant since the magnetization is almost free from the geometric constriction.

Total energy density

The total energy is a function of L and its general form is given by the sum of equations (4.17) and (4.20).

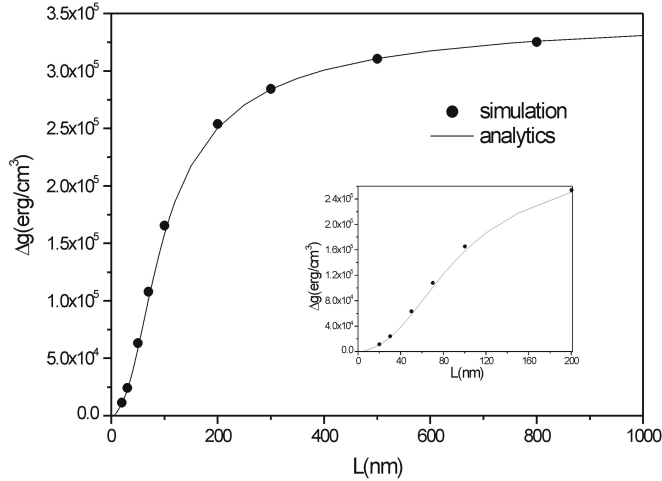


Figure 4.6: Energy gain due to the modulation of the anisotropy vs. L , width of the unit cell. For $L < 50$ nm the finite structure determines the energy increasing. For $L > 50$ nm the geometrical factor $\frac{1}{L}$ dominates and the energy tends asymptotically to the value $-\frac{k_1^{eff}}{2}$, see equation (4.23)

The gain in energy due to a modulated microstructure that forms for $L \neq 0$:

$$\Delta f_t(L) = f_t^{unif} - f_t^{mod}(L) \quad (4.22)$$

with $f_t^{mod}(L) = f_{ex}(L) + f_{ms}(L) + f_{an}(L)$. The value of f_t^{unif} is function of the weighted effective anisotropies. If $L_1 k_1^{eff} > L_2 k_2^{eff}$ the out-of-plane anisotropy dominates and $f_t^{unif} = k_{sh}$. If $L_1 k_1^{eff} < L_2 k_2^{eff}$ the in-plane anisotropy dominates and $f_t^{unif} = k_1 + k_2$.

If the effective anisotropies balance, i.e., $L_1 k_1^{eff} = L_2 k_2^{eff}$, the magnetization tilts at 45° for $L \rightarrow 0$ and $f_t^{unif} = k_{sh}$, as seen above. In this case equation (4.22) becomes:

$$\Delta f_t(L) = -\frac{k_1^{eff}}{2} + \frac{(1-m)A_{ex}}{\lambda^2} - \frac{4}{L}(k_1^{eff}\lambda + \frac{A_{ex}}{\lambda})(E(\phi_{\frac{L}{4}}|m) - E(\phi_0|m)) \quad (4.23)$$

Equation (4.23) is plotted as a function of L in Fig. 4.6 in the case of Ni on Cu(110) partially covered by H_2 . The energy gap is function of L , width of the unit cell. Comparison between Figures 4.4 and 4.5 shows that the anisotropy energy is at least one order of magnitude bigger than the exchange energy and therefore dominates the behavior of $\Delta f_t(L)$.

The energy gain $\Delta f_t(L)$ can be regarded as an anisotropy energy. Like in systems with uniaxial anisotropy the thermal stability of a particle of volume V is measured by $V\Delta f_t(L)$. If this activation energy is overcome by the thermal energy $k_B T$, the easy axis of the particle is undefined and the system in the superparamagnetic phase.

4.2 Role of the dipolar interaction

In this section we study the modifications of the energy and of the shape of the magnetic profiles induced by the dipolar interaction. The alternated anisotropies generate a modulation of the magnetization and thus of the surface charge density. The stripes with out-of-plane anisotropy have an higher average value of the surface charge density, defined as $\sigma = \mathbf{n} \cdot \mathbf{M}$. The stray field generated by these charges is higher than the one generated by the charges placed in the stripes with in-plane anisotropy. As a consequence the torque due to the stray field causes a rotation of the magnetic moments inside the stripe with in-plane anisotropy while inside the stripes with out-of-plane anisotropy it is negligible. Such a situation is plotted in Fig. 4.7 for a film of 4ML of Co grown on Pd(111) and partially covered by Pd so that $k_{Pd}^{eff} = -k_{Co}^{eff} = 0.48 \cdot 10^7 \frac{\text{erg}}{\text{cm}^3}$. The width of the unit cell is $L = 36$ nm and the magnetic characteristic length is $\lambda = 5.68$ nm. It has to be noticed that as a consequence of the rotation the magnetostatic energy reduces, while the anisotropy energy increases since the crystalline anisotropy points out-of-plane. Therefore the variation of the total energy is negligible, while the variation of the magnetostatic energy can be larger than 10%. The rotation is a function of: 1) the scale of the system, 2) the value of the effective anisotropy and 3) the thickness of the film. In the

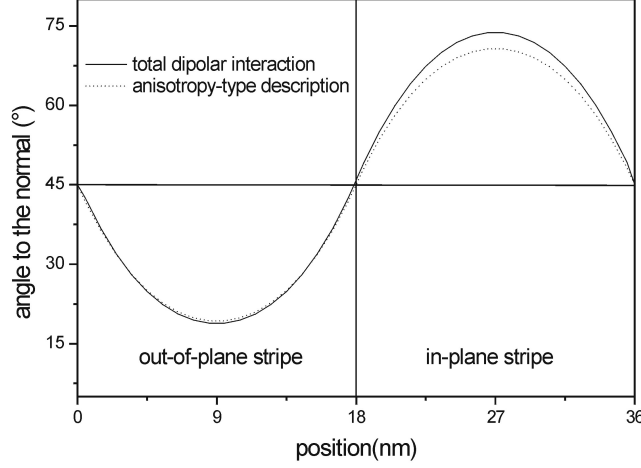


Figure 4.7: *Modification of the magnetic profile due to the influence of the stray field. The solid line is obtained considering the total dipolar interaction. The dotted line is the result of the anisotropy-type description. The curves differ in the region with in-plane anisotropy where the magnetic moments rotate because of the stray field. The angular difference $\Delta\theta$ in $\frac{L_2}{2}$ is function of the hardness of the material.*

following we study separately these three contributions although in real films they can mix one another.

Influence of the scale of the system

If the material parameters are fixed, the modification of the magnetic profiles is a function of the width of the unit cells. In Fig. 4.8 the variation of the magnetostatic energy is plotted versus L for the system mentioned above.

The straight line represents the value of the magnetostatic energy for films uniformly magnetized at 45° with respect to the normal. In this case the stray field does not modify the magnetic profile and the system is correctly described by means of the effective anisotropies. This value is obtained in the limit of very small or large unit cell, i.e., $L \rightarrow 0$ or $L \rightarrow \infty$. If the width of the unit cell is comparable or smaller than the magnetic characteristic length, i.e., $L \leq \lambda$, the exchange interaction is strong enough to keep the magnetization almost parallel. In this case the influence of the stray field is negligible and the magnetostatic energy has the same value as for a film uniformly magnetized at 45° with respect to the normal. For bigger unit cells the magnetization profile start to follow the constrictions of the magnetic anisotropy and the stray field can induce the rotation of the magnetic moments. As a consequence the magnetostatic energy decreases with L . The minimum is reached for $L=40$ nm (see Fig. 4.8) when the magnetic microstructure is fully developed. For $L > 40$ nm the effect of the rotation decays with power law $\sim -\frac{1}{L}$, like the magnetic potential.

Dependence on the effective anisotropy

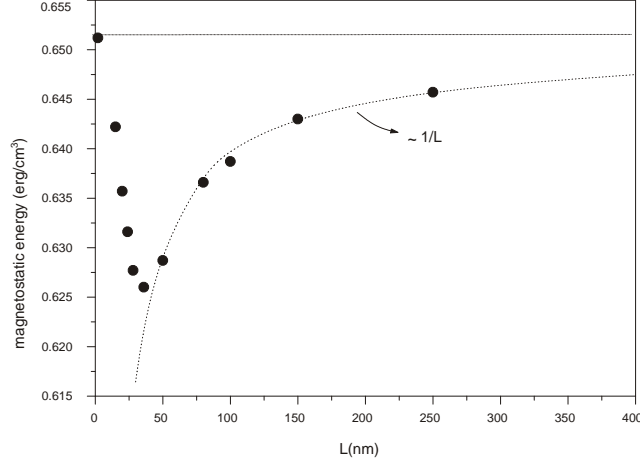


Figure 4.8: Variation of the magnetostatic energy versus the width of the unit cell. In the presence of the stray field the direction of the magnetization rotates and the magnetostatic energy deviates from the value obtained in the anisotropy-type description.

In this section we study the effect of the dipolar interaction on the magnetic microstructure as function of the effective anisotropy.

First we show that the hardness of the material is a function of the scale of the system. Let us define two magnetization profiles as equivalent if their shape is the same after re-scaling of the width of the unit cell. The re-scaling is performed as follows: given a certain magnetization profile we change the effective anisotropy and thus the magnetic characteristic length, i.e., $\lambda = \sqrt{\frac{A}{k_{eff}}}$. As a consequence the system reaches a new equilibrium with a new shape of the magnetization profile. Then we vary L until the original shape of the profile is recovered. The result of the re-scaling is reported in the inset of Fig. 4.9 and shows that it is sufficient to keep the ratio $\frac{L}{\lambda}$ constant to have the same shape of the magnetization profile. The total energy of the system is a function of the effective anisotropy and therefore of the width of the unit cell through the ratio $\frac{L}{\lambda}$. The depth of the minimum of the total energy, i.e., $\Delta f_t(L, \lambda)$, is calculated with equation (4.23) and is plotted in Fig. 4.9. This quantity measures the hardness of the material, i.e., the smaller $\Delta f_t(L, \lambda)$ is the softer is the system. Therefore we find (see Fig. 4.9) that the smaller L is, the harder is the material. Note that this dependency on L is opposite to the one shown in Fig. 4.6 where the effective anisotropy is kept constant.

So far the influence of the stray field has been neglected. The scaling law shown in the inset of Fig. 4.9 results from the analytical solution based on the anisotropy-type description. The influence of the dipolar interaction on the shape of magnetic profile can be measured by means of the variation of the magnetization direction $\Delta\theta$ at the center of the stripe with in-plane anisotropy. The variation is the bigger the smaller k_{eff} is, i.e.,

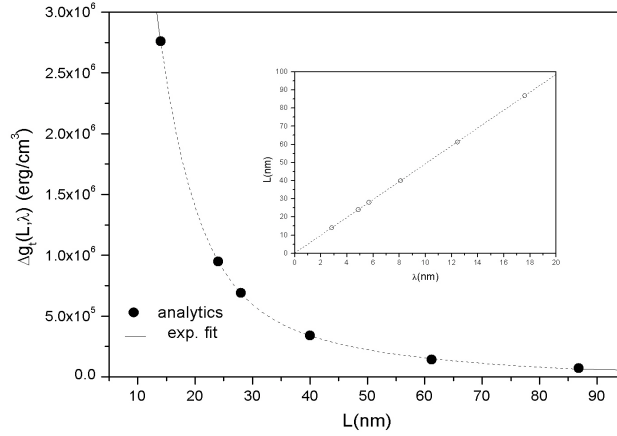


Figure 4.9: *Hardness of the material, represented by the depth of the minimum of the total energy $\Delta g_t(L, \lambda)$, vs. L , width of the unit cell. The curve results from the comparison of magnetic profiles of the same shape obtained for different scales of the system. The inset shows the values of L and λ that correspond to the same magnetic profile. The two quantities are proportional. Note that the plots are obtained varying the effective anisotropy k_{eff} and therefore $\lambda = \sqrt{\frac{A}{k_{eff}}}$*

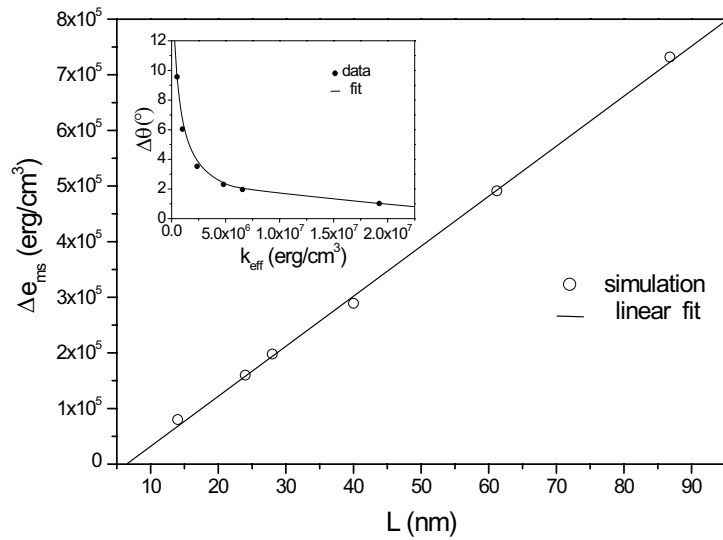


Figure 4.10: *Variation of the magnetostatic energy versus width of the unit cell. In the inset the change in magnetization direction due to the dipolar interaction is plotted as a function of the effective anisotropy. From the plots we see that the softer the material is, the stronger is the effect of the dipolar interaction.*

the softer the material is (see inset of Fig. 4.10). This behaviour is due to the stray field created by the surface charges in the stripes with out-of-plane anisotropy. In particular, the softer the material is, the stronger the effect of the stray field is. The variation of the magnetostatic energy versus the the width of the unit cell is plotted in Fig. 4.10. In general the effect of the stray field is to rotate the magnetization in-plane and thus to decrease the magnetostatic energy. In particular the effect of the stray field is to increase linearly the variation of the magnetostatic energy as function of the width of the unit cell.

Dependence on the thickness

The modification of the magnetic profiles is also a function of the film thickness. This is a consequence of the thickness dependence of the magnetostatic energy for films with perpendicular uniaxial anisotropy which we studied in section 2.3.1. For ultrathin films, i.e., $t \approx 0$, the effect of the non-local part of the magnetostatic energy is negligible and we do not expect any variation of the magnetization. For thicker films the stray field is strong enough to modify the magnetic profile. Here we study the thickness dependence for different hardness of the material.

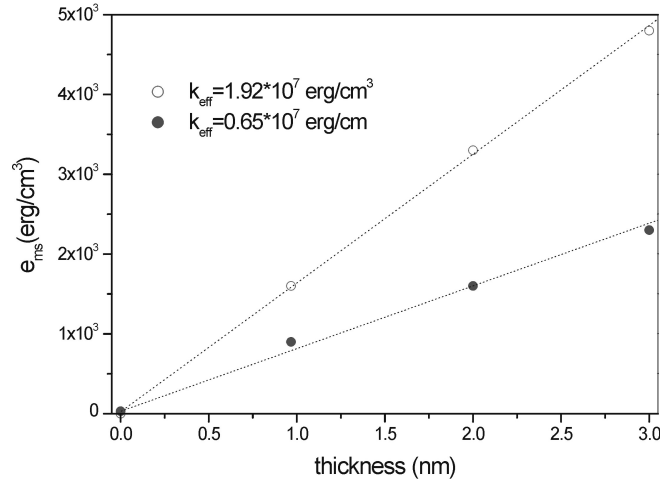


Figure 4.11: Variation of the magnetostatic energy versus t , thickness of the film. Δf_{ms} compares the values obtained in the anisotropy-type description with the those of the total dipolar interaction description. The gap increases with the thickness since the effect of the stray field becomes stronger. Besides, the softer the material is, the stronger this effect is and the steeper the linear dependence of the magnetostatic energy is.

We compare two systems with unit cell respectively $L = 14$ nm and $L = 28$ nm. The corresponding effective anisotropies are $k_{Pd}^{eff} = -k_{Co}^{eff} = 1.922 \cdot 10^7 \frac{\text{erg}}{\text{cm}^3}$ and $k_{Pd}^{eff} = -k_{Co}^{eff} = 0.656 \cdot 10^7 \frac{\text{erg}}{\text{cm}^3}$. With these parameters the shape of the magnetization profiles scales in the way plotted in the inset of Fig. 4.9. The energy of the magnetization profiles are a

function of the two effective anisotropies and of the thickness of the slab. In Fig. 4.11 is plotted the thickness dependence on the variation of the magnetostatic energy, indicated with Δf_{ms} , when the dipolar interaction is fully taken into account.

The variation of the magnetostatic energy grows linearly with the thickness and it increases with the softness of the material. Note that in reality the crystalline anisotropy is not constant but it is function of the thickness. Therefore the analysis performed is valid only in first approximation since in real systems the thickness dependence of the magnetostatic energy is in general not linear (see section 2.3.1).

Chapter 5

Engineered magnetic domains

5.1 Alternating in/out-of-plane patterned domains

From chapter 2 it comes out clearly that the driving force for the formation of a multi-domain configuration in systems with perpendicular uniaxial anisotropy is the dipolar interaction. Now we study the class of magnetic systems with spatially alternating uniaxial anisotropy. In chapters 3 and 4 we showed that it is possible to obtain states with non-uniform magnetization even neglecting the correction due to the stray field. The angle to the normal of the magnetization was always modulating between $0 \leq \theta \leq 90^\circ$. So far other possible orientations of the magnetization have been ignored. If the amplitude of the modulation is sufficiently large a Bloch wall ($0 \leq \theta \leq 180^\circ$) or a spiral configuration ($0 \leq \theta \leq 360^\circ$) may form. In this section we compare the magnetic profiles and the energies of various configurations as a function of the geometry of the system.

5.1.1 Tailoring the anisotropy and modifying the magnetic profiles

The magnetization of ultrathin films with easy axis perpendicular to the surface is uniform [21, 22]. In order to obtain magnetic domains we can reduce the wall energy by tuning the out-of-plane uniaxial anisotropy in a region L_2 around the wall. In this way, after relaxation, the system reaches a new minimum with an energy comparable with the one of a single domain state.

Let us consider an infinite film with thickness t crossed by an infinitely long stripe of width L_2 , see Fig. 5.1. In this region the value of the perpendicular uniaxial anisotropy is smaller than the value of the shape anisotropy and the effective anisotropy favors an in-plane magnetization, i.e., $k_{\text{eff},2} < 0$ and $Q_2 < 1$. In the rest of the film the uniaxial magnetocrystalline anisotropy dominates and the effective anisotropy points out-of-plane, i.e., $k_{\text{eff},1} > 0$ and $Q_1 > 1$.

Since the stripe is infinitely long and the film is thin the orientation of the magneti-

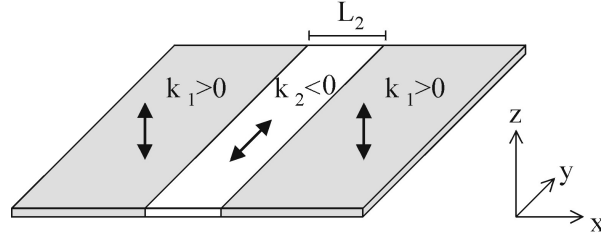


Figure 5.1: Film of thickness t crossed by an infinitely long stripe of width L_2 . Within the stripe $Q_2 < 1$ and the effective anisotropy lies in-plane. In the rest of the film it lies out-of-plane, i.e., $Q_1 > 1$.

zation is constant along the axis y and z and it varies only along the x direction.

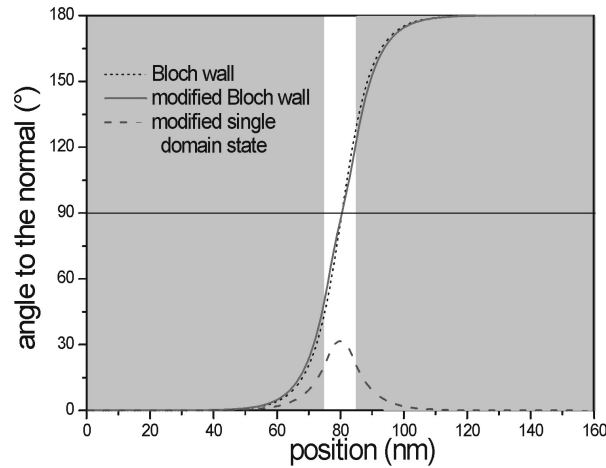


Figure 5.2: Magnetization profiles for a film with thickness equal to 0.3 nm , crossed by an infinite long stripe of width $L_2 = 10 \text{ nm}$. Since $L_2 \simeq 1.5 \cdot \lambda$ the magnetization of the single domain tends to rotate in-plane in the region of the stripe.

Besides, the divergence of the magnetization is minimized when the magnetic moments lie along the stripe, so that the angle to the normal is sufficient to fully describe the orientation of the magnetization. Therefore, the problem is one-dimensional and it is solved when the angle to the normal of the magnetization θ is known as a function of the position x on the sample.

The numerical magnetization profiles obtained for three different values of L_2 are plotted in Fig. 5.2 and 5.3. The region with out-of-plane anisotropy is shaded in grey. In each figure we plot three profiles: a Bloch wall and two magnetic states found after relaxation. The Bloch wall, obtained for $L_2 = 0$, is drawn as a reference in order to study the effect of the presence of the in-plane anisotropy. This effect shows up in the modified

Bloch wall state, where the magnetization rotates from out-of-plane to in-plane within the central stripe and rotates further to the opposite direction in the other side of the stripe. The shape of the profile is a function of L_2 . Similarly, the single domain state is affected by the presence of the in-plane anisotropy, as shown by the modified single domain state. Here the magnetization rotates in-plane in the central stripe but rotates back to the same orientation on the other side. The total energy of the system as a function of L_2 can be calculated in the framework of the anisotropy-type description. The result is plotted in Fig. 5.4. If the dipolar interaction is fully considered the energy slightly changes, as shown in Fig. 5.5.

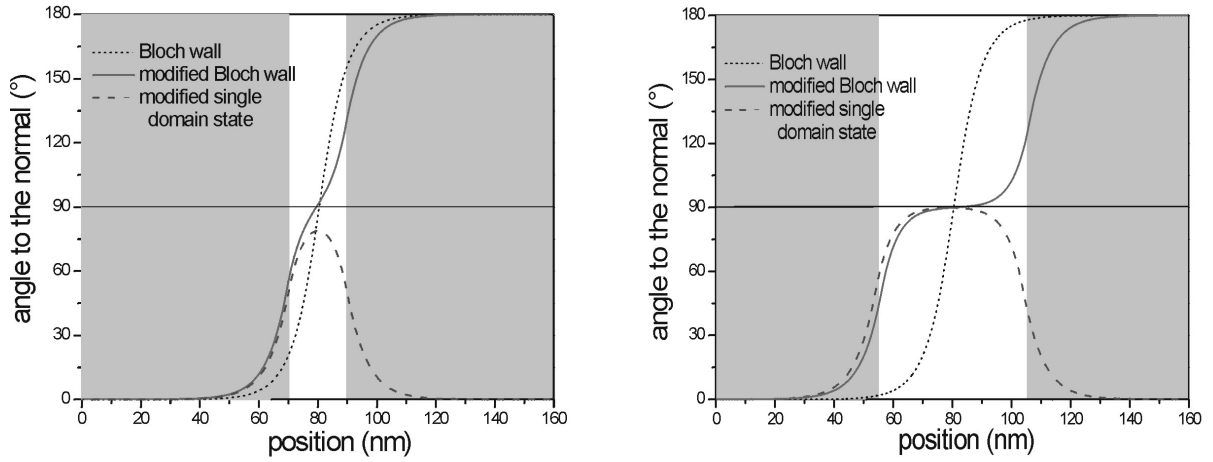


Figure 5.3: Magnetization profiles for $L_2 = 20$ nm and $L_2 = 50$ nm.

Now we analyze in more detail the total energy and the shape of the magnetization profiles as a function of L_2 . For $L_2 = 0$ the single domain state is the lowest in energy, as shown in Fig. 5.4. In general, in order to obtain an in-plane effective anisotropy, the value of the uniaxial out-of-plane anisotropy has to be reduced below the value of the shape anisotropy. As a consequence the magnetic anisotropy in the region L_2 is smaller than in the rest of the film. Since the Bloch wall is centered in this region, the wall energy and thus the total energy of the system decrease with L_2 , as shown in Fig. 5.4.

The black squares in Fig. 5.4 show that the total energy of the single domain state remains constant until L_2 exceeds a certain critical value when the exchange energy does not keep all the magnetic moments parallel. This case is represented by the dashed line in Fig. 5.2, where some spins of the single domain state rotate into the plane direction in order to minimize the effective anisotropy energy. In Fig. 5.2 the region with in-plane anisotropy is close to the magnetic characteristic length, $1.5 \cdot \lambda \simeq L_2 = 10$ nm. The shape of the modified Bloch wall and of the modified single domain change with L_2 increasing, as shown in the sequence of Fig. 5.3. If the width of the in-plane region is much larger than the characteristic length, $\lambda \ll L_2 = 50$ nm, the magnetization of both states lies in-plane at the centre of the stripe. As a consequence regions with in-plane magnetization

alternate with regions with out-of-plane magnetization forming a domain pattern. Fig. 5.4 shows that in this case (coverage=0.3125) the total energy of the two states is identical in the anisotropy-type description. Although the magnetic profiles differ with respect to $\theta = 90^\circ$, the exchange and anisotropy energy remain invariant.

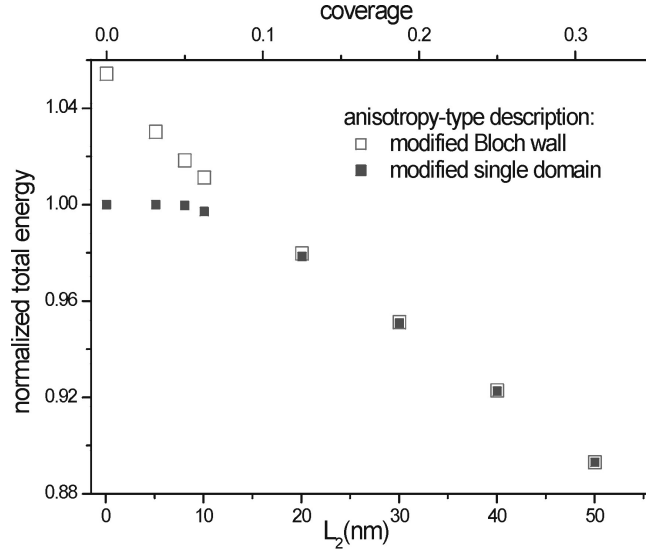


Figure 5.4: Total energy, normalized to the value of the single domain state, versus coverage. The plot is obtained in the anisotropy-type approximation. With L_2 increasing, the Bloch wall state modifies its shape while its total energy decreases following the trend of the anisotropy energy. The total energy of the single domain state is constant until a critical value of L_2 is reached, when the spins start to rotate into the plane and the total energy starts to decrease.

Until now we have seen that if a stripe with in-plane anisotropy is considered, the energies of the modified Bloch wall and of the modified single domain become comparable. Besides, a patterned domain configuration forms for $L_2 \gg \lambda$. These results are valid in the framework of the anisotropy-type description. As already explained in the previous chapters, the influence of the stray field in ultrathin films is negligible. Nevertheless the role of the correction to the magnetostatic energy becomes decisive when magnetic configurations with similar energies are compared, like in the case of the modified Bloch wall and the modified single domain states. The correction to the magnetostatic energy lowers the total energy of both the states. The change in total energy of the modified Bloch wall is shown in Fig. 5.5. For $L_2 \ll \lambda$ the correction reduces the energy gap between the two states, but the modified single domain state remains the lowest in energy. For $L_2 \gg \lambda$ the energy values of the two states are so close that the correction to the magnetostatic energy makes the modified Bloch wall state the lowest in energy, see inset of Fig. 5.5. Therefore a transition between the two states due to the stray field takes

place with increasing L_2 . Note that in Fig. 5.5 the transition is visible only for one value of L_2 , zoomed in the inset. In fact, for larger values of L_2 the stray field reduces and the transition is not possible. It has to be noticed that in the example considered the thickness of the slab is only 1 ML and the energy gap at the transition is minimal. In general since the stray field is a function of the thickness of the film (see eq. (2.14)) a thickness dependence of the energy gap between the two states can be expected.

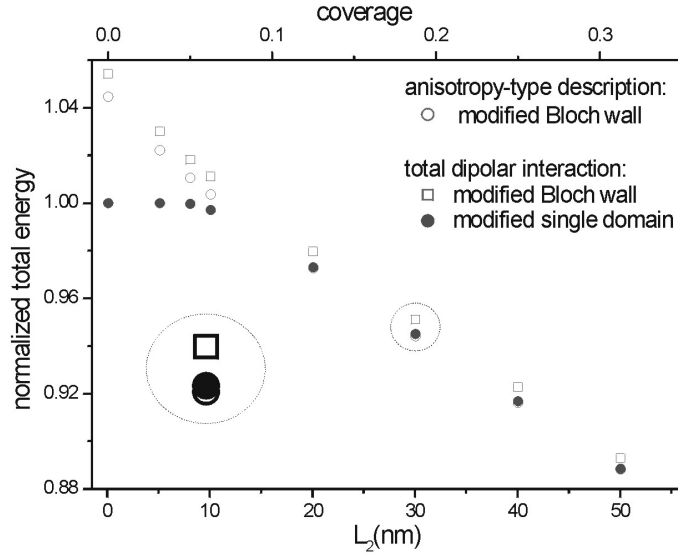


Figure 5.5: Total energy, normalized to the value of the single domain state, versus L_2 , width of the in-plane region. The dipolar interaction is totally considered in the dots. The effect of the magnetic field arising from the Bloch wall is evident by comparing squares and empty dots. As clear from the inset, we can see that the correction to the dipolar interaction is the driving force which cause the Bloch wall state to be of lower energy.

5.1.2 Types of multi-domain states

In this section we extend the analysis to a thin film crossed by an infinite number of stripes. In particular we analyze the possible magnetic configurations as function of the width of the unit cell.

In Fig. 5.6 we sketch the four possible states for systems with infinitely long stripes with alternating anisotropies. The arrows represent the direction of the magnetization in sufficiently large stripes. The state ' $\uparrow \rightarrow \uparrow \rightarrow$ ', that we have analyzed in the last two chapters, is the energy minimum for small width of the unit cell, as we will see. The state ' $\uparrow \rightarrow \uparrow \leftarrow$ ' differs at the center of the stripe of width L_1 where for symmetry reasons the magnetization is always out-of-plane. The state ' $\uparrow \rightarrow \downarrow \rightarrow$ ' is similar, but it has the symmetry point at the center of the stripe with in-plane anisotropy. Finally the magnetization of the state ' $\uparrow \rightarrow \downarrow \leftarrow$ ' rotates in the yz plane forming a spiral along the x direction.

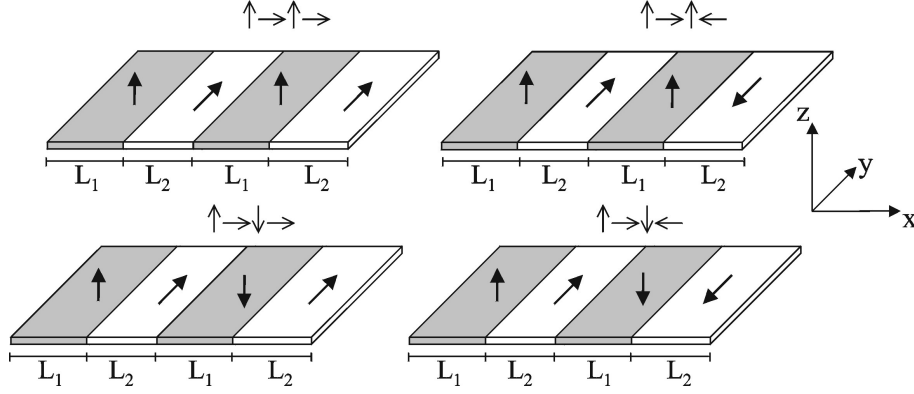


Figure 5.6: *Multi-domain states for systems with alternating effective anisotropy. The arrows represent the direction of the magnetization for sufficiently wide stripes. Periodic boundaries are imposed in the x and y directions.*

The energy minimum is a function of the width of the unit cell. In general the exchange energy dominates for small scales of the system, i.e., $L \ll \lambda$, while the dipolar interaction determines the minimum for large scales of the system, i.e., $L \gg \lambda$. This can be proven by calculating numerically the energies of an arbitrary system with alternating effective anisotropies $k_1^{eff} = -k_2^{eff} = 0.39 \cdot 10^7$ erg/cm³, saturation magnetization $M_s = 1440$ emu/cm³ and thickness $t = 1$ ML.

First we consider a system with unit cell $L = 40$ nm. In this case $L > \lambda = 5$ nm. The magnetic profiles of the four states are plotted in Fig. 5.7; the corresponding energies are given in Tab. 5.1. The state ' $\uparrow \rightarrow \uparrow \rightarrow$ ' is the energy minimum because of the absence of symmetry points (circles in Fig. 5.7) that force the magnetization to cross the center of the stripes increasing the value of the exchange energy. The reason is that the average angle between successive magnetic stripes enlarges. From Fig. 5.7 and Tab. 5.1 we notice that the higher the number of these symmetry points is, the higher is the value of the exchange energy. The main difference between the magnetic profiles of the states ' $\uparrow \rightarrow \uparrow \rightarrow$ ' and ' $\uparrow \rightarrow \uparrow \leftarrow$ ' is located inside the stripe with perpendicular magnetic anisotropy, see Fig. 5.7. Note that the higher value of exchange energy of the state ' $\uparrow \rightarrow \uparrow \leftarrow$ ' is partially compensated by the lower effective anisotropy energy. A similar analysis can be performed for the states ' $\uparrow \rightarrow \downarrow \rightarrow$ ' and ' $\uparrow \rightarrow \downarrow \leftarrow$ '. So far the comparison between states has shown that the state of lowest energy is determined by the exchange energy. The role of the stray field could become determinant when we compare states with opposite out-of-plane magnetization, like ' $\uparrow \rightarrow \uparrow \rightarrow$ ' and ' $\uparrow \rightarrow \downarrow \rightarrow$ '. The values of the energies calculated for these two states show that the correction due to the stray field is not important and the state ' $\uparrow \rightarrow \uparrow \rightarrow$ ' is still the lowest in energy. This analysis is performed for $L = 40$ nm, but it is also valid for smaller values of L . In fact shrinking L the weight of the exchange energy increases because the angle between neighbor magnetic moments enlarges.

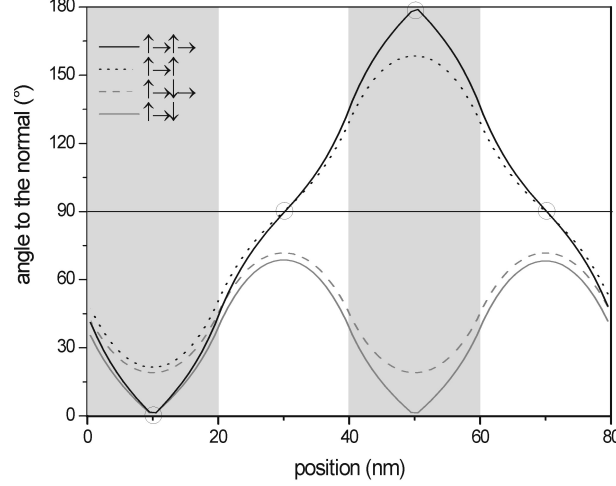


Figure 5.7: Magnetization profiles of the states sketched in Fig. 5.6 for $L = 40$ nm. With the circle are marked some points of symmetry in which the angle of the magnetization to the normal is either $\theta = 0^\circ$, $\theta = 90^\circ$ or $\theta = 180^\circ$.

state	e_{tot}	e_{ex}	e_{an}	e_{ms}
$\uparrow \rightarrow \uparrow \rightarrow$	0.947	0.034	0.419	0.494
$\uparrow \rightarrow \uparrow \leftarrow$	0.956	0.05	0.323	0.583
$\uparrow \rightarrow \downarrow \rightarrow$	0.952	0.05	0.487	0.416
$\uparrow \rightarrow \downarrow \leftarrow$	0.963	0.077	0.324	0.583

Table 5.1: Energies of the multi-domain states normalized to the total energy of the single domain magnetized out-of-plane. The values refer to the magnetization profiles plotted in Fig. 5.7 for $L = 40$ nm.

Now we extend our analysis to systems with larger values of the unit cell, i.e., for $L \gg \lambda$. In Fig. 5.8 we plot the magnetic profiles calculated for $L = 80$ nm. The corresponding energies are given in Tab. 5.2. For this value of the unit cell the magnetic microstructure is not significantly constrained by the width of the stripes and the total energy of the four states is similar. The configurations of lowest energy are those with successive out-of-plane stripes opposite magnetized ($\uparrow \rightarrow \downarrow \rightarrow$ ' and $\uparrow \rightarrow \downarrow \leftarrow$ '). Therefore, by increasing the width of the unit cell, the state of lowest energy change from ' $\uparrow \rightarrow \uparrow \rightarrow$ ' to ' $\uparrow \rightarrow \downarrow \rightarrow$ '. In the following we show that the stray field energy determines the state of lowest energy. Let us consider the states ' $\uparrow \rightarrow \uparrow \leftarrow$ ' and ' $\uparrow \rightarrow \downarrow \leftarrow$ ' (a similar analysis can be performed for the states ' $\uparrow \rightarrow \uparrow \rightarrow$ ' and ' $\uparrow \rightarrow \downarrow \rightarrow$ '). In Tab. 5.3 we report the energies obtained in the anisotropy-type description ($\uparrow \rightarrow \uparrow \leftarrow^*$ and ' $\uparrow \rightarrow \downarrow \leftarrow^*$ ') and in the fully dipolar description ($\uparrow \rightarrow \uparrow \leftarrow$ ' and ' $\uparrow \rightarrow \downarrow \leftarrow$ ').

In the first case the stray field is included in the anisotropy energy and the lowest

state	e_{tot}	e_{ex}	e_{an}	e_{ms}
$\uparrow \rightarrow \uparrow \rightarrow$	0.9007	0.0261	0.3789	0.4957
$\uparrow \rightarrow \uparrow \leftarrow$	0.901	0.0269	0.3754	0.4987
$\uparrow \rightarrow \downarrow \rightarrow$	0.8995	0.0265	0.3777	0.4953
$\uparrow \rightarrow \downarrow \leftarrow$	0.8999	0.0275	0.3743	0.4981

Table 5.2: Normalized energies of the multi-domain plotted in Fig. 5.8 for $L = 80$ nm.

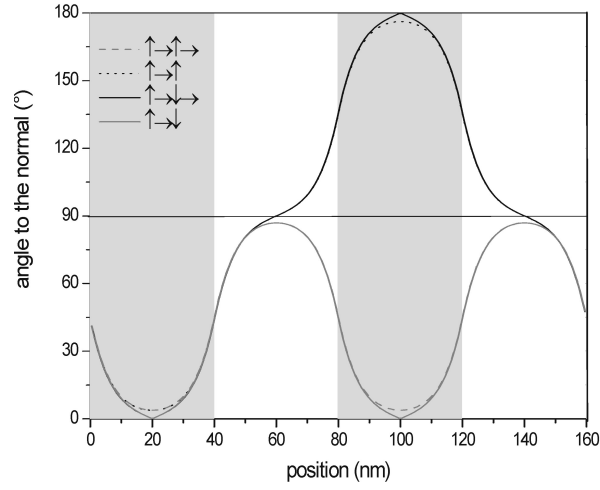


Figure 5.8: Magnetization profiles for $L = 80$ nm.

state in energy is ' $\uparrow \rightarrow \uparrow \leftarrow *$ '. Therefore, if the stray field is not fully considered, the lowest state in energy is the one with successive out-of-plane stripes parallel magnetized. In the second case the stray field is fully taken into account and the lowest state in energy is ' $\uparrow \rightarrow \downarrow \leftarrow$ '. Therefore, for $L \gg \lambda$, the lowest state in energy is determined by the stray field energy.

state	e_{tot}	e_{ex}	e_{an}	e_{ms}
$\uparrow \rightarrow \uparrow \leftarrow *$	0.9031	0.0269	0.3754	0.5008
$\uparrow \rightarrow \downarrow \leftarrow *$	0.9034	0.0275	0.3743	0.5016
$\uparrow \rightarrow \uparrow \leftarrow$	0.901	0.0269	0.3754	0.4987
$\uparrow \rightarrow \downarrow \leftarrow$	0.8999	0.0275	0.3743	0.4981

Table 5.3: Normalized energies in the anisotropy-type description and in the fully dipolar interaction description for $L = 80$ nm.

5.1.3 Diagram of the states for films with modulated anisotropies

We have seen that films with modulated anisotropies present different types of magnetic configurations as a function of the intrinsic and the extrinsic parameters. If the width of the unit cell is much smaller than the magnetic characteristic length, i.e., $L \ll \lambda$, the magnetization is either uniform or canted, see chapter 3. If the width of the unit cell is larger than the magnetic characteristic length, i.e., $L > \lambda$, various magnetic configurations are energetically comparable and a pattern domain configuration can form, see section 5.1.2. In particular if $L \gg \lambda$ the lowest state in energy is a pattern domain with alternating magnetization in the regions with out-of-plane anisotropy.

In this section we draw a diagram of the states obtained as a function of the ratios $\frac{L_1}{\lambda_1}$ and $\frac{L_2}{\lambda_2}$. As we will see, the invariance of these quantities represent a necessary condition to be fulfilled in order to have a scale invariance of the problem. Now we describe the different regions of the diagram 5.9. It is divided in four regions. Inside region 1 the film is magnetized uniformly out-of-plane. This happens if L_2 is too narrow to allow a rotation of the magnetization. Similarly, inside region 2 the film is magnetized uniformly in-plane. The dashed lines divide regions 1 and 2 from region 3 where the magnetization is non-uniform. Elmers calculated these lines of transition using the Jacobi criterion [75]. The analytical solution given in chapter 4 permits to calculate these lines as well. In fact the equations (4.11), (4.10) and (4.13) give the magnetization profile for each set of the parameters of the system and therefore allow to study the transition (see Fig. 4.3). Note that the regions of uniform magnetization 1 and 2 progressively reduce with $\frac{L_1}{\lambda_1}$ and $\frac{L_2}{\lambda_2}$. If for example we are in region 2 by decreasing the ratio $\frac{L_2}{\lambda_2}$ we reach a critical point where the width L_2 is too narrow to keep the system magnetized in-plane. The other transition to be analyzed is the one between regions 3 and 4. The border line between these two regions cannot be predicted by the analytical solution of chapter 4. This happens because the analytical model is based on the anisotropy-type description, while the transition is driven by the dipolar interaction. Therefore the border line has to be calculated numerically taking fully into account the dipolar interaction.

The straight line crossing the graph from bottom left to top right shows where the system has balanced weighted effective anisotropies. As shown in chapter 3 this is the condition necessary to obtain a canting in the limit of small unit cell, when $L \ll \lambda$. In Fig. 5.9 some values of the gap $\Delta\theta$, i.e., the angular difference between successive stripes, are given as a function of the ratio $\frac{L_1}{\lambda_1}$ and $\frac{L_2}{\lambda_2}$. We notice that $\Delta\theta$ decreases with L . In fact, as explained in chapter 3, the magnetization oscillates around an average value with an amplitude that is a function of the width of the unit cell.

The magnetization can reorient from in-plane to out-of-plane (or vice versus) crossing region 3. The sharpness of the transition, i.e., the interval necessary for the reorientation, decreases with L as evident by the narrowing of region 3. In the next section we will study in more detail the spin reorientation transition for systems with varying magnetic anisotropies.

Now we analyze the role played by the dipolar interaction in the determination of the

border lines in the diagram of the states. The asymmetry visible at the border between regions 3 and 4 is due to the different orientation of the magnetization in the stripes of width L_1 and L_2 . In order to understand this we consider the border at the point where $\frac{L_2}{\lambda_2} = \frac{L_1}{\lambda_1}$. From this point any enlargement of L_1 leads to a gain in magnetostatic energy because in these stripes the magnetization is alternated out-of-plane. Therefore, if we move to higher values of L_1 we enter region 4. If we increase L_2 from the starting point there are no changes in the magnetostatic energy because in these stripes the magnetization is in-plane. Therefore if we move to higher values of L_2 we stand on the border between the two regions.

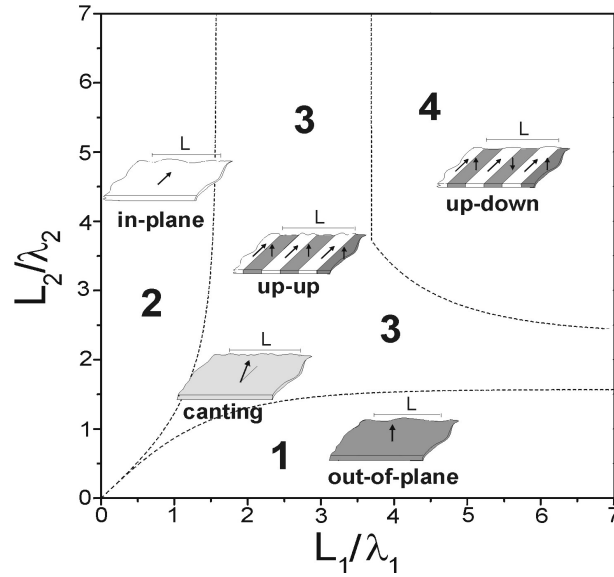


Figure 5.9: *Diagram of the magnetic configurations as function of the internal and external parameters. In regions 1 and 2 the film is uniformly magnetized respectively out-of-plane and in-plane. In region 3 the magnetization is canted for $L \ll \lambda$. For $L > \lambda$ patterned magnetic domains form. In region 4, $L \gg \lambda$ and the direction of the magnetization is alternating in the out-of-plane domains.*

The dipolar interaction affects the transition between regions 1 and 3 and regions 2 and 3 in different way. In fact, as pointed out by Elmers [75], the dipolar interaction scales with $\Delta\theta^4$ for $\theta \cong \frac{\pi}{2}$ and $\Delta\theta^2$ for $\theta \cong 0$, where $\Delta\theta$ is the angle between neighbor magnetic moments. As a consequence, since the exchange energy scales with $\Delta\theta^2$, the transition between the regions 2 and 3 is not influenced by the dipolar interaction. On the other hand, the transition between regions 1 and 3 changes under the action of the stray field. In particular region 1 reduces because the stray field tends to modify the magnetization profile. As explained in section 4.2 the role of the dipolar interaction increases with the thickness and thus region 1 further reduces. In the same way the gain in magnetostatic energy of the state with alternated out-of-plane magnetization shifts the

transition between regions 3 and 4 to lower values of $\frac{L_1}{\lambda_1}$ and $\frac{L_2}{\lambda_2}$ so that region 4 becomes larger.

Finally, also the effective anisotropy influence the border between different regions. In section 4.2 we showed that the softer the material is, the stronger is the effect of the stray field and thus the smaller is region 1. The energy density of the states with non-uniform magnetization belonging to region 3 reduces with the softness of the material, see Fig. 4.9. On the other hand, the energy density of the states of region 4 remains almost unchanged because it is dominated by the symmetry point so that the stray field hardly modify the magnetic profile. As a consequence, the softer the material is the smaller is region 4.

In conclusion of this section we take a brief overview to the scaling properties of the diagram in the framework of the anisotropy-type description. In section 4.2 we have defined two magnetic profiles whose shape is the same after re-scaling of the width of the unit cell as equivalent. The scale invariance of the system is obtained analyzing equations (4.11), (4.10) and (4.13). Equations (4.11) and (4.10) are invariant for $\frac{L_1}{\lambda_1} = a$, $\frac{L_2}{\lambda_2} = b$ and $\theta_0 = c$, where a , b , c are constants. The third condition can be substituted with $\frac{\lambda_1}{\lambda_2} = d$ by using equation (4.13). From the conditions of invariance it follows that each point of the diagram represent more than one state having equivalent magnetization profiles.

5.2 Spin reorientation transition

In thin films the breaking of symmetry at the surface generates an anisotropy that can favor either an in-plane or an out-of-plane magnetization [49]. In the first case the film is always in-plane magnetized because the shape anisotropy favors the same direction. In the second case the easy axis can turn from out-of-plane to in-plane with increasing thickness [50]. In fact, the contribution of the shape anisotropy extends all over the film thickness, while the influence of the surface anisotropy is confined to the two interfaces of the film. Also the increase of temperature can induce a reorientation of the magnetization from out-of-plane to in-plane. The reorientation is due to the different temperature dependence of the magneto crystalline anisotropy constant $k(T)$ and the shape anisotropy constant k_{sh} [88, 96]. With increasing temperature, the value of the crystalline anisotropy usually decreases more rapidly than the magnetization [89, 91]. As a consequence, if for $T = 0^\circ K$ the magnetization is perpendicular to the film surface, at a certain critical temperature T_R the system falls into a new state with magnetization parallel to the surface. An additional reason which brings the magnetization to be parallel to the surface is the increase in entropy [56, 89]. For small values of the temperature, i.e., $T < T_R$, the contribution of the entropy is negligible and the magnetization is perpendicular to the surface. For higher values of the temperature, i.e., $T > T_R$, the entropy is dominant and the magnetization is parallel to the surface [92].

The spin reorientation transitions (SRT) driven by the variation of the thickness or the temperature are widely studied and they are usually described in the framework of

the phenomenological uniform approach, see section 3.1. These transitions take place through either a state of canting or a state of coexistence. In the first case the transition is continuous, in the second it is discontinuous [68,123]. Note that the SRT involving magnetic domains can be also described in the framework of this approach [119]. This is valid if the wall width is much smaller than the domain width.

5.2.1 Lateral modulation of the anisotropy and SRT

In this section we show that the lateral variation of the anisotropy due to the presence of a capping material can induce a spin reorientation transition whose sharpness is a function of the density of the islands formed during the growth process.

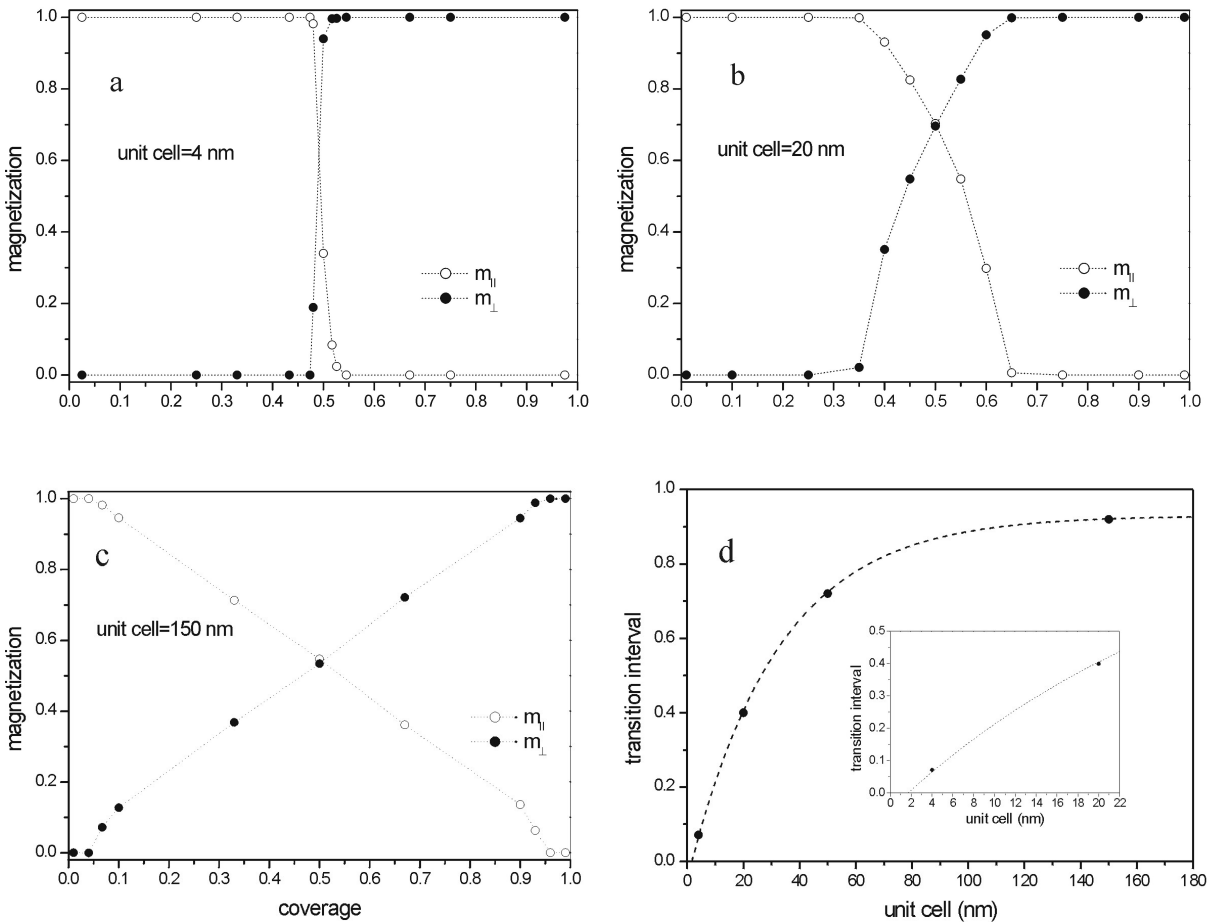


Figure 5.10: *Fig.a-c show the reorientation of the magnetization as a function of the coverage for various values of the width the unit cell. In each figure we plot the projection of average magnetization along the surface and along the normal to the surface, i.e., m_{\parallel} and m_{\perp} . The transition interval is the sharper the smaller the unit cell is, see Fig.d.*

The easy axis of a magnetic thin film can reorient either from in-plane to out-of-plane or vice versa [86, 93, 94] by deposition of a capping layer. In particular, if the coverage of the capping is partial (submonolayer coverage), i.e., $0 \leq L_1/L \leq 1$, the surface anisotropy changes only locally and a spin reorientation transition induced by the variation of the coverage can be expected [77]. The growth temperature is the fundamental parameter determining the size of the islands and thus the sharpness of the spin reorientation transition. In general, high density of small islands can be obtained at low deposition temperatures while bigger islands are obtained when the temperature is increased or the sample annealed [25, 95].

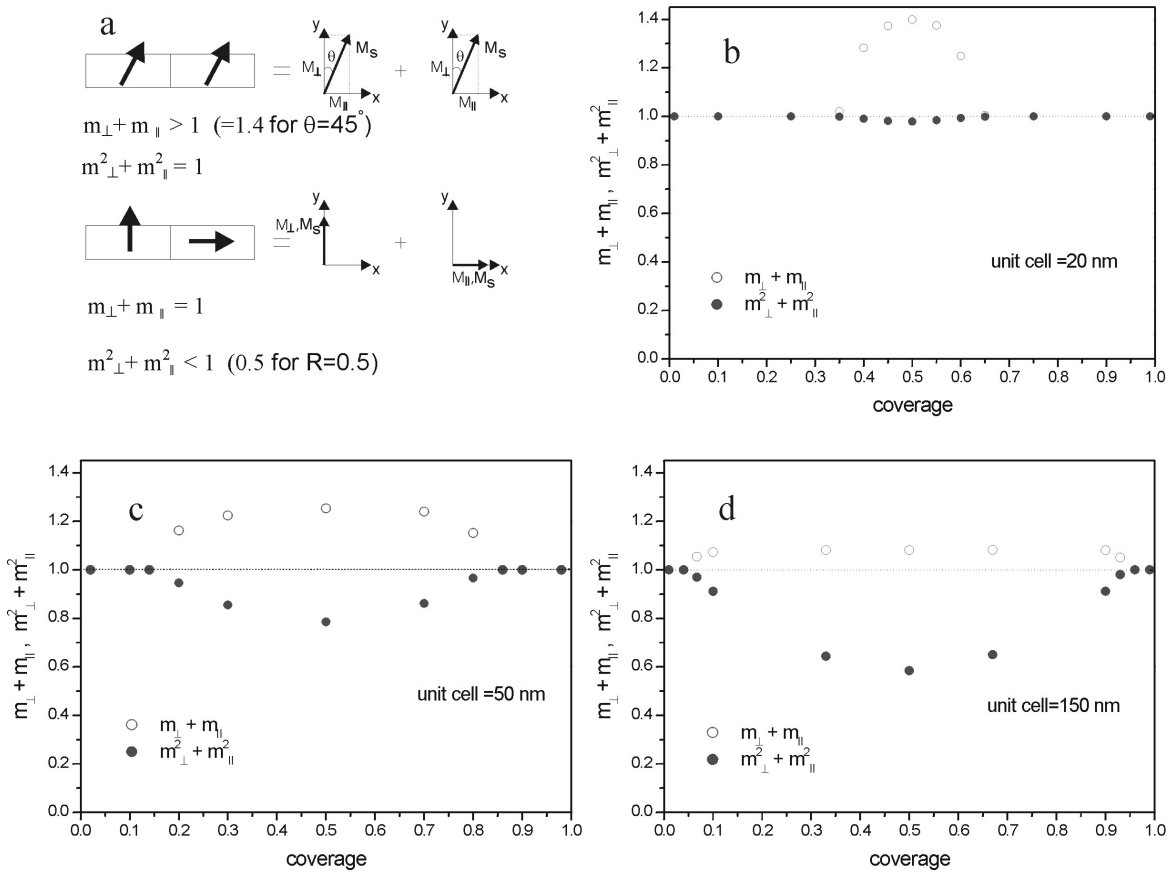


Figure 5.11: In Fig.a two states are sketched: the first of uniform magnetization, the second of non-uniform magnetization constituted by domains magnetized in-plane and out-of-plane. The quantities $m_{\perp} + m_{\parallel}$ and $m_{\perp}^2 + m_{\parallel}^2$ are macroscopic measures of the magnetic states. In Fig.b-d these quantities are plotted as a function of the coverage for various values of the unit cell. For $L = 20$ nm the magnetization is almost uniform along the entire coverage interval. By increasing the width of the unit cell the magnetization splits into magnetic domains due to the local variation of the anisotropies.

Let us study the SRT as a function of the submonolayer coverage and of the density of the stripes. For simplicity we analyze the 1-D case considering a unit cell of two stripes with periodic boundaries, as shown in the previous sections. The system considered is formed by 4ML Co on Pd(111) partially covered by island of Pd so that $k_{Pd}^{eff} = -k_{Co}^{eff} = 0.48 \cdot 10^7 \frac{\text{erg}}{\text{cm}^3}$. The width of the Pd stripes is L_1 ; the width of the Co stripe is L_2 . With increasing the submonolayer coverage, that we represent with $R = L_1/L$, the magnetization rotates from in-plane to out-of-plane. In Fig. 5.10a-c we show the results of numerical simulations performed for three different values of the unit cell. The magnetization is plotted versus the coverage. In particular we plot the average projection of the normalized magnetization along the surface and along the normal to the surface, i. e. $m_{\perp} = M_{\perp}/M_s = \sum_{i=1}^L m_{i,\perp}/L$ and $m_{\parallel} = M_{\parallel}/M_s = \sum_{i=1}^L m_{i,\parallel}/L$. In these formulas L is the width of the unit cell and i are the points in which it is divided. For $R = 0$ the film is magnetized in-plane which corresponds to region 2 in the diagram of the states of Fig. 5.9. By increasing the submonolayer coverage we move towards region 1 where the film is magnetized out-of-plane. From Fig. 5.9 it is evident that region 3 has to be crossed as the coverage increases. Therefore the state of non-uniform magnetization is involved and the reorientation is not discontinuous from in-plane to out-of-plane. The reorientation transition interval is defined as the submonolayer coverage to be added in order to reorient the magnetization from in-plane to out-of-plane. The interval is a function of the size of the unit cell and defines the sharpness of the transition, see Fig. 5.10d. The transitions reported in Fig. 5.10a-c are continuous and they are the sharper the smaller the unit cell is. In the limit of a wide unit cell the transition interval is directly determined by the magnetic characteristic length λ , i.e., $\varphi \sim 1 - 2\lambda/L$. In fact the minimum coverage necessary to rotate locally the magnetization direction is the ratio between magnetic characteristic length and width of the unit cell. The transition interval versus the width of the unit cell reduces with an exponential law. In the limit of small unit cell, i.e., $L \ll \lambda$ the transition tends to be discontinuous. Note that the narrowing of the transition interval corresponds to the reduction of the area of region 3 for values close to the origin of the diagram of the states, see Fig. 5.9.

The projections of the average magnetization can be used to study macroscopically the magnetic states involved in a reorientation transition [77]. If the magnetization is uniform the sum of the squares of the laterally averaged projections is equal to one, i.e., $m_{\perp}^2 + m_{\parallel}^2 = 1$, see Fig. 5.11. If the magnetization is alternating in-plane and out-of-plane the sum of the projections is equal to one, i.e., $m_{\perp} + m_{\parallel} = 1$. In Fig. 5.11b-d we plot the two sums as a function of the coverage. If the width of the unit cell is 20 nm, for $R \leq 0.35$ and $R \geq 0.65$ we have $m_{\perp}^2 + m_{\parallel}^2 = 1$. Therefore the magnetization is uniform. For $0.35 \leq R \leq 0.65$ the sum of the squares of the projections is close to one, $m_{\perp}^2 + m_{\parallel}^2 \approx 1$. This means that the magnetization is not completely uniform but slightly modulates due to the presence of the alternating anisotropies. The sum of the projections can be used to have additional information on the magnetization. In particular if the magnetization is almost uniform and its direction is at $\theta \simeq 45^\circ$ with respect to the normal the value of the sum is $m_{\perp} + m_{\parallel} \simeq 1.4$. Since in our example the effective anisotropies balance this

value is obtained for a coverage $R = 0.5$, for a width of the unit cell $L = 20$ nm. By increasing the width of the unit cell, see Fig. 5.11c-d, the interval of coverage in which the magnetization is uniform becomes narrower. Besides, $m_{\perp} + m_{\parallel}$ decreases showing the formation of magnetic domains due to the alternating anisotropies. A way to measure the splitting of the magnetization in magnetic domains is given by $m_{\perp}^2 + m_{\parallel}^2$. The minimum is obtained for $R = 0.5$. In this case splitting is maximum and the role played by the domain walls between successive domains is negligible.

Summarizing, in this section we have studied the spin reorientation transition driven by coverage variation in magnetic thin films with alternating anisotropies. The sharpness of the transition is a function of the density of the stripes and it involves different kinds of magnetic states. The transition is always continuous and it is as sharper as higher the density of the stripes is. During the spin reorientation, if the width of the unit cell is much smaller than the magnetic characteristic length, i.e., $L \ll \lambda$, the magnetization is only slightly non-uniform; if the width of the unit cell is much larger, i.e., $L \gg \lambda$, a patterned domain configuration form.

5.3 In-plane patterned domains

In this section we extend the analysis performed for systems with alternating in/out-of-plane uniaxial anisotropies to systems with patterned in-plane anisotropies. The main difference between these systems is the role played by the dipolar interaction that can determine the formation of magnetic domains. We have seen that in the monolayer regime the gain in magnetostatic energy vanishes and the single domain becomes favorable. In this limit magnetic domains form if the anisotropies modulate on a scale much bigger than the magnetic characteristic length of the system, i.e., $L \gg \lambda$. Similarly, thin films in-plane magnetized as single domain can split up into sub-structures if $L \gg \lambda$. Note that theoretically thin films with in-plane anisotropy are predicted to be single domain [88], as found experimentally for various systems [121, 122].

5.3.1 Experiment and micromagnetic simulation of Fe on W(001)

The magnetic anisotropy can be patterned on the nanometer scale by controlling the strain relief [4]. In this section we show how the magnetic properties of a thin film change as a function of the scale of the pattern. In particular we show that the coercivity and the anisotropy field can be varied on a wide range of values and that the state of magnetization depends on the scale considered. These experimental results, obtained for the system Fe/W(001), fully support the theoretical analysis developed in the previous chapters for systems with alternating in-out-of-plane effective anisotropies.

The growth mode of Fe on W(001) is a function of the temperature. At around 400 K the STM analysis reveals layer-by-layer growth. Below 6 ML, MOKE measurements show that the film is in-plane magnetized with a four-fold magnetic anisotropy with easy

directions along the $\langle 110 \rangle$ directions. The lattice mismatch causes a tensile strain of 10.4% in bcc Fe on W(001). Above 4 ML the strain is partially relieved by the formation of dislocation bundles along the $\langle 100 \rangle$ directions, see Fig. 5.12 [4]. As a consequence the four-fold symmetry breaks down locally and is substituted by an uniaxial anisotropy directed along the dislocation lines. In particular, the strain relief takes place where the film is locally 5 ML thick and islands in the $\langle 100 \rangle$ directions are formed. Since the dimension of the islands is a function of the growth temperature [95], the density of the stripes that constitute the network can be tuned, as shown in Fig. 5.12.

Now we correlate the film structure to the macroscopic magnetic properties by measuring the in-plane hysteresis loops in the $\langle 110 \rangle$ and $\langle 100 \rangle$ directions. In Fig. 5.13 we report the loops obtained with the MOKE technique for the films in Fig. 5.12. The typical size of the network, i.e., the unit cell of the structure, is $L = 5$ nm (loop on the left side) and $L = 40$ nm (loop on the right side). The easy axis is the $\langle 110 \rangle$ direction, as shown by the loops in black. Since for $L = 5$ nm the remanence is smaller than one, i.e., $R_{\langle 110 \rangle} = 0.84$, we deduce that around $H = 0$ Oe magnetic domains form. For the same reason the remanence measured in the $\langle 100 \rangle$ direction is $R_{\langle 100 \rangle} = 0.59$ instead of $R_{\langle 100 \rangle} = 0.71$, value obtained for a film uniformly magnetized in the $\langle 100 \rangle$ direction. By increasing the external field the film reaches the saturation after coherent rotation from the $\langle 110 \rangle$ to the $\langle 100 \rangle$ direction.

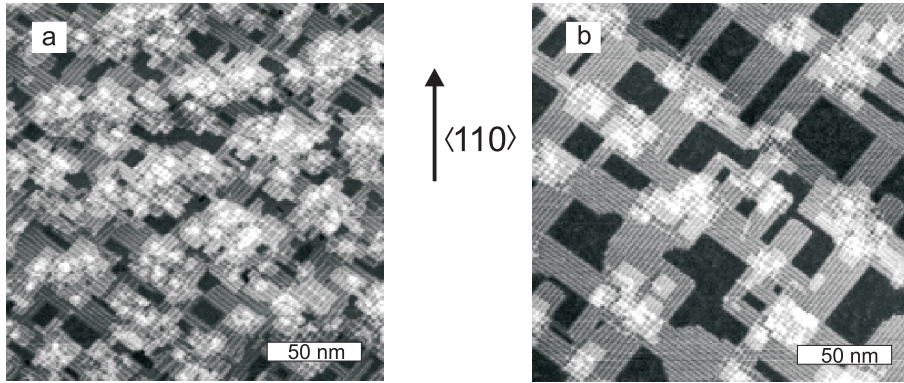


Figure 5.12: *STM images of Fe films on W(001) deposited between ≈ 360 and ≈ 440 °K. The network, that is 5 ML high, is formed by stripes elongated in the $\langle 100 \rangle$ directions. The anisotropy is uniaxial inside the stripes, directed along their main extension, and 4-fold in the rest of the film, in the $\langle 110 \rangle$ direction. In the figure the width of the stripes increases with the temperature, from picture a to b. (Images taken from [4])*

The main differences between the loops calculated for $L = 5$ nm and $L = 40$ nm is the increasing of the coercive field and of the anisotropy field. The coercivity as a function of the pattern size is reported in Fig. 5.14a. It increases exponentially, steeply around $L = 75$ nm. Interestingly this length is equal to the width of a 90° -Néel wall [4]. These

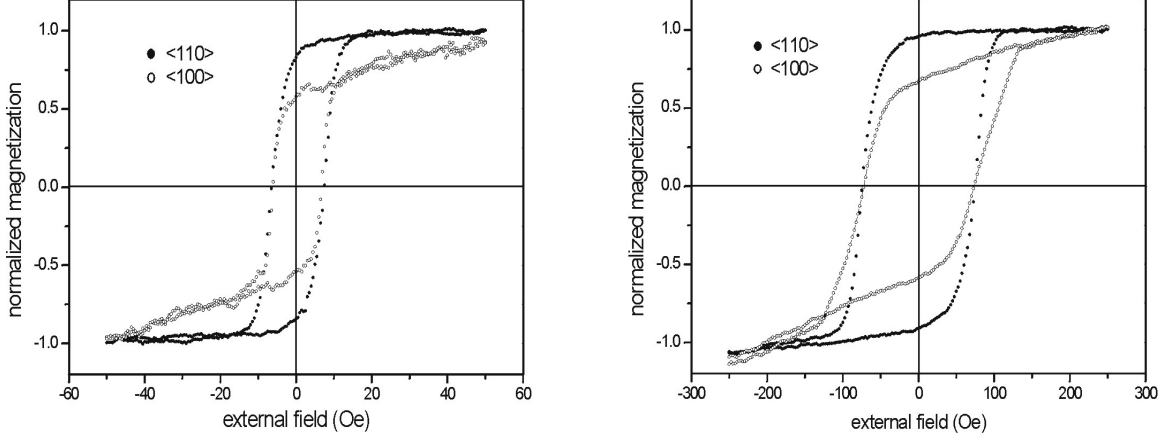


Figure 5.13: *Hysteresis loops obtained by means of MOKE measurements. The loops refers to the films of Fig. 5.12. The unit cell is $L = 5$ nm (loops on left) and $L = 40$ nm (loops on right). Each figure shows the loops measured in the $\langle 110 \rangle$ direction (black dots) and in the $\langle 100 \rangle$ direction (open dots). (The loops were kindly provided by W. Wulfhekel)*

data can be interpreted as follow. For $L \ll \lambda$ the exchange energy dominates keeping the magnetization uniform. The material is soft and the coercive field smaller than 50 Oe. For $L \gg \lambda$ the magnetization adapts to the constriction of the anisotropies. As a consequence the material becomes harder, as already shown in chapter 3 for systems with alternated anisotropies.

The above analysis is based on average quantities, as obtained by means of MOKE measurements. By means of micromagnetics we can have a deeper insight into the magnetism of these systems. Our goal is to relate the macroscopic picture as obtained by MOKE with the microscopic one obtained by computer simulation. In the following we investigate the anisotropy field as a function of the pattern size. The unit cell used simulate the network of Fig. 5.12 is drawn in Fig. 5.15a. The figure contains four segments formed by regions with four-fold anisotropy (4 ML thick areas) and by regions with uniaxial anisotropy (5 ML thick areas). The values of the anisotropy constants are respectively $k_4 = 0.44 \text{ M} \frac{\text{erg}}{\text{cm}^3}$, as measured by MOKE in flat films of 4ML, and $k_u = 1 \text{ M} \frac{\text{erg}}{\text{cm}^3}$, as measured by a highly sensitive optical deflection technique combined with MOKE [125]. The coverage is $\varphi = 0.82$, close to the experiment as deduced from Fig. 5.12. Boundary conditions are imposed to simulate the infinity of the film. The starting condition for the simulation is a single domain state along the $\langle 110 \rangle$ direction, that is the easy axis for $L = 5$ nm and $L = 40$ nm as shown in Fig. 5.13. Fig. 5.15b-d give the result of the simulation, respectively for a unit cell of $L = 5$ nm, $L = 40$ nm and $L = 250$ nm. As supposed above the magnetization is uniform for $L \ll \lambda$ and non-uniform for $L \gg \lambda$. From these states obtained at remanence we calculate the anisotropy field by applying an external magnetic field in the $\langle 100 \rangle$ direction. The anisotropy field obtained as a function

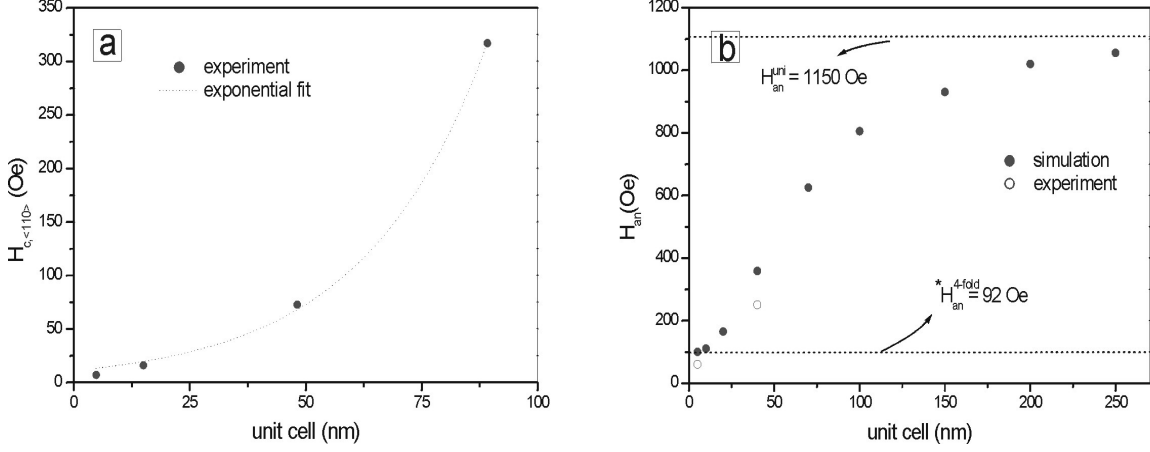


Figure 5.14: The plot on the left side shows the coercive field versus the width of the unit cell. The measurement is performed in the $\langle 110 \rangle$ direction. The plot on the right side gives the anisotropy field as a function of the width of the unit cell. These values are obtained by increasing the external field in the $\langle 100 \rangle$ direction until saturation.

of the unit cell are plotted in Fig. 5.14b. For $L \ll \lambda$ on each magnetic moment acts the same average anisotropy, that is in the $\langle 110 \rangle$ direction. In fact the average uniaxial anisotropy points in the $\langle 110 \rangle$ with an intensity that is a function of the scale of the system, see Fig.3.10. As a consequence for $L \ll \lambda$ its contribution is not important and only the four-fold anisotropy survives. The anisotropy field of a flat film with four-fold anisotropy $k_4 = 0.44 \text{ M} \frac{\text{erg}}{\text{cm}^3}$ in the $\langle 110 \rangle$ direction is $H_{an} = 510$ Oe. Since the region with four-fold anisotropy is only 18% of the entire film, the value of the effective anisotropy is $*H_{an}^{4-fold} = 0.18 * 510 \text{ Oe} = 92 \text{ Oe}$, as shown in Fig. 5.14b. For $L = 40$ nm, see Fig. 5.15c, the magnetization is not completely uniform and starts to follow the constriction of the anisotropy. Stripes elongated in different directions start to be magnetically decoupled and the contribution of the uniaxial anisotropy is no more negligible. For $L \gg \lambda$, see Fig. 5.15d, the magnetization follows more clearly the anisotropy so that the initial single domain state transforms in a multi-domain state. The value of the anisotropy energy becomes a function of the position and the anisotropy field tends to the value obtained for a flat film with uniaxial anisotropy $k_u = 1 \text{ M} \frac{\text{erg}}{\text{cm}^3}$, i.e., $H_{an} = 1150$ Oe.

In conclusion, we have shown that controlled partial strain relief can be used in Fe/W(001) to locally pattern the magnetic anisotropies. In these films the macroscopic magnetic analysis based on MOKE measurements shows a rapid increase of the coercive field and of the anisotropy field as a function of the scale of the system. These macroscopic properties can be explained by studying the system at microscopic level. In this way we have found that for small values of the scale of the system, i.e., $L < \lambda$, the exchange energy dominates leading to a uniform magnetization, while as soon as the scale of the system exceeds the magnetic characteristic length of the system, i.e., $L > \lambda$, the

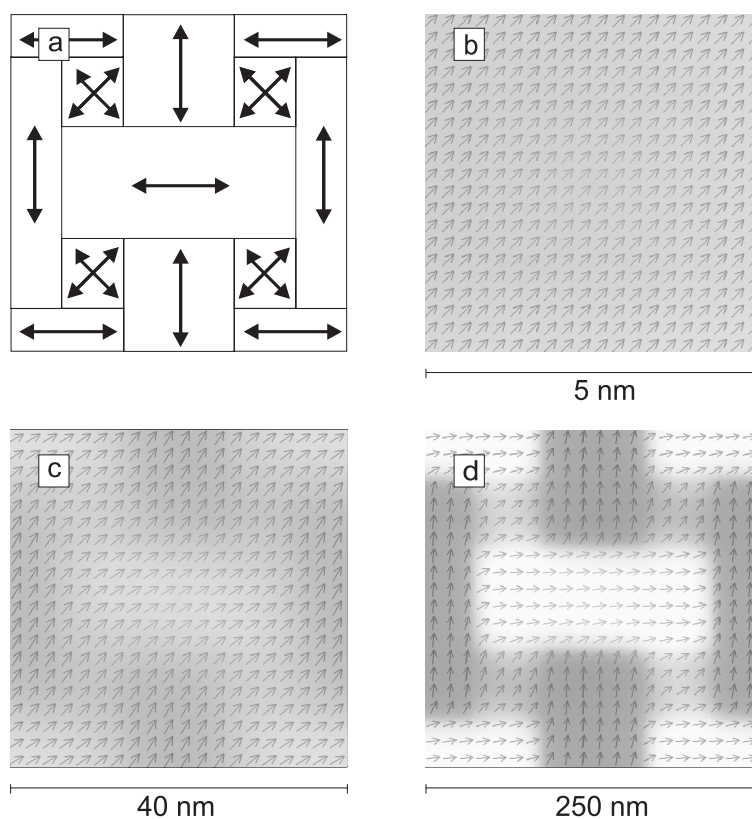


Figure 5.15: *Relation between scale of the pattern and magnetization. Fig.a, that sketches the anisotropy directions, contains four unit cell. The uniaxial anisotropy is in the $\langle 100 \rangle$ directions. The 4-fold anisotropy is in the $\langle 110 \rangle$ directions. Fig.b-d give the result of the micromagnetic simulation. By increasing the dimension of the unit cell the magnetization varies from a state of single domain to a state of multi-domains. The gray scale is associated to the directions of the magnetic moments indicated by the arrows.*

anisotropy energy dominates favoring the formation of in-plane structures in the 100 nm range.

Chapter 6

Discussion and conclusion

6.1 Introduction

In ultrathin films with spatially varying magnetic anisotropies the magnetization is forced to follow the constriction of the anisotropy. The relative importance of the various energy terms is a function of the scale of the anisotropy patterning. For a geometric scale of the patterning (indicated with L) smaller or comparable to the magnetic characteristic length (indicated with λ) the magnetic configuration is modulated. For a geometric scale much bigger than the magnetic characteristic length large regions of uniform magnetization are separated by domain walls.

At this point we can notice two important facts. The first is that the patterning of the anisotropy may induce regions with uniform magnetization separated by walls. This is interesting because ultrathin films with uniform perpendicular anisotropy are predicted to be single domain [21, 38, 40], as found experimentally [22]. Here magnetic domains induced by the patterning of the anisotropy can form, even if the stray field is insufficient to form them. In these structures, the role of the stray field has to be carefully evaluated. On the one hand, the film is too thin to permit a spontaneous formation of magnetic domains. On the other hand, the stray field may determine the direction of the magnetization inside the regions with uniform magnetization for $L \gg \lambda$, i.e., when the walls do not dominate. The second fact to be considered is that states with modulated magnetization may appear when the walls dominate, i.e., for $L \leq \lambda$. In this case the dipolar interaction will play a marginal role and the magnetic configuration is totally determined by the values of the anisotropy and the exchange. This magnetic configuration is somehow similar to the one obtained in the regime of the spin reorientation transition where the shape anisotropy compensates the surface anisotropy. The difference is the origin of the two structures. In fact, in the first case the magnetization is determined by the stray field at compensation of the two anisotropies. In the second case the configuration is due to the local variation of the anisotropies pointing in different directions. Summarizing, these arguments tell us that two kinds of magnetic configurations may be expected as a function of the geometric scale of the system: a modulated state and a multi-domain state, both induced by the local

variation of the anisotropy. In particular, we may notice that the modulated state shall transform in a single domain state if one of the local magnetic anisotropies is dominant.

In this work, the state of lowest energy as a function of the system parameters has been calculated by solving the micromagnetic equation of Brown associated to our problem. This has been done by using two levels of approximation. In the first the dipolar interaction is considered anisotropy-like and the calculations are performed analytically ('anisotropy-type' description). In the second the dipolar interaction is fully considered and the analysis is numerical ('fully dipolar interaction' description). In the 'anisotropy-type' description the dipolar energy takes the form of a "local" quantity. In literature this description is often used under the assumption that either the magnetization is uniform [23, 54] or the film thickness is negligible [75]. In general for films with spatially varying magnetic anisotropies we expect to have a non-uniform magnetization. However, the 'anisotropy-type' description may be used to study the modulated configuration because in this limit the exchange and the anisotropies determine the structure and because we study films only a few monolayers thick. In principle this approximation can be used also to study the magnetic domains induced by the anisotropy patterning. Nevertheless this choice could be a limit because states with stripes magnetized parallel ('up-up' configuration) would have the same energy of states with stripes magnetized anti-parallel ('up-down' configuration). Therefore in order to study the system for large scales, i.e., $L \gg \lambda$, the more suitable 'fully-dipolar interaction' description was used.

6.2 Discussion

In order to make the reading easier the discussion is grouped in four subsections. Some of the points discussed, like the canting, rigidly belong to one subsection. Some others, like the spin reorientation transition, are analyzed in various subsections.

6.2.1 Characterization

The macroscopic investigation based on the analysis of the hysteresis loops calculated numerically reveals two types of magnetic behaviour as a function of the scale of the system (section 3.2.2). If the width of the unit cell is smaller or comparable to the magnetic characteristic length the stripes are tightly exchange coupled. If it is larger the stripes are weakly exchange coupled. This behavior is different from the one shown by the system of nanostripes of Fe on W(110) intensively studied in the last years [6, 17]. In this case the stripes with out-of-plane anisotropy show an anti-parallel arrangement of magnetostatic origin [135]. The period of the system (about 10 nm) is too narrow to allow any rotation of the magnetization, if the measured anisotropy constant and the bulk value of the exchange stiffness are used. In subsection 6.2.4 we discuss how to lift this contradiction. However, the anti-parallel arrangement indicates that the stripes are weakly exchange coupled, like we expect to have for large scales of the system. The

coercive field of weakly exchange coupled stripes of the experiment (narrow period) can be compared with the one of the simulation (large period). The coercive field in the experiment is two orders of magnitude smaller than for the simulation. In the first case the system is soft, in the second is hard. The difference may be explained by the kind of magnetization process. In the simulation the rotation is coherent. In the experiment probably it takes place through domain wall motion. Actually, spin-polarized tunneling spectroscopy images reveal that the stripes are subdivided in domains with walls directed perpendicularly to the stripe elongation [136]. We remark that the anisotropy of the in-plane stripes has the same direction of the walls and therefore it encourage their formation. In our case, no preferential direction is imposed in-plane and we find single domain out-of-plane magnetized stripes. The difference plays an important role in view of a possible utilization of nanostripes as perpendicular recording media where each stripe correspond to one bit.

The magnetic properties of the system studied in this thesis are a function of its scale. In particular the coercive field decreases with the scale of the pattern. This behavior is due to a compensation of the local anisotropies that average out with scale decrease. At macroscopic level we can compare thin films with locally varying magnetic anisotropies with magnetic materials formed by grains [26, 28]. In these materials, if the grain size is sufficiently small the exchange acts not only inside each grain but also from grain to grain. As a consequence the exchange coupling tends to align the magnetization of neighbor grains in the same direction. Groups of grains form regions of uniform magnetization characterized by a local effective anisotropy whose value is a function of the grain size. The scale dependence of the effective anisotropy is reflected on the coercive field that decreases with the grain size [126]. Also the coercive field of Fe on W(100) with anisotropies locally patterned by partial strain relief is a function of the scale of the system (sec. 5.3.1) [4]. The film is made of regions with uniaxial anisotropy of easy axis along the $\langle 100 \rangle$ directions and of regions with four-fold anisotropy with easy axis along the $\langle 110 \rangle$ directions. The system is in-plane magnetized and the coercive field increases with the scale of the anisotropy pattern. The trend is coherent with the one shown by polycrystalline magnetic materials. However, in Fe on W(100) with anisotropies locally patterned the coercive field increases with exponential law, while in polycrystals it increases with power law L^6 (here L is the grain size) [126].

The macroscopic analysis outlines the main characteristics of the system, but it does not explain them. A deeper understanding can be achieved at microscopic level by spatial investigation of the magnetization. In particular in this thesis, the macroscopic picture obtained with the analysis of the hysteresis loops is explained at microscopic level by means of micromagnetic calculations. For Fe on W(110) with in-plane patterned anisotropies micromagnetics indicates that for $L \ll \lambda$ the uniaxial anisotropy averages out and a state of uniform magnetization determined by the four-fold anisotropy forms. For $L \gg \lambda$ the magnetization adapts to the constriction of the anisotropies and in-plane patterned structures in the 100 nm range form. The averaging out for small scales looks like the compensation mechanism between different anisotropies obtained in thin films in the regime

of the spin reorientation transition [54, 61], but it is different from the one taking place in polycrystalline materials. In the latter case the effective anisotropy is given by the average of anisotropies locally random directed. In films with patterned anisotropies the average is between locally well defined directions. The difference between the two systems leads to the two mentioned power laws. Nanocrystals embedded in matrix give rise to a broad range of coercive fields as a function of the grain size and of the anisotropies of the materials used. The difference in coercivity is due to the nanostructure rather than to the composition [127]. Also the examination of exchange coupled multilayers shows that the properties of the system strongly depend on the microstructure [100]. By partial capping and patterning techniques it is possible to obtain compound ultrathin films that are expected to show a variety of magnetic behaviors. The investigation of the magnetization process as a function of the scale and the composition has not yet been performed and is a challenge for future studies.

6.2.2 Uniform magnetization

The analysis of the hysteresis loops for films with spatially varying magnetic anisotropies indicates that in the limit of small scales of the patterning the system behaves like a uniformly magnetized single particle. In this limit, we have modeled the system by means of a second order anisotropy constant. The direction of the magnetization, either in-plane or out-of-plane, is determined by the weight of the two stripes (sec. 3.2.3). A reorientation of the easy axis is induced by coverage increase. Experimentally this transition has been observed for Fe on Cu(100) capped by submonolayer films of Co [77]. In this experiment the order of the transition has not been investigated. From our model, based on the assumption of uniform magnetization, a first order spin reorientation transition is expected. The study of magnetic thin films in proximity of the transition point is important from a fundamental point of view and for the applications. Samples with controllable easy axis may be used as switches. In particular at the critical point of compensation of the anisotropies completely soft magnetic samples might be obtained. In the past, the study of fcc Fe on Cu(100) using spin-polarized secondary-electron spectroscopy showed a vanished remanent magnetization in the regime of the spin reorientation driven by temperature increase [129]. SEMPA measurements showed that the absence of remanence is due to the formation of magnetic domains [64]. In other systems, Fe on Ag(100) for instance [115], higher order anisotropies shows up at compensation. In these cases the magnetic system is not completely soft. The numerical investigation of our system shows that at compensation a state of canting appears and the model based on the second order anisotropy fails. The canting can be described by a higher order anisotropy term due to the microstructure. The value of the fourth order anisotropy constant decreases with the scale of the system, but it never vanishes. As a consequence the hardness of the material may be engineered tuning the scale and the coverage of the system, but the magnet is never completely soft. This behavior is similar to the one obtained by MOKE measurements for films of Co on Cu(110) exposed to CO and partially capped by Cu [70]. In

this case an absence of remanence was measured at room temperature at compensation. This result cannot be obtained with our calculations because they are performed at zero temperature.

By weighting the anisotropies out of the point of compensation magnets of the wished hardness may be created. In order to engineer the hardness of the sample it is necessary to know the values of the anisotropy constants. As it will be discussed later, these constants may be obtained by comparison of the analytical solution of the micromagnetic problem with the magnetization profiles measured in experiments.

6.2.3 Modulation

The state of canting has been explained neither by the macroscopic analysis nor by the model based on the assumption of uniform magnetization. The next step is to consider the magnetization as non-uniform. This is essential not only to study the system in the regime of canting, but also in the regime of modulation, i.e., for small scales outside the compensation, and for large scales where the magnetization is free to adapt to the constriction of the anisotropy patterning. For simplicity we modeled the system in one-dimension. Brown and Shtrikman showed that in a one-dimensional homogeneous ferromagnet all the solutions in which the magnetization is non-uniform are unstable [36]. As a consequence a second dimension had to be considered to study systems containing walls [27]. At this point it has to be remarked that the stability of our analytical solution in absence of an applied external field is guaranteed by the non-homogeneity of the anisotropy.

The analytical solution of the 1-D problem is given in the framework of the 'anisotropy-type' description (sec. 4.1). By solving the equation of Brown we obtained the magnetization profile and the expression of the energies as a function of the system parameters. The solution of the problem shows that for $L \leq \lambda$ the magnetization is uniform if one of the effective anisotropies dominates (as modeled by means of second order anisotropies) while it is non-uniform if they balance. Therefore the macroscopic picture is coherent with the micromagnetic analysis only if one of the effective anisotropies dominates. Otherwise the magnetization slightly oscillates around an average value that macroscopically appears like a uniform canting. Therefore the origin of this state is related to the oscillation and thus to the spatially alternating anisotropies. Later in this section we will discuss this relation in the framework of a simplified model. At this point we underline that this result is obtained in the framework of the 'anisotropy-type' description. As a consequence the dipolar interaction does not play any role in the formation of the magnetic microstructure that is rather due to the balance between the exchange and the effective anisotropies.

The problem of the determination of the geometrical size under which the sample is uniform magnetized was solved by Brown in the case of fine particles with uniaxial anisotropy [19]. The author rigorously proved that a sphere is uniformly magnetized below a certain critical radius determined by the exchange and the anisotropy constants. In the case of thin film, Thiaville and Fert showed that for transition metals the magnetization is either in-plane or out-of-plane, but never modulated (or twisted) in the vertical direction

[23]. In this case, in spite of the local variation of the anisotropy the exchange stiffness constant is considered to be strong enough to keep all the magnetic moments aligned in the same direction. This result allowed us to reduce our analysis to one-dimension, i.e., the magnetization is considered to vary only laterally. The first author who addressed the problem for ultrathin films with laterally varying magnetic anisotropies was Elmers, who calculated the transition point to the uniform configuration using the Jacobi criterion [75]. This result defines the regions of uniform and non-uniform magnetization, but does not clarify how the transition point is reached. By means of the solution given in section 4.1.1 it is possible to study the magnetization profile as a function of the driving parameter of the transition. For example the transition between non-uniform and uniform magnetization may be studied by shrinking the scale of the system. Later in the discussion we will consider the transition between uniform states (from in-plane to out-of-plane) as a function of the coverage and of the scale of the system. These transitions are continuous because they involve the state with modulated magnetization.

The comparison of the analytical solution with the magnetization profile obtained experimentally by laterally resolving techniques [10–12] allows the direct determination of the anisotropy constants. In general, the magnetic anisotropy can be deduced from the dynamic or the static response of the magnetic system [104]. The methods used to measure the dynamic response, the ferromagnetic resonance (FMR) [62, 105, 106] and the Brillouin light scattering (BLS) [107, 113] need a sophisticated experimental set-up. The static response can be measured by torsion oscillating magnetometry (TOM) [50, 116] or by the magneto optic Keer-effect (MOKE) [117]. This last method is the most widely used, but is limited because very large external fields are necessary to saturate the material [118]. If the magnetization direction is a function of the thickness, it is possible to calculate the anisotropy constants studying the system in the regime of the spin-reorientation transition. This method, proposed by Oepen et al. [119], is based on the direct imaging of different magnetic phases obtained in wedge-shape samples of increasing thickness. Another possible spin-reorientation mechanism is the one induced by the capping of the film with an additional overlayer. The critical thickness at which the transition takes place is function of the relative thickness of the two layers. From this dependence it is possible to extract the anisotropy constants of the system [94]. The method that we propose is based on the same physical effect, but only a modulation of the magnetization and not the complete reorientation is considered. The advantage of our approach is that a single deposition is sufficient to determine the anisotropy constants in the as grown state by the direct comparison of the analytical solution with the magnetization profile obtained experimentally. Besides, once the sample has been prepared, the study of the temperature dependence of the anisotropy constants becomes immediate since it is sufficient to map the evolution of the magnetic profile during the increasing of temperature.

A simplification of the one-dimensional micromagnetic model in the limit of small scales of the system can be given considering the magnetization as non-uniform (sec. 3.2.3). Inside each stripe the magnetization is assumed to be uniform and described by a single magnetic moment. At compensation each magnetic moment spilt following the direction

of the local anisotropy. As a consequence, a fourth-order anisotropy term appears that describes the canting due to the magnetic microstructure. In literature many systems are described in the framework of the phenomenological model based on uniform magnetization [54]. In this case both the surface and the bulk contribute to the second and the fourth order anisotropy terms. Usually, due to the thickness or the temperature increase the canting shows up at compensation between surface and shape anisotropies. In flat films like Fe/Ag(100) [115] or Co/Ho [58] and in stepped systems like Ni/Cu(100) [110] the canting can rise from higher orders of the bulk magnetic anisotropy. We underline that in thin films with spatially varying magnetic anisotropies the fourth order term is not introduced to describe the canting found macroscopically, but it is the result of the alternating anisotropies. Therefore, the fourth order is a consequence of the microstructure, i.e., a geometric property, and is not directly due to the crystalline anisotropy, i.e., a material property. This is the result of the micromagnetic analysis. Of course the system may be described as well at macroscopic level. In this case the modulation of the magnetization is neglected and a fourth order term is introduced ad hoc to describe the reorientation of the easy axis. As soon as the scale of the system increases, the modulation cannot be neglected anymore. As a consequence the phenomenological model used in literature for uniform magnetized systems is no more feasible to describe the system.

As mentioned, in thin films with magnetic anisotropy locally changed by the presence of a capping material a spin reorientation transition (SRT) can be induced by the variation of the coverage [77]. In the 1-D case of stripes with alternating anisotropies we have studied the SRT induced by coverage variation as a function of the density of the stripes (sec. 5.2.1). We have found that the sharpness of the transition is a function of the density of the stripes, it is always continuous and is the sharper the higher the density of the stripes is. This investigation has been performed for films magnetically flat, but is in principle valid also for films with roughness. In this case the local variation of the anisotropy is due to the thickness dependence of the anisotropy constant. In general the presence of the roughness leads to a dipolar surface anisotropy that may be not negligible [111]. The effect is due to the magnetic charges located at the steps' discontinuities. If the magnetization rotates along the steps, like in our case, the effect is not present. In other geometries, like in Fe growth on stepped W(110) [6], the magnetization rotates perpendicularly to the steps. Therefore the dipolar surface anisotropy contributes to the magnetostatic energy. The correction is a function of the average deviation from ideal flat film and lateral size of the flat areas. In the regime of the SRT islands with in-plane anisotropy appear in a film out-of-plane magnetized. In this case, if the size of the islands is smaller than the exchange length the film is uniformly out-of-plane magnetized. If the islands are larger than the exchange length the magnetization rotates in-plane. However, the effect of the dipolar surface anisotropy should be negligible because the extension of the islands is of some nanometers [9] while the step discontinuity is of atomic order. The presence of islands has the same qualitative effect if the material is the same of the underlayer or not. Therefore the SRT induced by the lateral variation of the anisotropy is always possible. The question is weather this reorientation mechanism plays a role in the SRT driven by

the thickness or temperature increasing. In many systems [64, 67, 119] magnetic domains induced by the dipolar interaction are observed in the regime of the spin reorientation transition. In these systems the local variation of the anisotropy may contribute to the nucleation of the domains in the first stage of the transition. However, the role of the anisotropies is marginal in comparison with the one of the dipolar interaction. The SRT induced by the local variation of the anisotropy can be studied only far away from the point of compensation between shape and crystalline anisotropies, i.e., where no domains induced by the dipolar interaction are expected.

At the end of this section, we mention that in literature stripes domains due to a modulation of the magnetization around an average values are reported also for Fe-Ni alloy thin films [28]. In this system the magnetization rotates just a few degree from the average. The configuration is due to the balance between perpendicular anisotropy and stray field. We remark that in our case, the origin of the canting is exclusively the local variation of anisotropy, while the role played by the dipolar interaction is not important.

6.2.4 Patterned magnetic domains

Patterned magnetic domains form if the geometric scale of the system is larger than the magnetic characteristic length. In this case, the exchange is no more dominant and the magnetization is free to follow the constriction of the anisotropy patterning. Such a configuration has been obtained in Co/Pt multilayers patterned by ion-beam irradiation [108]. The film was initially magnetized out-of-plane. After irradiation alternatively in-plane and out-of-plane regions were detected. This state is metastable, but not the lowest in energy. Actually our investigation shows that different magnetic configurations are possible. For small scales of the system the state with stripes parallel magnetized ('up-up' configuration) is the lowest in energy. For large scales the state with stripes anti-parallel magnetized ('up-down' configuration) is the lowest (sec. 5.1). The transition between the two configurations is driven by the dipolar interaction that favors the 'up-down' state. A system in which the dipolar interaction leads to the 'up-down' configuration is Fe growth on vicinal W(110) crystal [6]. In this system 1ML stripes with in-plane easy axis and 2 ML stripes with out-of-plane easy axis Fe grow in step-flow mode parallel to the step edges of the substrate. The periodicity of the system is about 10 nm and the anisotropy constants determined by magnetometry. In order to explain the micromagnetic structure, Elmers *et al.* [82] assumed a value of the exchange stiffness constant one order smaller than the bulk value. Spin-polarized scanning tunneling spectroscopy measurements confirm the existence of the 'up-down' configuration [17] and show that the magnetization profile can not be explained with the assumption of Elmers, since the analysis of walls in the 2 ML stripes lead to estimate the value of the exchange stiffness constant like in bulk. The solution may be given by considering different values of the exchange constant in the stripes with 1 ML or 2 ML. If the constant in the 2 ML stripes is assumed like in bulk and much smaller in the 1 ML stripes, neighbor stripes are weakly exchanged coupled. As a consequence the magnetization in the 1 ML stripe is completely in-plane, as measured

in the experiment [17]. We remark that a recent measure in 1 ML in-plane magnetized stripes leads to a value of the exchange stiffness much smaller than in bulk [137], proving our assumption.

Now we discuss the possible utilization of thin films with spatially varying magnetic anisotropy as high-density magnetic storage media. The increase in the capacity of the conventional granular recording media is due to the reduction of the grain size [109]. This leads to a critical size under which the grain is superparamagnetic, i.e., the magnetization direction is not defined. In order to overcome this limit single magnetic objects like dots or pillars have been designed by lithography and etching techniques [2]. The thermal stability of the object is determined by the blocking temperature, i.e., by the anisotropy and the volume of the particle. Since the media is made of a collection of objects, the magnetostatic coupling has to be considered. It has been shown that the coercive field of an ensemble of Ni nanowires is a function of the number of wires [112]. Therefore neighbor objects influence one another. Of course, in order to store the bit information the coupling has to be sufficiently small to avoid the rotation of the magnetization. This condition is fulfilled in ultrathin films with spatially varying magnetic anisotropies, because the role of the dipolar interaction is negligible, as proven by the comparable energy of the 'up-up' and 'up-down' states (sec. 4.2). The writing process should be easy, known the anisotropy of the stripes out-of-plane magnetized. The reading process might be more difficult because of the weak magnetostatic field created by the stripes. We remark that the thermal stability of the stripes is guaranteed by their infinite length. In fact, since the thickness of the stripes is in the monolayer regime and their width is of the order of 10 nm, their length has to be at least of the order of 100 nm. Moreover, in the out-of-plane stripes we can exclude domains' formation that leads to a non divergence-free configuration. The uniform magnetization of the stripes, that results from our simulations, is a necessary condition in order to store one bit information inside each stripe. It may be remarked that patterned magnetic domains induced by the local variation of the anisotropies are possible only in the limit of ultrathin films where magnetic domains induced by the stray field may be excluded, at least at low temperatures [21, 22].

The various magnetic configurations obtained as a function of the system parameters are summarized in a diagram of the states (sec. 5.1.3). In literature similar diagrams have been proposed by Thiaville and Fert [23] and by Elmers [75]. These diagrams are the result of analytical calculations where the dipolar interaction is considered anisotropy-like. This choice is limiting because it leads to neglect the region where the 'up-down' configuration is the lowest in energy. As a consequence a richer diagram of the states is obtained if the anisotropy-type description is substituted by the fully-dipolar interaction description. We underline that for large scales of the system the 'up-up' and the 'up-down' configurations are comparable in energy since the role of the dipolar interaction is small. However, the dipolar interaction is sufficient to make the 'up-down' state the lowest in energy.

Finally we remark that thin films with laterally varying magnetic anisotropies might be used for domain wall resistivity studies. In particular, since the resistivity of a sample is a function of the wall width and of the ratio between the wall width and the domain

size [138] samples with various characteristics may be obtained by tuning geometric and material parameters.

6.3 Conclusion

Micromagnetic modeling has been applied to ultrathin films with spatially varying magnetic anisotropies. From this study we conclude that the anisotropy pattern plays the main role in the determination of the magnetic configuration. A marginal role is played by the dipolar interaction that is negligible in first approximation. As a consequence magnetic domains induced by the dipolar interaction are not found and the state of magnetization is only a function of the length scale of the anisotropy pattern.

The macroscopic description of the system based on the hypothesis of uniform magnetization is not satisfactory. The explanation of the macroscopic behavior is found only with the analysis of the magnetic microstructure. We conclude that micromagnetics gives the necessary information for the understanding of systems with spatially varying magnetic anisotropy on the nanometric scale.

The variety of characteristics of ultrathin films with spatially varying magnetic anisotropies might be utilized in new magnetoelectronics devices. This possibility is connected to the development of low-cost nanopatterning techniques. Moreover, high resolution magnetic imaging is required in order to prove the validity of the micromagnetic modeling.

Zusammenfassung

Diese Arbeit beschäftigt sich mit der Modellierung ultradünner Filme mit auf der Nanometerskala räumlich veränderlichen magnetischen Anisotropien im Konzept der mikromagnetischen Theorie. Das Interesse an diesen Strukturen begründet sich in der Möglichkeit der Herstellung dünner, strukturierter, magnetischer Filme in der Nanotechnologie. Im Besonderen kann die magnetische Anisotropie durch eine teilweise Bedeckung der Schicht oder auch Spannungsabbau in der Schicht lokal angepasst werden. Die mikromagnetische Modellierung verbindet die intrinsischen Eigenschaften des Materials mit der im Herstellungsvorgang erzielten morphologischen Struktur. Dabei ergibt sich die folgende Frage: Wie wird die magnetische Konfiguration durch Material- und Geometrieparameter bestimmt?

Das hier untersuchte Modellsystem besteht aus einer Serie von unendlich langen Streifen mit alternierender, uniaxialer Anisotropie. Die Einheitszelle des Modellsystems besteht aus zwei Streifen der Breite L_1 und L_2 , deren leichte Magnetisierungsrichtung senkrecht bzw. in der Schichtebene liegt. Die statische mikromagnetische Gleichung nach Brown wird gelöst, um die magnetische Gleichgewichtskonfiguration zu erhalten. Analytische Lösungen wurden mit Hilfe der Variationsrechnung erhalten. In diesem Fall wird die dipolare Wechselwirkung nur als lokal wirkende Entmagnetisierungsenergie berücksichtigt und ist in dem Anisotropieterm enthalten. Ein Iterationsverfahren wurde verwendet, um numerische Lösungen zu erhalten, die die dipolare Wechselwirkung vollständig berücksichtigen.

In dieser Arbeit wird einerseits das makroskopische Verhalten der Magnetisierung, wie es mit räumlich mittelnden Methoden gemessen werden kann, im Rahmen der mikromagnetischen Theorie erklärt. Andererseits wird auch direkt das Verhalten von magnetischen Nanostrukturen, wie es durch hochauflösende magnetische Mikroskopie untersucht werden kann, behandelt.

Im folgenden werden die Ergebnisse meiner Arbeit zusammengefasst. Dabei beschreibt L die geometrische Länge des Systems und λ ist die charakteristische magnetische Länge.

- *Makroskopische Eigenschaften.* Die mittlere Magnetisierung als Funktion eines angelegten äußeren Feldes wurde berechnet. Die Analyse der Hystereseschleife zeigt, daß das System für $L \leq \lambda$ wie ein einzelnes Teilchen mit gleichförmiger Magnetisierung verhält. Für $L \gg \lambda$ ist die Magnetisierung nicht mehr gleichförmig und folgt der lokalen Anisotropie.
- *Mikroskopische Eigenschaften.* Das makroskopische Verhalten des Systems wird

durch die magnetische Theorie erklärt. Insbesondere wurde die magnetische Härte der Schicht als Funktion der Längenskala L in numerischen Rechnungen untersucht. Für $L \leq \lambda$ werden die lokalen Anisotropieunterschiede in der Magnetisierung ausgemittelt. Das Koerzitivfeld ist klein, d.h. die Struktur ist magnetisch weich. Für $L \gg \lambda$ verursachen die Anisotropieunterschiede eine räumlich veränderliche Magnetisierungsrichtung in der Sicht und das Koerzitivfeld steigt an. Die Schicht wird magnetisch hart. Die Resultate werden mit experimentellen Messungen des magneto-optischen Kerr Effektes an dem System Fe auf W(100), welches ein räumlich veränderliches Muster der Anisotropie aufgrund von teilweisen Spannungsabbau zeigt, verglichen.

- *1-D Modell.* Nach Lösung der Brownschen Gleichung erhält man das Magnetisierungsprofil als Funktion der Materialparameter. Ein Übergang von räumlich variierender zu gleichförmiger Magnetisierung erfolgt, wenn die Längenskala L des Systems reduziert wird.
- *Verkippte Magnetisierung.* Im Grenzfall $L \leq \lambda$ wurde ein Zustand mit schräger Magnetisierungsrichtung gefunden, falls keine der beiden Anisotropien dominieren. Die Verkipfung, die hier in einem System mit nur zweiter Ordnung Anisotropiekonstanten auftritt, wird durch die Mikrostruktur, d.h. eine geometrische Eigenschaft, und nicht durch eine magnetokristalline Anisotropie höherer Ordnung, d.h. einer Materialeigenschaft, hervorgerufen.
- *Spinreorientierungsübergang. (SRT)* Ein SRT wird durch Variation der relativen Breite L_1/L_2 der Streifen hervorgerufen. Die Schärfe des Übergangs ist eine Funktion der Längenskala L und wird mit kleiner werdenden L immer schärfer.
- *Einfluß der dipolaren Wechselwirkung.* Die Korrekturen an dem Magnetisierungsverlauf durch den nichtlokalen Anteil des Streufeldes wurde durch Vergleich der analytischen Näherungslösungen mit der numerische exakten Lösungen der Brownschen Gleichung abgeschätzt. Diese Korrektur ist eine Funktion der Längenskala L und der effektiven Anisotropien.
- *Magnetische Domänen.* Verschiedene magnetische Konfigurationen wurden als Funktion der Systemparameter miteinander verglichen. Insbesondere wurden Konfigurationen mit parallel magnetisierten Streifen (up-up Konfiguration) und anti-parallel magnetisierten Streifen (up-down) miteinander verglichen. Für kleine Ausdehnungen des Systems, $L \leq \lambda$, hat die 'up-up' Konfiguration die geringste Energie, für große Ausdehnungen, $L \gg \lambda$, hat dagegen die 'up-down' Konfiguration die geringste Energie. Der Übergang zwischen beiden Konfigurationen wird durch die Dipolwechselwirkung bestimmt.
- *Zustandsdiagramm.* Das magnetische Zustandsdiagramm eines Systems mit räumlich variierender Magnetisierung als Funktion der Systemparameter festgestellt.

Bibliography

- [1] K. O'Grady, H. Laidler, J. Magn. Magn. Mater. **200**, 616 (1999)
The limits to magnetic recording-media considerations
- [2] S.Y. Chou, Proceedings of the IEEE **85**, 652 (1997)
Patterned magnetic nanostructures and quantized magnetic disks
- [3] O. Fruchart, M. Klaua, J. Bartel, J. Kirschner, Phys. Rev. Lett. **83**, 2769 (1999)
Self-organized growth of nanosized vertical magnetic Co pillars on Au(111)
- [4] W. Wulfhekel, F. Zavaliche, F. Porrati, H. P. Oepen, J. Kirschner, Europhys. Lett. **49**, 651 (2000)
Nano-patterning of magnetic anisotropy by controlled strain relief
- [5] C. Teichert, J. Barthel, H. P. Oepen, J. Kirschner, Appl. Phys. Lett. **74**, 588 (1999)
Fabrication of nanomagnet arrays by shadow deposition on self-organized semiconductors substrates
- [6] J. Hauschild, H. J. Elmers, U. Gradmann, Appl. Phys. Lett. **57**, R677 (1998)
Dipolar superferromagnetism in monolayer nanostripes of Fe(110) on vicinal W(110) surfaces
- [7] S. Y. Chou, P. R. Krauss, L. Kong, J. Appl. Phys. **79**, 6101 (1996)
Nanolithographically defined magnetic structures and quantum magnetic disk
- [8] J. Shen, R. Skomski, M. Klaua, H. Jenniches, S. Manoharan, J. Kirschner, Phys. Rev. B **56**, 2340 (1997)
Magnetism in one dimension: Fe on Cu(111)
- [9] A. Kubetzka, O. Pietzsch, M. Bode, R. Wiesendanger, Phys. Rev. B **63**, 140407 (2001)
Magnetism of nanoscale Fe islands studied by spin-polarized scanning tunneling spectroscopy
- [10] P. Grütter, H. J. Mamin, D. Rugar, Springer-Verlag Berlin, Heidelberg (1991)
Scanning Tunneling Microscopy II
- [11] K. Koike, K. Hayakawa, Appl. Phys. Lett. **45**, 585 (1984)
Observation of magnetic domains with spin-polarized secondary electrons
- [12] W. Wulfhekel, J. Kirschner, Appl. Phys. Lett. **75**, 1944 (1999)
Spin-polarized scanning tunneling microscopy on ferromagnets

- [13] S. Heinze, M. Rode, A. Kubetzka, O. Pietzsch, X. Nie, S. Blugel, R. Wiesendanger, *Science* **288**, 1805 (2000)
Real-space imaging of two-dimensional antiferromagnetism on the atomic scale
- [14] W. F. Brown Jr., Interscience-Wiley, New York (1963)
Micromagnetics
- [15] H. Kronmüller, World Scientific (1996)
from *Aspect of modern magnetism*, edited by F. C. Pu, Y. Wang, C. H. Shang
- [16] P. Bruno *Phys. Rev. Lett.* **83**, 2425 (1999)
Geometrically constrained magnetic wall
- [17] O. Pietzsch, A. Kubetzka, M. Bode, R. Wiesendanger *Phys. Rev. Lett.* **84**, 5212 (2000)
Real-space observation of dipolar antiferromagnetism in magnetic nanowires by spin-polarized scanning tunneling spectroscopy
- [18] N. Garcia, M. Muñoz, Y.-W. Zhao *Phys. Rev. Lett.* **82**, 2923 (1999)
Magnetoresistance in excess of 200% in ballistic Ni nanocontacts at room temperature and 100 Oe
- [19] W. F. Brown, *J. Appl. Phys.* **39**, 993 (1968)
Micromagnetics and fine particles
- [20] P. Politi, M. G. Pini, *Eur. Phys. J. B* **2**, 475 (1998)
Shape anisotropy and magnetic domain structures in striped monolayers
- [21] A. B. Kashuba, V. L. Pokrovsky, *Phys. Rev. B* **48**, 10335 (1993)
Stripe domain structures in a thin ferromagnetic film
- [22] A. Berger, H. Hopster, *Phys. Rev. Lett.* **76**, 519 (1996)
Nonequilibrium magnetization near the reorientation phase transition of Fe/Ag(100) films
- [23] A. Thiaville, A. Fert, *J. Magn. Magn. Mater.* **113**, 161 (1992)
Twisted spin configurations in thin magnetic layers with interface anisotropy
- [24] B. Dieny, A. Vedyanev, *Europhys. Lett.* **25**, 723 (1994)
Crossover from easy-plane to perpendicular anisotropy in magnetic thin films: canted anisotropy due to partial coverage or interfacial roughness
- [25] W. Wulfhekel, Ph.D. thesis, Jul 3234 (1997)
Kinetic growth manipulation during molecular beam epitaxy
- [26] G. Bertotti, Academic-Press (1998)
Hysteresis in magnetism
- [27] A. Aharoni, Oxford University Press (1996)
Introduction to the theory of ferromagnetism

- [28] S. Chikazumi, Oxford University Press (1997)
Physics of ferromagnetism
- [29] A. Hubert, R. Schäfer, Springer-Verlag (1998)
Magnetic domains
- [30] C. Kittel, in *Solid state physics*, Academic-Press (1956)
Ferromagnetic domain theory
- [31] B. D. Cullity, Addison-Wesley (1972)
Introduction to magnetic materials
- [32] M. Cinal, D. M. Edwards, J. Mathon, Phys. Rev. B **50**, 3754 (1994)
Magnetocrystalline anisotropy in ferromagnetic films
- [33] W. F. Brown, A. E. LaBonte, J. Appl. Phys. **36**, 1380 (1965)
Structure and energy of one-dimensional domain walls in ferromagnetic thin films
- [34] A. E. LaBonte, J. Appl. Phys. **40**, 2450 (1969)
Two-dimensional Bloch-type domain walls in ferromagnetic films
- [35] A. Hubert, Phys. stat. sol. **32**, 519 (1969)
Stray-field-free magnetization configurations
- [36] W. F. Brown, S. Shtrikman, Phys. Rev. **125**, 825 (1962)
Stability of one dimensional ferromagnetic microstructures
- [37] M. Scheinfein
LLG *Micromagnetic Simulator*TM
Copyright ©1988 and 1999 by M. Scheinfein and E. Price
- [38] B. Kaplan, G.A. Gehring, J. Magn. Magn. Mater. **128**, 111 (1993)
The domain structure in ultrathin magnetic films
- [39] C. Kittel, Phys. Rev. **70**, 965 (1946)
Theory of the structure of ferromagnetic domains in films and small particles
- [40] Z. Malek, V. Kambersky, Czechosl. Journ. Phys. **8**, 416 (1958)
On the theory of the domain structure of thin films of magnetically uniaxial materials
- [41] In this integration no periodical boundary conditions are considered. This assumption brings to underestimate the value of the domain size.
- [42] B. Kooy, U. Enz, Philips Res. Rep. **15**, 7 (1960)
Experimental and theoretical study of the domain configuration in thin layers of BaFe₁₂O₁₉

- [43] M. Speckmann, Ph.D. thesis, Julich (1996)
Mikromagnetische Strukturen und magnetischer Reorientierungsübergang in Co/Au(111)
- [44] R. Skomski, H.P. Oepen, J. Kirschner, Phys. Rev. B **58**, 3223 (1998)
Micromagnetics of ultrathin films with perpendicular magnetic anisotropy
- [45] The equation is valid for a system of stripes uniformly magnetised. For a checkerboard pattern the equation has the same form, but the factor that multiplies the exponential is smaller. As a consequence the total energy for a checkerboard pattern is higher than for a system of stripes.
- [46] A.L.Sukstanskii, K.I. Primak, J. Magn. Mater. **169**, 31 (1997)
Domain structure in an ultrathin ferromagnetic film
- [47] R. Skomski
Private communication.
- [48] The infinite film is numerically obtained by imposing periodical boundary conditions in the x and y directions. The boundary in the x direction forms an additional Bloch wall at the edges of the structure.
- [49] J. G. Gay, R. Richter, Phys. Rev. Lett. **56**, 2728 (1986)
Spin anisotropy of ferromagnetic films
- [50] U. Gradmann, J. Muller, Phy. Stat. Sol. **27**, 313 (1968)
Flat ferromagnetic, epitaxial 48Ni/52Fe(111) films of few atomic layers
- [51] U. Gradmann in *Handbook of magnetic materials* by K. H. J. Buschow **7**, (North-Holland, Amsterdam, 1993)
Magnetism in transition metal ultrathin films
- [52] M. T. Johnson, P. J. H. Bloemen, F. J. A. den Broeder, J. J. de Vries, Rep. Prog. Phys. **59**, 1049 (1996)
Magnetic anisotropy in metallic multilayers
- [53] M. N. Barber in *Phase transitions and critical phenomena* by C. Domb, J. L. Lebowitz **8**, 145 (Academic, London, 1993)
Finite-size scaling
- [54] Y. Millev, J. Kirschner, Phys. Rev. B **54**, 4137 (1996)
Reorientation transitions in ultrathin ferromagnetic films by thickness- and temperature-driven anisotropy flows
- [55] L. M. Levinson, M. Luban, S. Shtrikman, Phys. Rev. **187**, 715 (1969)
Microscopic model for reorientation of the easy axis of magnetization
- [56] P. J. Jensen, K. H. Bennemann, Phys. Rev. B **42**, 849 (1990)
Direction of the magnetization of thin films and sandwiches as a function of temperature

- [57] M. Farle, W. Platow, A. N. Anisimov, B. Schulz, K. Baberschke, J. Magn. Magn. Mater. **165**, 74 (1997)
The temperature dependence of magnetic anisotropy in ultra-thin films
- [58] G. Garreau, M. Farle, E. Beaurepaire, J. P. Kappler, J. Magn. Magn. Mater. **184**, 289 (1998)
Spin-reorientation phase transition in Co/Tb and Co/Ho ultrathin films
- [59] G. Garreau, E. Beaurepaire, M. Farle, J. P. Kappler, Europhys. Lett, **39**, 557 (1997)
Second- and fourth-order anisotropy constants near the spin reorientation transition in Co/Ho thin films
- [60] M. Farle, B. Mirwald-Schulz, A. N. Anisimov, W. Platow, K. Baberschke, Phys. Rev. B **55**, 3708 (1997)
Higher-order magnetic anisotropies and the nature of the spin-reorientation transition in the face-centred-tetragonal Ni(001)/Cu(001)
- [61] H. Fritzsche, J. Kohlhepp, H. J. Elmers, U. Gradmann, Phys. Rev. B. **49**, 15665 (1994)
Angular dependence of perpendicular magnetic surface anisotropy and the spin-reorientation transition
- [62] B. Schulz, K. Baberschke, Phys. Rev. B **50**, 13467 (1994)
Crossover from in-plane to perpendicular magnetization in ultrathin Ni/Cu(001) films
- [63] V. Grolier, J. Ferre', A. Maziewski, E. Stefanowicz, D. renard, J. Appl. Phys. **73**, 5939 (1993)
Magneto-optical anisometry of ultrathin cobalt films
- [64] R. Allenspach, M. Stampanoni, A. Bischof, Phys. Rev. Lett. **69**, 3385 (1992)
Magnetization direction switching in Fe/Cu(100) epitaxial films: Temperature and thickness dependence
- [65] M. Speckmann, H. P. Oepen, H. Ibach, Phys. Rev. Lett. **75**, 2035 (1995)
Magnetic domain structures in ultrathin Co/Au(111): on the influence of film morphology
- [66] R. P. Cowburn, J. Ferre', J. -P. Jamet, S. J. Gray, J. A. C. Bland, Phys. Rev. B **55**, 11593 (1997)
Role of remanent domain structure and cubic anisotropy in the reorientation phase transition of ultrathin Ag/Fe/Ag(001) epitaxial films
- [67] H. F. Ding, S. Pütter, H. P. Oepen, J. Kirschner, Phys. Rev. B **63**, 134425 (2001)
Spin reorientation transition in thin films studied by the component-resolved Kerr effect
- [68] K. Ha, R. C. O'Handley, J. Appl. Phys. **87**, 5946 (2000)
Magnetization canting in epitaxial Cu/Ni/Cu/Si(001)
- [69] R. C. O'Handley, J. P. Woods, Phys. Rev. B **42**, 6568 (1990)
Static magnetization direction under perpendicular surface anisotropy
- [70] S. Hope, E. Gu, B. Choi, J. A. C. Bland, Phys. Rev. Lett. **80**, 1750 (1998)
Spin engineering in ultrathin Cu/Co/Cu(110)

- [71] A. Rettori, L. Trallori, P. Politi, M. G. Pini, M. Maccio', J. Magn. Magn. Mater. **140**, 639 (1995)
Surface magnetic reconstruction
- [72] H. Tang, D. Weller, T. G. Walker, J. C. Scott, C. Chappert, H. Hopster, A. W. Pang, D. S. Dessau, D. P. Pappas, Phys. Rev. Lett. **71**, 444 (1993)
Magnetic reconstruction of the Gd(0001) surface
- [73] Xiao Hu, Y. Kawazoe, Phys. Rev. B **49**, 3294 (1994)
Theory of the capping effect in magnetic double-film systems
- [74] C. S. Arnold, D. P. Pappas, A. P. Popov, Phys. Rev. Lett. **83**, 3305 (1999)
Second- and first-order phase transitions in the magnetic reorientation of ultrathin Fe on Gd
- [75] H. J. Elmers, J. Magn. Magn. Mater. **185**, 274 (1998)
Magnetization states in ultrathin films with laterally modulated anisotropies
- [76] H. P. Oepen, F. Porrati, J. Kirschner, to be published
On the influence of spatially varying magnetic anisotropies on the magnetic properties of ultrathin films
- [77] M. A. Torija, J. P. Pierce, J. Shen, Phys. Rev. B **63**, 92404 (2001)
Magnetic capping layer induced spin reorientation: Co on Fe/Cu(100)
- [78] M. Farle, H. Poppa, bulletin PAS, (2001)
Ni/Cu covered by Fe islands
- [79] B. Heinrich, T. Monchesky, R. Urban, pre-print of J. Magn. Magn. Mater. (2001)
Role of interfaces in higher order angular terms of magnetic anisotropies. Ultrathin film structures
- [80] J. C. Slonczewski, Phys. Rev. Lett. **67**, 3172 (1991)
Fluctuation mechanism for biquadratic exchange coupling in magnetic multilayers
- [81] N. Weber, N. Wagner, H. J. Elmers, J. Hauschild, U. Gradmann, Phys. Rev. B **55**, 14121 (1997)
Nanoscale spatial switching of magnetic anisotropy in pseudomorphic Fe(110) on W(110)
- [82] H. J. Elmers, J. Hauschild, U. Gradmann, Phys. Rev. B **59**, 3688 (1999)
Onset of perpendicular magnetization in nanostripe arrays of Fe on stepped W(110) surfaces
- [83] S. D. Bader, J. Magn. Magn. Mater. **100**, 440 (1991)
SMOKE
- [84] E. C. Stoner, E. P. Wohlfarth, Phil. Trans. Roy. Soc. **A 240**, 599 (1948)
A mechanism of magnetic hysteresis in heterogeneous alloys
- [85] J. Kohlhepp, Ph.D. thesis, Technischen Universität Clausthal (1994)
Torsions-Oszillations-Magnetometrie an ultradünnen Kobalt-Epitaxie-Schichten

- [86] J. Kohlhepp, U. Gradmann, J. Magn. Magn. Mater. **139**, 347 (1995)
Magnetic surface anisotropies of Co(0001)- based interfaces from in situ magnetometry of Co films on Pd(111), covered with ultrathin films of Pd and Ag
- [87] G. Bochi, C. A. Ballentine, H. E. Inglefield, C. V. Thompson, R. C. O'Handley, Phys. Rev. B **53**, R1729 (1996)
Evidence for strong surface magnetoelastic anisotropy in epitaxial Cu/Ni/Cu(001) sandwiches
- [88] P. Politi, Comm. Cond. Mat. Phys. **18**, 191 (1998)
Domain structures in ultrathin magnetic films
- [89] D. Pescia, V. L. Pokrovsky, Phys. Rev. Lett. **65**, 2599 (1990)
Perpendicular versus in-plane magnetization in a 2D Heisemberg monolayer at finite temperatures
- [90] N. D. Mermin, H. Wagner, Phys. Rev. Lett. **17**, 1133 (1966)
Absence of ferromagnetism or antiferromagnetism in one- or two- dimensional isotropic Heisemberg models
- [91] D. Pescia, V. L. Pokrovsky, Phys. Rev. Lett. **70**, 1185 (1993)
Comment on "Perpendicular versus in-plane magnetization in a 2D Heisemberg monolayer at finite temperatures"- reply
- [92] A. Moschel, K. D. Usadel, Phys. Rev. B **49**, 12868 (1994)
Influence of the dipole interaction on the direction of the magnetization in thin ferromagnetic films
- [93] J. Lee, G. Lauhoff, J. A. C. Bland, Phys. Rev. B **56**, R5728 (1997)
Perpendicular magnetic anisotropy of the epitaxial Fcc Co/60-Å-Ni/Cu(100) system
- [94] J. Shen, A. K. Swan, J. F. Wendelken, App. Phys. Lett. **75**, 2987 (1999)
Determination of critical thickness of spin reorientation in metastable magnetic ultrathin films
- [95] J. A. Venables, G. D. T. Spiller, M. Hanbucken, Rep. Prog. Phys. **47**, 399 (1984)
Nucleation and growth of thin films
- [96] M. Kowaleski, C. M. Schneider, B. Heinrich, Phys. Rev. B **47**, 8748 (1993)
Thickness and temperature dependence of magnetic anisotropies in ultrathin fcc Co(001) structures
- [97] H. P. Oepen, J. Kirschner, Scanning Microscopy **5**, 1 (1991)
Imaging of magnetic microstructures at surfaces: the scanning electron microscope with spin polarization analysis
- [98] Y. Suzuki, W. Nabhan, K. Tanaka, Appl. Phys. Lett. **71**, 3153 (1997)
Magnetic domains of cobalt ultrathin films observed with a scanning tunneling microscope using optically pumped GaAs tips
- [99] Xiao Hu, Physical Review B **55**, 8382 (1997)
Magnetization reversal and coercive force in ultrathin films with perpendicular surface anisotropy: micromagnetic theory

- [100] T. Leineweber, H. Kronmüller, J. Magn. Magn. Mater. **176**, 145 (1997)
Micromagnetic examination of the exchange coupled ferromagnetic nanolayers
- [101] I. N. Bronstein, K. A. Semendyayev, Springer-Verlag Berlin Heidelberg (1998)
Handbook of mathematics
- [102] M. Abramowitz, I. A. Stegun, M. Danos, J. Rafelski, Verlag Harri Deutsch (1984)
Handbook of mathematical functions
- [103] I. S. Gradshteyn, I. M. Ryzhik Academic Press (1994)
Tables of integrals, series, and products
- [104] J. A. C. Bland, B. Heinrich Springer-Verlag (1994)
Ultrathin magnetic structures
- [105] K. B. Urquhart, B. Heinrich, J. F. Cochran, A. S. Arrott K. Myrtle, J. Appl. Phys. **64**, 5334 (1988)
Ferromagnetic resonance in ultrahigh vacuum of bcc Fe(001) films grown on Ag(001)
- [106] B. Heinrich, J. F. Cochran, M. Kowalewski, J. Kirschner, Z. Celinski, A. S. Arrott, K. Myrtle, Phys. Rev. B **44**, 9348 (1991)
Magnetic anisotropies and exchange coupling in ultrathin fcc Co(001) structures
- [107] B. Hillebrands, P. Baumgart, G. Güntherodt, Phys. Rev. B **36**, 2450 (1987)
In situ Brillouin scattering from surface-anisotropy-dominated Damon-Eshbach modes in ultrathin epitaxial Fe(110) layers
- [108] C. Chappert, H. Bernas, J. Ferré, V. Kottler, J.-P. Jamet, Y. Chen, E. Cambril, T. Devolder, F. Rousseaux, V. Mathet, H. Launois, Science **280**, 1919 (1998)
Planar patterned magnetic media obtained by ion irradiation
- [109] B. D. Terris, L. Folks, D. Weller, J. E. E. Baglin, A. J. Kellock, H. Rothuizen, P. Vettiger, Appl. Phys. Lett. **75**, 403 (1999)
Ion-beam patterning of magnetic films using stencil masks
- [110] S. S. Dhesi, H. A. Dürr, G. van der Laan, Phys. Rev. B **59**, 8408 (1999)
Canted spin structures in Ni films on stepped Cu(001)
- [111] P. Bruno, J. Appl. Phys. **64**, 3154 (1988)
Dipolar magnetic surface anisotropy in ferromagnetic thin films with interfacial roughness
- [112] R. Hertel, J. Appl. Phys. **90**, 5758 (2001)
Micromagnetic simulations of magnetostatically coupled Nickel nanowires
- [113] P. Krams, F. Lauks, R. L. Stamps, B. Hillebrands, G. Güntherodt, Phys. Rev. Lett. **69**, 3674 (1992)
Magnetic anisotropies of ultrathin Co(001) films on Cu(001)

- [114] N. D. Mermin, H. Wagner, Phys. Rev. Lett. **17**, 1133 (1966)
Absence of ferromagnetism or antiferromagnetism in one- or two-dimensional isotropic Heisenberg models
- [115] Z. Q. Qiu, J. Pearson, S. D. Bader, Phys. Rev. Lett. **70**, 1006 (1993)
Asymmetry of the spin reorientation transition in ultrathin Fe films and wedges grown on Ag(100)
- [116] H. J. Elmers, T. Furubayashi, M. Albrecht, U. Gradmann, J. Appl. Phys. **70**, 5764 (1991)
Analysis of the magnetic anisotropies in ultrathin films by magnetometry in situ in UHV
- [117] C. Liu, E. R. Moog, S. D. Bader, J. Appl. Phys. **64**, 5325 (1988)
Polar Kerr-effect observation of perpendicular surface anisotropy for ultrathin ferromagnetic films: fcc Fe/Cu(100)
- [118] D. E. Fowler, J. V. Barth, Phys. Rev. B. **53**, 5563 (1996)
Magnetic anisotropy of glide-distorted fcc and of bcc ultrathin Fe/Cu(001) films
- [119] H. P. Oepen, M. Speckmann, Y. Millev, J. Kirschner, Phys. Rev. B. **55**, 2752 (1997)
Unified approach to thickness-driven magnetic reorientation transitions
- [120] R. Vollmer, Th. Gutjahr-Löser, J. Kirschner, S. van Dijken, B. Poelsema, Phys. Rev. B **60**, 6277 (1999)
Spin-reorientation transition in Ni films on Cu(001): the influence of H₂ adsorption
- [121] H. P. Oepen, M. Benning, H. Ibach, C. M. Schneider, J. Kirschner, J. Magn. Magn. Mater. **86**, L137 (1990)
Magnetic domain structure in ultrathin Cobalt films
- [122] H. J. Elmers, J. Hauschild, G. H. Liu, U. Gradmann, J. Appl. Phys. **79**, 4984 (1996)
Critical phenomena in the two-dimensional XY magnet Fe(100) on W(100)
- [123] A. Moschel, K. D. Usadel, Phys. Rev. B **51**, 16111 (1995)
Reorientation transitions of first and second order in thin ferromagnetic films
- [124] E. Y. Vedmedenko, H. P. Oepen, A. Ghazali, J.-C. S. Lévy, J. Kirschner, Phys. Rev. B **84**, 5884 (2000)
Magnetic microstructure of the spin reorientation transition: a computer experiment
- [125] A. Enders, D. Sander, J. Kirschner, J. Appl. Phys. **85**, 5280 (1999)
Strain dependence of the magnetic properties of nm Fe films on W(100)
- [126] G. Herzer, J. Magn. Magn. Mat. **112**, 258 (1992)
Nanocrystalline soft magnetic materials
- [127] J. Arcas, A. Hernando, J. M. Barandiarán, C. Prados, M. Vázquez, P. Marín, A. Neuweiler, Phys. Rev. B **58**, 5193 (1998)
Soft to hard magnetic anisotropy in nanostructured magnets

- [128] A. Hernando, I. Navarro, C. Prados, D. García, M. Vázquez, J. Alonso, Phys. Rev. B **53**, 8223 (1996)
Curie-temperature enhancement of ferromagnetic phases in nanoscale heterogeneous systems
- [129] D. P. Pappas, C. R. Brundle, H. Hopster, Phys. Rev. B **45**, 8169 (1992)
Reduction of macroscopic moment in ultrathin Fe films as the magnetic orientation changes
- [130] C. Chappert, H. Bernas, J. Ferré, V. Kottler, J.-P. Jamet, Y. Chen, E. Cambril, T. Devolder, F. Rousseaux, V. Mathet, H. Launois, Science **280** 1919 (1998)
Planar patterned magnetic media obtained by ion irradiation
- [131] J. Fidler, T. Schrefl, J. Phys. D **33**, R135 (2000)
Micromagnetic modelling-the current state of the art
- [132] M. R. Scheinfein, J. L. Blue, J. Appl. Phys. **69**, 7740 (1991)
Micromagnetic calculations of 180° surface domain walls
- [133] M. R. Scheinfein, J. Unguris, J. L. Blue, K. J. Coakley, D. T. Pierce, R. J. Celotta, P. J. Ryan, Phys. Rev. B **43**, 3395 (1991)
Micromagnetics of domain walls at surfaces
- [134] W. F. Brown, J. Appl. Phys. **49**, 1937 (1978)
Domains, micromagnetics, and beyond: reminiscences and assessments
- [135] J. Hauschild, U. Gradmann, H. J. Elmers, App. Phys. Lett. **72**, 3211 (1998)
Perpendicular magnetization and dipolar antiferromagnetism in double layer nanostripe arrays of Fe(110) on W(110)
- [136] M. Bode, O. Pietzsch, A. Kubetzka, S. Heinze, R. Wiesendanger, Phys. Rev. Lett. **86**, 2142 (2001)
Experimental evidence for intra-atomic noncollinear magnetism at thin film probe tips
- [137] M. Pratzner, H. J. Elmers, M. Bode, O. Pietzsch, A. Kubetzka, R. Wiesendanger, Phys. Rev. Lett. **87**, 127201 (2001)
Atomic-scale magnetic domain walls in quasi-one-dimensional Fe nanostripes
- [138] A. D. Kent, J. Yu, U. Rüdiger, S. S. P. Parkin, J. Phys. Cond. Matt. **13**, R461 (2001)
Domain wall resistivity in epitaxial thin film microstructures

Appendix A

Derivation of equations

Derivation of equation (4.5)

Equations (4.4) and (4.5) are obtained by applying the variational method to equation (4.1). Here, I show how to calculate equation (4.5), defined in the stripe with in-plane anisotropy. The procedure to obtain equation (4.4) is similar. The energy per unit area for the stripe of width L_2 is:

$$G_{L_2} = \int_0^{L_2} (A \left(\frac{d\theta}{dx} \right)^2 + k_{sh} + k_2^{eff} \sin^2 \theta) dx \quad (\text{A.1})$$

This functional can be minimized by considering an arbitrary small variation $\delta\theta(x)$. In this way the variation of the energy results:

$$\delta G_{L_2} = 2 \int_0^{L_2} (A \frac{d}{dx} \frac{d\theta}{dx} + k_2^{eff} \sin \theta \cos \theta) \delta\theta dx \quad (\text{A.2})$$

Integration by parts brings to:

$$\delta G_{L_2} = 2 \int_0^{L_2} (-A \frac{d^2\theta}{dx^2} + k_2^{eff} \sin \theta \cos \theta) \delta\theta dx \quad (\text{A.3})$$

where the condition of symmetry, that gives $\theta(0) = \theta(L_2)$, has been used. The extreme of equation (A.1) is obtained if $\delta G_{L_2} = 0$ for each arbitrary variation $\delta\theta(x)$. This condition brings to the Euler-Lagrange equation of the problem that is given by:

$$\lambda_2^2 \frac{d}{dx} \frac{d\theta}{dx} + \sin \theta \cos \theta = 0 \quad (\text{A.4})$$

with $\lambda_2 = \sqrt{-\frac{A}{k_2^{eff}}} > 0$. By multiplying for $\frac{d\theta}{dx}$ and integrating by parts, we obtain equation (4.5):

$$\left(\frac{d\theta}{dx}\right)^2 = -\frac{\sin^2 \theta}{\lambda_2^2} + c_2 \quad (\text{A.5})$$

Elliptical integral of the first kind

$$F(\varphi|m) = \int_0^\varphi \frac{1}{\sqrt{1 - m \sin^2 \theta}} d\theta \quad (\text{A.6})$$

Elliptical integral of the second kind

$$E(\varphi|m) = \int_0^\varphi \sqrt{1 - m \sin^2 \theta} d\theta \quad (\text{A.7})$$

Definitions

Sine and cosine amplitude:

$$\text{sn}(F(\varphi|m)) = \sin \varphi \quad \text{cn}(F(\varphi|m)) = \cos \varphi \quad (\text{A.8})$$

Useful properties

Introducing the notation $\xi = F(\varphi|m)$ for the elliptical integral of the first kind we have:

$$\text{sn}^2 \xi + \text{cn}^2 \eta = 1 \quad (\text{A.9})$$

$$F(\alpha|m) = \frac{F(\beta|m^{-1})}{\sqrt{m}} \quad (\text{A.10})$$

with $\sin \alpha = \sin \beta / \sqrt{m}$

$$\frac{d \text{sn} \xi}{d u} = \sqrt{(1 - \text{sn}^2 \xi)(1 - m \text{sn}^2 \xi)} \quad (\text{A.11})$$

$$\int \text{sn}^2 \xi d\xi = \frac{\xi - E(\varphi|m)}{m} \quad (\text{A.12})$$

$$\int \text{cn}^2 \xi d\xi = \frac{E(\varphi|m) - (1 - m)\xi}{m} \quad (\text{A.13})$$

Derivation of equations (4.10) and (4.11)

$$F(\theta_x|m) - F(\theta_0|m) = \frac{x}{\lambda_2 \sqrt{m}} \quad (\text{A.14})$$

with $m = 1/\sin^2 \theta_{\frac{L_2}{2}}$. By using the relation (A.10) equation (A.14) becomes:

$$F(\phi_x|m^{-1}) - F(\phi_0|m^{-1}) = \frac{x}{\lambda_2} \quad (\text{A.15})$$

with

$$\sin \phi_x = \sqrt{m} \sin \theta_x \quad \sin \phi_0 = \sqrt{m} \sin \theta_0 \quad (\text{A.16})$$

The system of equations (A.15) and (A.16) can be compacted in the following manner by inserting relations (A.16) in equation (A.15):

$$F\left(\arcsin\left(\frac{\sin \theta_x}{\sin \theta_{\frac{L_2}{2}}}\right) \middle| \sin^2 \theta_{\frac{L_2}{2}}\right) - F\left(\arcsin\left(\frac{\sin \theta_0}{\sin \theta_{\frac{L_2}{2}}}\right) \middle| \sin^2 \theta_{\frac{L_2}{2}}\right) = \frac{x}{\lambda_2} \quad (\text{A.17})$$

that is equation (4.10). The analogous of equation (A.14) for the case $-L_1 \leq x \leq 0$ can be deduced from equation (4.6) and results:

$$F\left(\frac{\pi}{2} - \theta_x|m\right) - F\left(\frac{\pi}{2} - \theta_0|m\right) = -\frac{x}{\lambda_1 \sqrt{m}} \quad (\text{A.18})$$

with $m = 1/\cos^2 \theta_{-\frac{L_1}{2}}$. By using the relation (A.10) equations (A.18) becomes:

$$F(\phi_x|m^{-1}) - F(\phi_0|m^{-1}) = -\frac{x}{\lambda_1} \quad (\text{A.19})$$

with

$$\sin \phi_x = \sqrt{m} \cos \theta_x \quad \sin \phi_0 = \sqrt{m} \cos \theta_0 \quad (\text{A.20})$$

Substituting relations (A.20) in equation (A.19) we obtain equation (4.11):

$$F\left(\arcsin\left(\frac{\cos \theta_x}{\cos \theta_{-\frac{L_1}{2}}}\right) \middle| \cos^2 \theta_{-\frac{L_1}{2}}\right) - F\left(\arcsin\left(\frac{\cos \theta_0}{\cos \theta_{-\frac{L_1}{2}}}\right) \middle| \cos^2 \theta_{-\frac{L_1}{2}}\right) = -\frac{x}{\lambda_1} \quad (\text{A.21})$$

Derivation of equation (4.17)

The following integrals contained in equation (4.16) have to be solved:

$$I_1 = \int_{-\frac{L_1}{2}}^0 \left(\frac{d\theta_x}{dx}\right)^2 dx \quad (\text{A.22})$$

$$I_2 = \int_0^{\frac{L_2}{2}} \left(\frac{d\theta_x}{dx}\right)^2 dx \quad (\text{A.23})$$

Equation (A.16) can be written as:

$$\theta_x = \arcsin(\sqrt{m_2} \sin \phi_x) \quad (\text{A.24})$$

with $m_2 = \sin^2 \theta_{\frac{L_2}{2}}$. By using relations (A.8), (A.9) and (A.11) the derivative of equation (A.24) becomes:

$$\frac{d\theta_x}{dx} = \frac{\sqrt{m_2}}{\lambda_2} \text{cn}(F(\phi_x|m_2)) \quad (\text{A.25})$$

Substituting in integral (A.23) we obtain:

$$I_2 = \frac{m_2}{\lambda_2} \int_0^{\frac{L_2}{2}} \text{cn}^2 z dz \quad (\text{A.26})$$

where $z = \frac{x}{\lambda_2} + F(\phi_0|m_2)$ and equation (A.15) has been used. Using relation (A.13) integral (A.26) becomes:

$$I_2 = \frac{E(\phi_{\frac{L_2}{2}}|m_2) - E(\phi_0|m_2) - (1 - m_2)\frac{L_2}{2\lambda_2}}{\lambda_2} \quad (\text{A.27})$$

From equation (A.22) in the same way we obtain:

$$I_1 = \frac{E(\phi_{-\frac{L_1}{2}}|m_1) - E(\phi_0|m_1) - (1 - m_1)\frac{L_1}{2\lambda_1}}{\lambda_1} \quad (\text{A.28})$$

with $m_1 = \cos^2 \theta_{-\frac{L_1}{2}}$. Finally, substituting integrals (A.27) and (A.28) in equation (4.16) we obtain equation (4.17).

Derivation of equation (4.20)

To calculate equation (4.20) we need to solve the following integrals:

$$I_1 = \int_{-\frac{L_1}{2}}^0 \sin^2 \theta_x dx \quad (\text{A.29})$$

$$I_2 = \int_0^{\frac{L_2}{2}} \sin^2 \theta_x dx \quad (\text{A.30})$$

Using relation (A.20) equation (A.29) becomes:

$$I_1 = \frac{L_1}{2} - m_1 I_1^* \quad (\text{A.31})$$

with $m_1 = \cos^2 \theta_{-\frac{L_1}{2}}$ and:

$$I_1^* = \int_{-\frac{L_1}{2}}^0 \sin^2 \phi_x dx \quad (\text{A.32})$$

Considering equations (A.8) and (A.19) integral (A.32) becomes:

$$I_1^* = \int_{-\frac{L_1}{2}}^0 \operatorname{sn}^2\left(-\frac{x}{\lambda_1} + F(\phi_x|m_1)\right) dx \quad (\text{A.33})$$

After the change of variable $z = -\frac{x}{\lambda_1} + F(\phi_x|m_1)$, using relation (A.12) we obtain:

$$I_1^* = \frac{L_1}{2m_1} - \frac{\lambda_1}{m_1} (E(\phi_{-\frac{L_1}{2}}|m_1) - E(\phi_0|m_1)) \quad (\text{A.34})$$

Substituting in (A.31) we have:

$$I_1 = \lambda_1 (E(\phi_{-\frac{L_1}{2}}|m_1) - E(\phi_0|m_1)) \quad (\text{A.35})$$

In a similar way we calculate integral I_2 using equations (A.15) and (A.16):

$$I_2 = \int_0^{\frac{L_2}{2}} \operatorname{sn}^2\left(\frac{x}{\lambda_2} + F(\phi_x|m_2)\right) dx \quad (\text{A.36})$$

with $m_2 = \sin^2 \theta_{\frac{L_2}{2}}$. Using the new variable $z = \frac{x}{\lambda_2} + F(\phi_x|m_2)$ and equation (A.12) we obtain:

$$I_2 = \frac{L_2}{2} - \lambda_2 (E(\phi_{\frac{L_2}{2}}|m_2) - E(\phi_0|m_2)) \quad (\text{A.37})$$

Finally, inserting integrals (A.36) and (A.37) in equation (4.19) we obtain equation (4.20).

Appendix B

Curriculum vitae

Personal data:

Name: Fabrizio Porrati
Date of birth: Januar 31, 1968
Place of birth: Milano, Italy

Education:

Sept. 1974 – June 1979 Primary school in Milano, Italy.
Sept. 1979 – June 1982 Secondary school in Milano and Torino, Italy.
Sept. 1982 – July 1987 High school, Liceo Scientifico Statale "Galileo Ferraris" in Torino, Italy.
Sept. 1987 – March 1997 "Università degli Studi" in Torino, Italy. Degree in Physics with the thesis: *Correlation measurements and Barkhausen effect in soft magnetic materials* made at the "Istituto Elettrotecnico Nazionale G. Ferraris".
Supervisors: Dr. Gianfranco Durin, Prof. Giorgio Bertotti
Nov. 1997 – Nov. 2001 Ph. D. candidate at Max-Planck-Institut für Mikrostrukturphysik in Halle(Saale), Germany.
Thesis: *Spatially varying magnetic anisotropies in ultrathin films*.
Supervisor: Prof. Dr. Jürgen Kirschner

Halle, November 26, 2001 Fabrizio Porrati

Appendix C

Erklärung

Ich versichere hiermit, die vorliegende Dissertation

Spatially varying magnetic anisotropies in ultrathin films

selbständig verfasst und keine anderen als die von mir angegebenen Quellen und Hilfsmittel verwendet zu haben. Die den benutzten Werken wörtlich oder inhaltlich entnommenen Stellen sind als solche kenntlich gemacht.

Halle, November 26, 2001

Fabrizio Porrati

Appendix D

Acknowledgments

At the end of this work I wish to express my gratitude to my Supervisor Prof. Jürgen Kirchner. He gave me the chance to spend a good time of professional growth at the Institute supporting me in these years of study.

I wish to thank Prof. Hans-Peter Oepen for the time spent in teaching me basics of micromagnetics. Our dialogues have been always a challenge for me. At the beginning he gave important hints to my work, that he continued to examine after his leaving to Hamburg.

Special thanks are for Dr. Wulf Wulffhekel. His suggestions have been always precious during my Ph. D. He helped me to 'put order' into my thesis reading it critically. His support and kindness go much beyond physics.

In these years of study I could interact with many people and take advantage of their experience in thin film magnetism. In particular I would like to mention Dr. Gerold Steierl and Dr. Wim Lutzke that contributed to 'set' the bases of my thesis. I certainly gained a lot in being the 'third men' in their office! Another special thank goes to Dr. Haifeng Ding. As Ph.D. student he shared with me a lot of time at the Institute. He helped me to solve a lot of problems about physics and computer stuff. He has shown me that physics sometime is simple (given my basic complexity this is an incomparable merit!).

Another special thank is for my master Prof. Giorgio Bertotti. His beautiful book about magnetism has been a reference and a very helpful background during this period of study.

I would like to acknowledge for fruitful discussions Dr. Riccardo Hertel, Dr. Olivier Fruchard, Prof. Patrick Bruno, Prof. U. Gradmann and Dr. Vollmer. Thanks also to Dr. Simona Bodea and Mr Yaroslav Pavlyukh that corrected part of my thesis.

I would like to express my gratitude to all the members of the computer support group, the mechanical and the electrical workshops who helped me in the first year of work in the lab. Thanks also to Mr Gerth and Mr Roger Pflanz who helped me at the beginning of my staying at the institute.

I wish also to thank Dimitre Iorgov, Dirk Sander, Gianfranco Durin, Carlo Sasso, Enzo Ferrara and Marek Przybylski for their friendship and encouragement.

Francesco Offi shared with me this experience in Germany. He has been present in the difficult moments of my Ph.D. and he constantly pushed and encouraged me. He and Paola provided me also some Italian specialties helping me to survive to homesickness.

I would like also to thank all my friends at the Institute: Roger, Wim, Sabina, Wulf, Haifeng, Dimitri, Gulei, Gerold, Florin, Simona, Yaroslav, Olena, Vio, Uta, Marcus, Jonathan, Norbert, Sha, Riccardo, Yurek, Peter, Miroslav, Matthieu. I shared with all of them very good moments and interesting discussions.

In Halle and in Italy heaps of people supported me with words of wisdom, friendship and encouragement: Po', Maurizio, Giorgio, Nelly, Franco, Anja, Regina, Hannes, Marit, Christian, KSG friends, Campus friends, EG friends, Maria, Edo, Fulvio, Marco, Larry, Alberto, Randy and Sybilla.

To them and to my parents, to Pipa and Damaris that continuously poured out on me love in these years of study this thesis is dedicated.